Geo-neutrinos and earth's interior

Gianni Fiorentini[a, b], Marcello Lissia[c, d, *], Fabio Mantovani[b, e, f]

[a]*Dipartimento di Fisica, Università di Ferrara, I-44100 Ferrara, Italy*
[b]*Istituto Nazionale di Fisica Nucleare, Sezione di Ferrara, I-44100 Ferrara, Italy*
[c]*Istituto Nazionale di Fisica Nucleare, Sezione di Cagliari, I-09042 Monserrato, Italy*
[d]*Dipartimento di Fisica, Università di Cagliari, I-09042 Monserrato, Italy*
[e]*Dipartimento di Scienze della Terra, Università di Siena, I-53100 Siena, Italy*
[f]*Centro di GeoTecnologie CGT, I-52027 San Giovanni Valdarno, Italy*

Abstract

The deepest hole that has ever been dug is about 12 km deep. Geochemists analyze samples from the Earth's crust and from the top of the mantle. Seismology can reconstruct the density profile throughout all Earth, but not its composition. In this respect, our planet is mainly unexplored. Geo-neutrinos, the antineutrinos from the progenies of U, Th and ^{40}K decays in the Earth, bring to the surface information from the whole planet, concerning its content of natural radioactive elements. Their detection can shed light on the sources of the terrestrial heat flow, on the present composition, and on the origins of the Earth. Geo-neutrinos represent a new probe of our planet, which can be exploited as a consequence of two fundamental advances that occurred in the last few years: the development of extremely low background neutrino detectors and the progress on understanding neutrino propagation. We review the status and the prospects of the field.
© 2007 Elsevier B.V. All rights reserved.

Contents

* Corresponding author. Tel.: +39 070 675 4899; fax: +39 070 510212.
E-mail addresses: fiorenti@fe.infn.it (G. Fiorentini), marcello.lissia@ca.infn.it (M. Lissia), fabio.mantovani@unisi.it (F. Mantovani).

1. Introduction

The deepest hole that has ever been dug is about 12 km deep, a mere dent in planetary terms. Geochemists analyze samples from the Earth's crust and from the top of the mantle. Seismology can reconstruct the density profile throughout all Earth, but not its composition. In this respect, our planet is mainly unexplored.

Geo-neutrinos, antineutrinos from the progenies of U, Th, and K decays in the Earth, bring to Earth's surface information coming from the whole planet. Differently form other emissions of the planet (e.g., heat, noble gases), they are unique in that they can escape freely and instantaneously from Earth's interior.

Detection of geo-neutrinos is becoming practical as a consequence of two fundamental advances that occurred in the last few years: (a) development of extremely low background neutrino detectors and (b) progress on understanding

neutrino propagation. In fact, KamLAND has reported in 2005 (Araki et al., 2005a) evidence of a signal originating from geo-neutrinos, showing that the technique for geo-neutrino detection is now available.

Geo-neutrinos look thus a promising new probe for the study of global properties of Earth and one has to examine their potential. Let us enumerate a few items which, at least in principle, can be addressed by means of geo-neutrinos.[1]

What is the radiogenic contribution to terrestrial heat production? There are large uncertainties on Earth's energetics, both on the value of the heat flow (estimated between 30 and 45 TW) and on the separate contributions to Earth's energy supply (radiogenic, gravitational, chemical...). Estimates of radioactivity in the Earth's crust, based on observational data, account for at least some 8 TW. The canonical Bulk Silicate Earth (BSE) model provides about 20 TW of radiogenic heat. However, on the grounds of available geochemical and/or geophysical data, one cannot exclude that radioactivity in the present Earth is enough to account for even the highest estimate of terrestrial heat flow.

An unambiguous and observationally based determination of the radiogenic heat production would provide an important contribution for understanding Earth's energetics. It requires determining how much uranium, thorium and potassium are inside the Earth, quantities which are strictly related to the anti-neutrino luminosities from these elements.

Test of the bulk silicate Earth model. The BSE model presents a chemical composition of the Earth similar to that of CI chondritic meteorites see, e.g. (McDonough, 2003; Palme and O'Neill, 2003). The consistency between their composition and that of the solar photosphere points towards considering CI representatives of the material available in the pre-solar nebula and the basic material from which our planet has been formed. Some authors, however, have argued for a genetic relationship of our planet with other chondrites, such as enstatite chondrites, which are richer in long lived radioactive elements (Javoy, 1995).

We remind that BSE is a basic geochemical paradigm consistent with most observational data, which however regard mostly the crust and an undetermined portion of the mantle. The global abundance of no element in the Earth can be estimated on the basis of observational data only. Geo-neutrinos could provide the first direct test of BSE (and/or its variants) by measuring the global abundances of natural heat radiogenic elements.

Heat generating elements in the crust: *a test of the estimated abundances.* The amount of radioactivity in the Earth's crust is reasonably well constrained by observational data, with the exception of the lowest portion. Most of the uncertainty on the amount of radioactivity in the crust arises from the different estimates about the lower crust. In this respect, a detector located well in the middle of a continent, being most sensitive to geo-neutrinos from the crust, might provide a significant check of the estimates on the crustal content of heat generating elements.

A measurement of heat generating elements in the mantle. The estimated content in the mantle is based on cosmochemical arguments and implies that abundances in deep layers have to be much larger than those measured in samples originating from the uppermost layer (Jochum et al., 1983; Zartman and Haines, 1988). Uncertainties on the heat generating elements content of the Earth essentially reflect the lack of observational data on the bulk of the mantle. A geo-neutrino detector located far from continents would be mainly sensitive to heat radiogenic elements in the whole mantle, as the oceanic crust is thin and poor in these elements.

What can be said about the core? Geochemical arguments are against the presence of radioactive elements in the core, although alternative hypothesis have been advanced see, e.g. (Herndon, 1996; Rama Murthy et al., 2003).

Present nondirectional detectors can say little about the core; however some extreme hypothesis can already be tested. If a natural fission reactor were present in the Earth's core, as advocated by Herndon in a series of paper (Hendron, 1998,2003; Herndon and Hollenbach, 2001), it would produce antineutrinos with a spectrum similar to that of man-made reactors. An excess of "reactor like" antineutrinos events could be detected. A detailed analysis already excludes a natural reactor producing more than about 20 TW (Dye et al., 2006; Fogli et al., 2005).

On the other hand, "non c'è rosa senza spine".[2] We list here the main difficulties and limitations encountered when detecting geo-neutrinos:

- First of all, even huge detectors cannot provide more than some hundreds of geo-neutrino events per year.
- Geo-neutrino events are to be disentangled from reactor neutrino events, which provide a severe background at many locations.

---

[1] Additional goals for geo-neutrinos (e.g., the distribution of radio-elements in the core, discrimination among models of mantle circulation, and the possibility of detecting plumes in the mantle (Fiorentini et al., 2005c)) appear presently too ambitious for the available technology.

[2] There is no such thing as a rose without a thorn.

- Some 80% of the geo-neutrino events are expected to arise from uranium decay chain and only 20% from thorium chain. Due to the low yield, it will be hard to extract information on thorium abundance from the difference in the spectra.
- Geo-neutrinos from K cannot be observed by means of inverse beta on free protons, the classical reaction for antineutrinos detection.
- Present detectors cannot provide directional information.

In the next section, we shall outline the main properties (sources, spectra and cross sections) of geo-neutrinos and in Section 3 we present how the field has evolved. Available information on the radioactivity content of the Earth is summarized in Section 4 and the debated issue of the sources and flow of terrestrial heat is examined in Section 5. Section 6 presents a reference model for geo-neutrino production, i.e. a calculation of geo-neutrino fluxes based upon the best available information on Earth's interior. This model is refined in Section 7 for a specific location (the Kamioka mine, Japan) with a detailed calculation of the flux generated in the region. Section 8 provides a strategy for determining Earth's radioactivity from geo-neutrino measurements. This approach is developed in detail for KamLAND, the results of this experiment being presented and interpreted in Section 9. The role of reactor neutrinos, which are generally a significant background for geo-neutrino detection, is discussed in Section 10. The prospects of the field are summarized in the final section.

As a rule, when a section is divided into subsections, the first one contains an overview of the main points, so that the reader can decide whether the more detailed information presented in the foregoing subsections is of interest to him/her.

2. Geo-neutrino properties

2.1. Overview

The natural radioactivity of present Earth arises mainly from the decay (chains) of nuclear isotopes with half-lives comparable to or longer than Earth's age[3]: ^{238}U, ^{232}Th, ^{40}K, ^{235}U, and ^{87}Rb.

Properties[4] of these isotopes and of the (anti)neutrinos produced from their decay (chains) are summarized in Table 1. Actually neutrinos are produced only in electron capture of ^{40}K. In contrast to the Sun, Earth shines essentially in antineutrinos.

The energy of ^{87}Rb neutrinos is so low that it is very unlikely that its flux could be measured. Also heat production from ^{87}Rb is at the level of 1% of the total.[5] For these reasons, from now on we shall consider only U, Th, and ^{40}K and refer to these three elements as the heat generating elements (HGEs) and to the antineutrinos from their decay (chains) as geo-neutrinos.

For each isotope there is a strict connection between the geo-neutrino luminosity L (anti-neutrinos produced in the Earth per unit time), the radiogenic heat production rate H_R and the mass m of that isotope in the Earth:

$$L = 7.46 \times m(^{238}\text{U}) + 31.94 \times m(^{235}\text{U}) + 1.62 \times m(^{232}\text{Th}) + 23.16 \times m(^{40}\text{K}), \tag{1}$$

$$H_R = 9.52 \times m(^{238}\text{U}) + 55.53 \times m(^{235}\text{U}) + 2.67 \times m(^{232}\text{Th}) + 2.85 \times m(^{40}\text{K}), \tag{2}$$

where units are 10^{24}s^{-1}, 10^{12} W and 10^{17} kg, respectively. By using the natural isotopic abundances in Table 1 these equations can be written in terms of the masses of the three elements[6]:

$$L = 7.64 \times m(\text{U}) + 1.62 \times m(\text{Th}) + 27.10 \times 10^{-4} \times m(\text{K}), \tag{3}$$

$$H_R = 9.85 \times m(\text{U}) + 2.67 \times m(\text{Th}) + 3.33 \times 10^{-4} \times m(\text{K}). \tag{4}$$

---

[3] Isotopes in the list have abundances and decay rates sufficiently large to give contributions of order 1% or more to the estimated radiogenic heat production: other radioactive elements such as ^{176}Lu, ^{147}Sm, ^{187}Rn, give contributions of order 10^{-4} or less.

[4] In the Table and in the rest of the paper, unless differently specified, nuclear data are taken from (Firestone and Shirley, 1996).

[5] This estimate is obtained assuming an abundance of ^{87}Rb about 50 times the one of uranium.

[6] The coefficients are slightly different from those quoted in Fiorentini et al. (2003b, 2005b), which did not include ^{235}U contribution.

Table 1
Properties of ^{238}U, ^{232}Th, ^{40}K, ^{235}U, and ^{87}Rb and of their (anti)neutrinos

Decay	Natural isotopic abundance	$T_{1/2}$ $(10^9\,\mathrm{yr})$	$E_{\max}$ (MeV)	Q (MeV)	Q_{eff} (MeV)	$\varepsilon_{\bar{\nu}}$ $(\mathrm{kg}^{-1}\,\mathrm{s}^{-1})$	ε_H $(\mathrm{W\,kg}^{-1})$	$\varepsilon'_{\bar{\nu}}$ $(\mathrm{kg}^{-1}\,\mathrm{s}^{-1})$	ε'_H $(\mathrm{W\,kg}^{-1})$
$^{238}\mathrm{U}\rightarrow{}^{206}\mathrm{Pb}+8{}^4\mathrm{He}+6e+6\bar{\nu}$	0.9927	4.47	3.26	51.7	47.7	7.46×10^7	0.95×10^{-4}	7.41×10^7	0.94×10^{-4}
$^{232}\mathrm{Th}\rightarrow{}^{208}\mathrm{Pb}+6\ {}^4\mathrm{He}+4e+4\bar{\nu}$	1.0000	14.0	2.25	42.7	40.4	1.62×10^7	0.27×10^{-4}	1.62×10^7	0.27×10^{-4}
$^{40}\mathrm{K}\rightarrow{}^{40}\mathrm{Ca}+e+\bar{\nu}$ (89%)	1.17×10^{-4}	1.28	1.311	1.311	0.590	2.32×10^8	0.22×10^{-4}	2.71×10^4	2.55×10^{-9}
$^{40}\mathrm{K}+e\rightarrow{}^{40}\mathrm{Ar}+\nu$ (11%)	1.17×10^{-4}	1.28	0.044	1.505	1.461	$=$	0.65×10^{-5}	$=$	0.78×10^{-9}
$^{235}\mathrm{U}\rightarrow{}^{207}\mathrm{Pb}+7\ {}^4\mathrm{He}+4e+4\bar{\nu}$	0.0072	0.704	1.23	46.4	44	3.19×10^8	0.56×10^{-3}	2.30×10^6	0.40×10^{-5}
$^{87}\mathrm{Rb}\rightarrow{}^{87}\mathrm{Sr}+e+\bar{\nu}$	0.2783	47.5	0.283	0.283	0.122	3.20×10^6	0.61×10^{-7}	8.91×10^5	0.17×10^{-7}

For each parent nucleus the table presents the natural isotopic mass abundance, half-life, antineutrino maximal energy (or neutrino energy), Q value, $Q_{\mathrm{eff}} = Q - \langle E_{(\nu,\bar{\nu})}\rangle$, antineutrino and heat production rates for unit mass of the isotope ($\varepsilon_{\bar{\nu}}$, ε_H), and for unit mass at natural isotopic composition ($\varepsilon'_{\bar{\nu}}$, ε'_H). Note that antineutrinos with energy above threshold for inverse beta decay on free proton ($E_{\mathrm{th}} = 1.806\,\mathrm{MeV}$) are produced only in the firsts two decay chains.
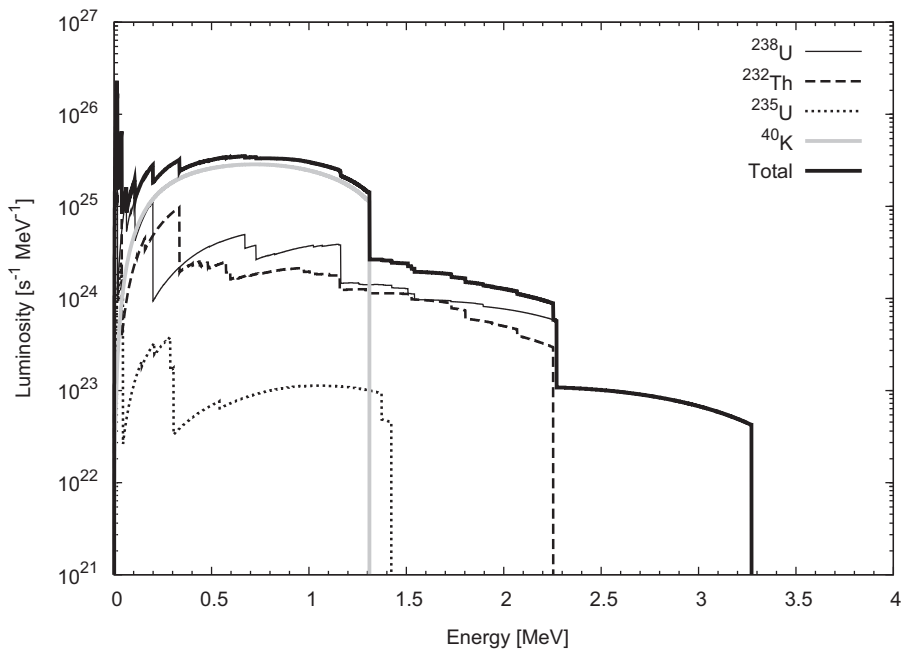

Fig. 1. Differential geo-neutrino luminosity, from Enomoto (2005). Data are from Enomoto's web page: http://www.awa.tohoku.ac.jp/~sanshiro/geoneutrino/spectrum/index.html. One assumes the following global abundances: $a(^{238}\mathrm{U}) = 15$ ppb, $a(^{235}\mathrm{U}) = 0.1$ ppb, $a(^{232}\mathrm{Th}) = 55$ ppb, $a(^{40}\mathrm{K}) = 160$ ppm (McDonough, 1999).

The geo-neutrino spectrum depends on the shapes and rates of the individual decays, and on the abundances and spatial distribution of the terrestrial elements. It is shown in Fig. 1 for a specific model.

The complete geo-neutrino spectrum depends on a large number of beta transitions in the uranium and thorium decay chains and it is essentially a result of theoretical calculations. These should be checked by measurements of the corresponding beta spectra, at least for the most important decays which contribute to the geo-neutrino signal: those of ^{214}Bi and ^{234}Pa$_m$ in the uranium chain, ^{212}Bi and ^{228}Ac in the thorium chain.

Geo-neutrinos originating from different elements can be distinguished—at least in principle—due to their different energy spectra, e.g., geo-neutrinos with $E > 2.25$ MeV are produced only in the uranium chain.

Geo-neutrinos from ^{238}U and ^{232}Th (not those from ^{235}U and ^{40}K) are above threshold for the classical anti-neutrino detection reaction, the inverse beta on free protons:

$$\bar{\nu}_e + p \rightarrow e^+ + n - 1.806\,\mathrm{MeV}. \tag{5}$$

Note that anti-neutrinos from the Earth are not obscured by solar neutrinos, which cannot yield reaction (5). On the other hand, antineutrinos from nuclear power plants are a significant source of background, as first observed in Lagage (1985) and discussed in more detail in Section 10.

An order of magnitude estimate of the geo-neutrino luminosity can be obtained by assuming that a large fraction of the heat released from Earth, $H \approx 40$ TW, arises from the decay chains of uranium and thorium. Table 1 shows that each of the N geo-neutrinos from each chain is associated with energy release $\Delta E \approx Q/N \approx 10$ MeV, so that:

$$L(\text{U+Th}) \approx H/\Delta E \approx 2.5 \times 10^{25}\,\text{s}^{-1}. \tag{6}$$

The order of magnitude of the produced flux is $\Phi^{(\text{pro})}(\text{U+Th}) \approx L/(4\pi R_{\oplus}^2)$, where $R_{\oplus}$ is the Earth's radius. The flux arriving at detectors will be smaller than that produced due to neutrino oscillations, $\Phi^{(\text{arr})}(\text{U+Th}) = \langle P_{ee} \rangle \Phi^{(\text{pro})}(\text{U+Th})$, where $\langle P_{ee} \rangle \approx 0.6$ is the average survival probability. All this gives:

$$\Phi^{(\text{arr})}(\text{U+Th}) \approx 2 \times 10^6\,\text{cm}^{-2}\text{s}^{-1}. \tag{7}$$

This is a flux comparable to that of solar neutrinos from ^{8}B decay (Castellani et al., 1997), however the detection of geo-neutrinos is a much more difficult task: their smaller energy implies that the signal is smaller and is in an energy region where background is larger.

For an order of magnitude estimate of the signal rate in a one-kton detector (containing some 10^{32} free protons), we observe that the cross section for inverse beta decay at few MeV is $\sigma \sim 10^{-43}$ cm^2 and the fraction of antineutrinos above threshold is $f \approx 0.05$. This gives a signal $S(\text{U+Th}) \approx \sigma f \Phi^{(\text{arr})}(\text{U+Th}) N_p \approx 30\,\text{yr}^{-1}$.

More precisely, the signal rates $S(\text{U})$ and $S(\text{Th})$ in a detector containing N_p free protons are

$$S(\text{U}) = 13 \times \frac{\Phi^{(\text{arr})}(\text{U})}{10^6\,\text{cm}^{-2}\,\text{s}^{-1}} \times \frac{N_p}{10^{32}}\,\text{yr}^{-1}, \tag{8}$$

$$S(\text{Th}) = 4.0 \times \frac{\Phi^{(\text{arr})}(\text{Th})}{10^6\,\text{cm}^{-2}\text{s}^{-1}} \times \frac{N_p}{10^{32}}\,\text{yr}^{-1}, \tag{9}$$

where $\Phi^{(\text{arr})}(\text{U})$ and $\Phi^{(\text{arr})}(\text{Th})$ are the fluxes of antineutrinos from ^{238}U and Th arriving at the detector.

Events rates are conveniently expressed in terms of a Terrestrial Neutrino Unit (TNU), defined as one event per 10^{32} target nuclei per year, or 3.17×10^{-40} s^{-1} per target nucleus. This unit, which is analogous to the solar neutrino unit (SNU) (Bahcall, 1989), is practical since one kton of liquid scintillator contains about 10^{32} free protons (the precise value depending on the chemical composition) and the exposure times are of order of a few years.

Concerning the relative contributions of thorium and uranium to geo-neutrino events, Eqs.(8) and (9) together with Eq. (1) give

$$\frac{S(\text{Th})}{S(\text{U})} = 0.32 \times \frac{\Phi^{(\text{arr})}(^{232}\text{Th})}{\Phi^{(\text{arr})}(^{238}\text{U})} \approx 0.32 \times \frac{L(^{232}\text{Th})}{L(^{238}\text{U})} \approx \frac{1}{16} \times \frac{m(^{232}\text{Th})}{m(^{238}\text{U})}. \tag{10}$$

Since one estimates that in our planet $m(\text{Th})/m(\text{U}) \approx 4$, one expects $S(\text{Th})/S(\text{U}) \approx 1/4$. Note that, although the global thorium mass is four times than that of uranium, it contributes just 1/5 of the total signal $S(\text{U+Th})$.

2.2. Decay chains and geo-neutrino spectra from uranium and thorium

One needs antineutrino spectra for two main reasons: the calculation of the specific elemental heat production and of the signal in the detector.

Heat production rate is calculated by subtracting from the Q value the energy $\langle E \rangle$ of antineutrinos averaged over the whole spectrum. In the case of ^{238}U and ^{232}Th chains[7] the average antineutrino energy is about 8% and 6% of the total available energy: an error of 10% on the calculation of $\langle E \rangle$ is sufficient to determine the elemental heat production to better the 1%. For this reason in the literature individual determinations of beta spectra have not been used to determine neutrino energy loss. Instead, the approximate relationship that, on average, neutrinos carry 2/3 of the decay energy for beta decay has been applied (van Schmus, 1995). This approximation can be checked or improved if the complete spectrum is known.

---

[7] Concerning ^{235}U, its contribution to the heat production is just a few per cent, so that the energy subtracted by antineutrinos is not relevant.

For calculating the signal in a detector we need to integrate the spectrum times the cross section: only the spectrum above the detection threshold is needed for this aim.

On these grounds we shall concentrate on the antineutrino energy spectra from ^{238}U and ^{232}Th decay chains. In general, the chain involves many different β decays and the total antineutrino spectrum results from the sum of the individual spectra.

For each decay chain, if the sample of material contains n_i nuclei of type i, the number of alpha and beta decays $i \to j$ per unit time is

$$r_{i,j} = n_i \lambda_i b_{i,j}, \tag{11}$$

where λ_i, is the inverse of the mean-life and $b_{i,j}$ is the branching ratio, $\sum_j b_{i,j} = 1$. The probability of each decay in the chain is

$$R_{i,j} = \frac{n_i \lambda_i b_{i,j}}{\sum_j r_{h,j}}, \tag{12}$$

where h indicates the decay-chain head. The $R_{i,j}$ form a network, with an isotope at each node. Generally the network has the following properties:

- $\frac{R_{i,j}}{R_{i,k}} = \frac{b_{i,j}}{b_{i,k}}$ (by definition),
- $\sum_j R_{h,j} = 1$ (normalization);

assuming that the chain is in secular equilibrium, one has

- $\sum_k R_{k,i} = \sum_j R_{i,j}$, at each node i (equilibrium).

These three conditions fully determine the network.[8]

In general the beta decay $i \to j$ involves transitions to different nuclear states which yield spectra with different endpoints: we call $I_{i,j;k}$ the percentage intensity of the kth beta transition[9] and $f_{i,j;k}(E)$ the corresponding antineutrino energy spectrum normalized to 1 (see below).

Then the antineutrino spectrum generated from the sample is

$$f(E) = \sum_{ij} R_{i,j} \sum_k I_{i,j;k} f_{i,j;k}(E). \tag{13}$$

Lifetimes $1/\lambda_i$, branching ratios $b_{i,j}$ and intensities $I_{i,j;k}$, can be found in Firestone and Shirley (1996).

A somehow delicate point is the expression to be used for the antineutrino spectra $f_{i,j;k}(E)$ of the β decay of nucleus i to the nucleus j into the state k. It can be derived from that for electron energy spectrum $\phi_{i,j;k}(W)$ by using energy conservation

$$f_{i,j;k}(E) = \phi_{i,j;k}(W)|_{W=W_{\max}-E}, \tag{14}$$

where W is the total electron energy and $W_{\max} = m_e c^2 + E_{\max}$ with $E_{\max}$ being the maximal neutrino energy for the transition and m_e the electron mass.

For allowed decays the electron energy spectrum has the well-known universal shape:

$$\phi_{i,j;k}(W) = \frac{1}{N} W (W_{\max} - W)^2 (W^2 - m_e^2 c^4)^{\gamma - 1/2} e^{\pi y} |\Gamma(\gamma + iy)|^2, \tag{15}$$

where

$$\gamma = \sqrt{1 - (\alpha Z)^2}, \quad y = \alpha Z \frac{W}{\sqrt{W^2 - m_e^2 c^4}}, \tag{16}$$

---

[8] It can be seen as a circuit where $R_{i,j}$ are the currents and $b_{i,j}$ the inverse of the resistance, and where it flows a unit of current.

[9] Our notation corresponds to the normalization $\sum_k I_{i,j;k} = 1$. A different normalization, $\sum_k I_{i,j;k} = b_{i,j}$ is used in Firestone and Shirley (1996).

with Z denoting the nuclear charge of the daughter nucleus and α the fine structure constant. N is a normalization constant such that

$$\int_{m_e c^2}^{W_{\max}} dW \, \phi_{i,j;k}(W) = 1. \tag{17}$$

Eq. (15) is generally used to estimate geo-neutrino spectra and this requires a few comments.

(1) Eq. (15) considers the effect of the bare Coulomb field through the relativistic Fermi function. Electron screening and finite nuclear size effects are not considered. These provide corrections to the spectrum shape of order of few per cent, a quantity which is not significant in comparison with the uncertainties mentioned below.

(2) All important contributions actually arise from (first) parity forbidden decays. In this case the spectrum does not need to have a universal shape, since it involves also momentum-dependent nuclear matrix elements. However experimental data show that many forbidden decays of high-Z nuclei have spectra *close* to the allowed one: the theoretical explanation is that these decays are dominated by momentum-independent matrix elements or matrix elements whose relevant momentum is the electron momentum near the nucleus $pR \approx Z\alpha$, which is weakly dependent on the emerging momentum (ξ approximation). This provides a partial justification for using Eq. (15). The resemblance with the allowed spectrum depends on the nucleus and it is difficult to study at low electron energy; in few cases one finds significant differences[10], e.g., ^{210}Bi (for an experimental review see, e.g., Daniel (1968).

(3) Measurements of electron spectra would be very useful—in particular at low energy—in order to check the predictions for geo-neutrino spectra, which are mostly theoretical. In this respect an experimental study of the beta decay of ^{214}Bi would be most significant.

Regarding the intensities $I_{i,j;k}$, the experimental errors on some of them should be reduced: at the moment they imply a few percent uncertainty on the total geo-neutrino signal (see Tables 3 and 5 and relative comments).

2.2.1. The ^{238}U decay chain

^{238}U decays into ^{206}Pb through a chain of eight α decays and six β decays.[11] In secular equilibrium the complete network (see Fig. 2) includes nine β-decaying nuclei[12] summarized in Table 2.

Only three nuclides (^{234}Pa, ^{214}Bi, ^{210}Tl) yield antineutrinos with energy larger than 1.806 MeV and contribute to the geo-neutrino signal. The contribution from ^{210}Tl is negligible, due to its small occurrence probability and the uranium contribution to the geo-neutrino signal comes from five β decays: one from ^{234}Pa and four from ^{214}Bi (see Table 3 and Fig. 3). In fact, 98% of the uranium signal arises from the first two transitions in Table 3 and an accuracy better than 1% is achieved by adding the third one.

In the last column of Table 3 we show the contribution of each decay to the total (U+Th) geo-neutrino signal: this is calculated using a ratio of Th to U signal $S_{\mathrm{Th}}/S_{\mathrm{U}} = 0.270$, that comes from the ratio between the average cross sections $\langle\sigma\rangle_{^{232}\mathrm{Th}}/\langle\sigma\rangle_{^{238}\mathrm{U}} = 0.127/0.404 = 0.314$ (see Section 2.4) and an assumed chondritic ratio[13] for the masses $m(\mathrm{Th})/m(\mathrm{U}) = 3.9$. Present errors on the intensities of the second and third decay of Table 3 imply corresponding errors to the total signal of 1.5% and 0.5%, respectively.

2.2.2. The ^{232}Th decay chain

^{232}Th decays into ^{208}Pb through a chain of six α decays and four β decays. In secular equilibrium the complete network (see Fig. 4) includes five β-decaying nuclei[14] summarized in Table 4.

---

[10] Spectra of high-Z nuclei, that do not follow the allowed spectra, are explained theoretically by cancelations of dominant terms: a detailed knowledge of the relative weights and signs of the nuclear matrix elements becomes necessary.

[11] If we call N_α the number of α decays and N_β the number of β decays, A and Z (A' and Z') the atomic number and charge of the initial (final) nucleus, then $N_\alpha = (A - A')/4$ and $N_\beta = Z' - Z + (A - A')/2$.

[12] This accounts for all branches with probability $> 10^{-5}$.

[13] The corresponding ratio of fluxes is $\Phi_{\mathrm{Th}}/\Phi_{\mathrm{U}} = (4/6) \times (m(\mathrm{Th})/m(\mathrm{U})) \times (238/232) \times (\tau_{\mathrm{U}}/\tau_{\mathrm{Th}}) \times (1/0.9927) = 0.8579$.

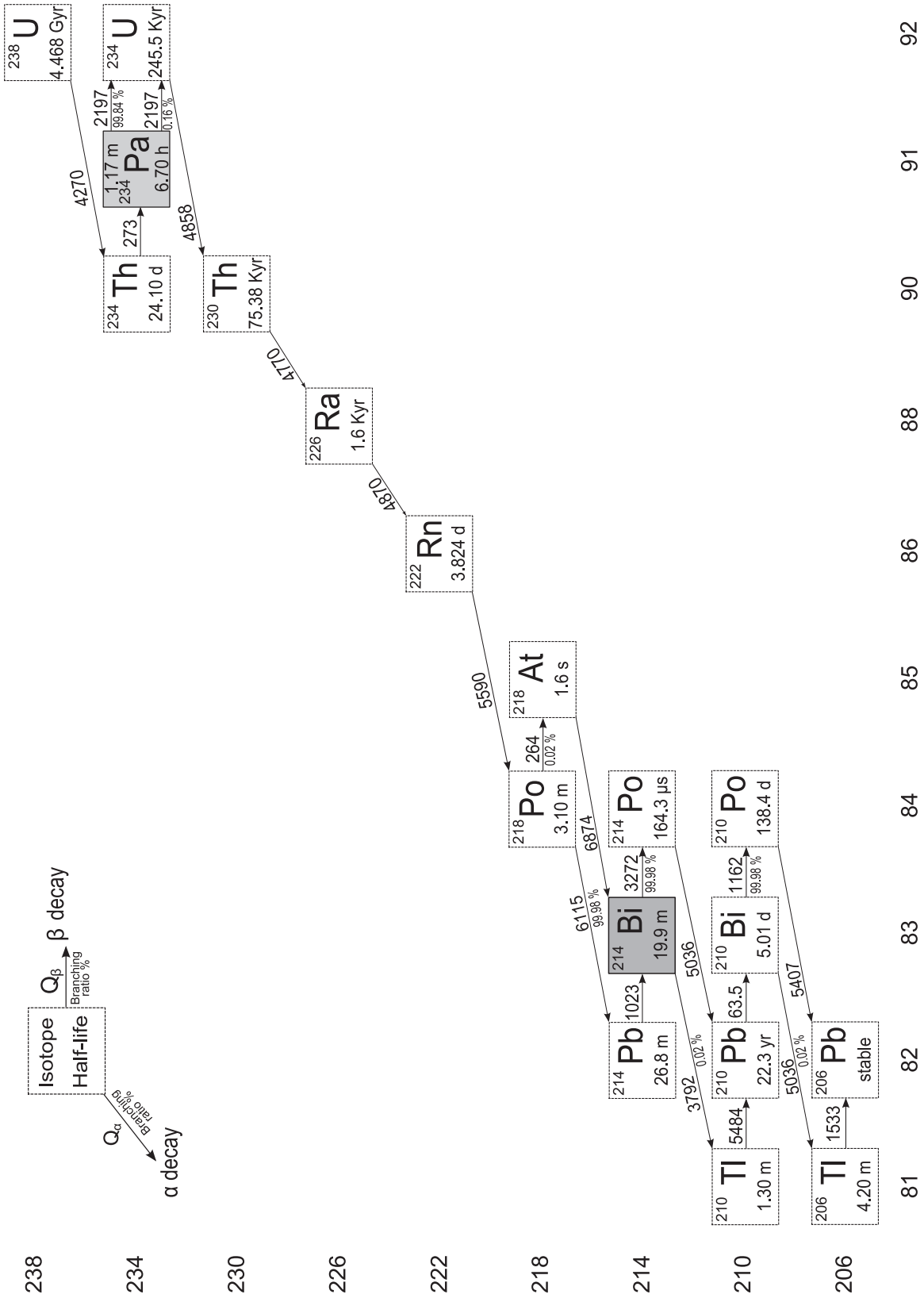[14] This accounts for all the branches with probability $> 10^{-5}$.

Fig. 2. The ^{238}U decay chain. The two nuclides inside the grey boxes (^{234}Pa and ^{214}Bi) are the main sources of geo-neutrinos.

Table 2
Beta decays in the ^{238}U chain

$i \to j$	$R_{i,j}$	$E_{\max}$ (keV)	Effective transitions
^{234}Th$\to ^{234}$Pa	1.0000	199.08	0
^{234}Pa$_m \to ^{234}$U	0.9984	2268.92	1
^{214}Pb$\to ^{214}$Bi	0.9998	1024	0
^{214}Bi$\to ^{214}$Po	0.9998	3272	4
^{210}Pb$\to ^{210}$Bi	1.0000	63.5	0
^{210}Bi$\to ^{210}$Po	0.9999	1162.1	0
^{234}Pa$\to ^{234}$U	0.0016	1247.15	0
^{218}Po$\to ^{218}$At	0.0002	< 265	0
^{206}Tl$\to ^{206}$Pb	0.0001	1533.5	0
^{210}Tl$\to ^{210}$Pb	0.0002	4391.3	5

For each decay we present the probability, the maximal antineutrino energy and the number of effective transitions, defined as those producing antineutrinos with $E > 1806$ keV.

Table 3
Effective transitions in the ^{238}U chain

$i \to j$	$R_{i,j}$	$E_{\max}$ (keV)	I_k	ΔI_k	Type (%)	S_{U} (%)	S_{tot}
^{234}Pa$_m \to ^{234}$U	0.9984	2268.92	0.9836	0.002	1st forbidden $(0^-) \to 0^+$	39.62	31.21
^{214}Bi$\to ^{214}$Po	0.9998	3272.00	0.182	0.006	1st forbidden $1^- \to 0^+$	58.21	45.84
		2662.68	0.017	0.006	1st forbidden $1^- \to 2^+$	1.98	1.55
		1894.32	0.0743	0.0011	1st forbidden $1^- \to 2^+$	0.18	0.14
		1856.51	0.0081	0.0007	1st forbidden $1^- \to 0^+$	0.01	0.01

In addition to quantities defined in Table 2 we present the intensity I_k, its error ΔI_k, type and percentage contributions to the uranium geo-neutrino signal, and to the (U + Th) geo-neutrino signal. For this last column we assume the chondritic ratio for the masses (Th/U = 3.9), which implies that 79% of the geo-neutrino signal comes from uranium.

Only two nuclides (^{228}Ac and ^{212}Bi) yield antineutrinos with energy larger than 1.806 MeV. The thorium contribution to the geo-neutrino signal comes from three β decays: one from ^{212}Bi and two from ^{228}Ac (see Table 5 and Fig. 5). In fact, 99.8% of the signal arises from the first two transitions in Table 5. The present error on the intensity of the second decay of Table 5 implies a corresponding error to the total signal of 0.9%.

2.3. Geo-neutrinos from ^{40}K

^{40}K undergoes branching decay to ^{40}Ca (via β decay) and ^{40}Ar (via electron capture), both of which are stable: the simplified decay scheme of ^{40}K is shown in Fig. 6. The half life is 1.277×10^9 yr, with a 10.7% probability of decaying to ^{40}Ar and an 89.3% probability of decaying to ^{40}Ca. All decays to ^{40}Ca proceed directly to the ground state, but most of the decays to ^{40}Ar reach an excited state, see Table 6.

Kelley et al. (1959) determined the spectrum of β particles emitted in the decay to ^{40}Ca (Fig. 7). From these data van Schmus (1995) obtained a mean β energy of 0.598 MeV, or about 45% of the total; the remainder, 0.722 MeV (55%), is carried away by the antineutrino.[15]

We remind that the antineutrinos from ^{40}K ($E_{\max} = 1.311$ MeV) are below the threshold for inverse beta on free protons. Note also that the monochromatic neutrinos from ^{40}K have a very small energy (44 keV).

---

[15] We checked that by using Eq. (15) times the non-relativistic correction factor appropriate for a 3rd forbidden decay, $S(p_e, p_\nu) \sim p_{\bar{\nu}}^6 + p_e^6 + 7p_{\bar{\nu}}^2 p_e^2 (p_{\bar{\nu}}^2 + p_e^2)$, one finds the same average energy as Van Schmus. Note that the value of the maximal energy used by Van Schmus, $W_{\max} = 1.32$, should be replaced with the more resent value: $W_{\max} = 1.31109$. In this case the average β energy becomes 0.588 MeV.
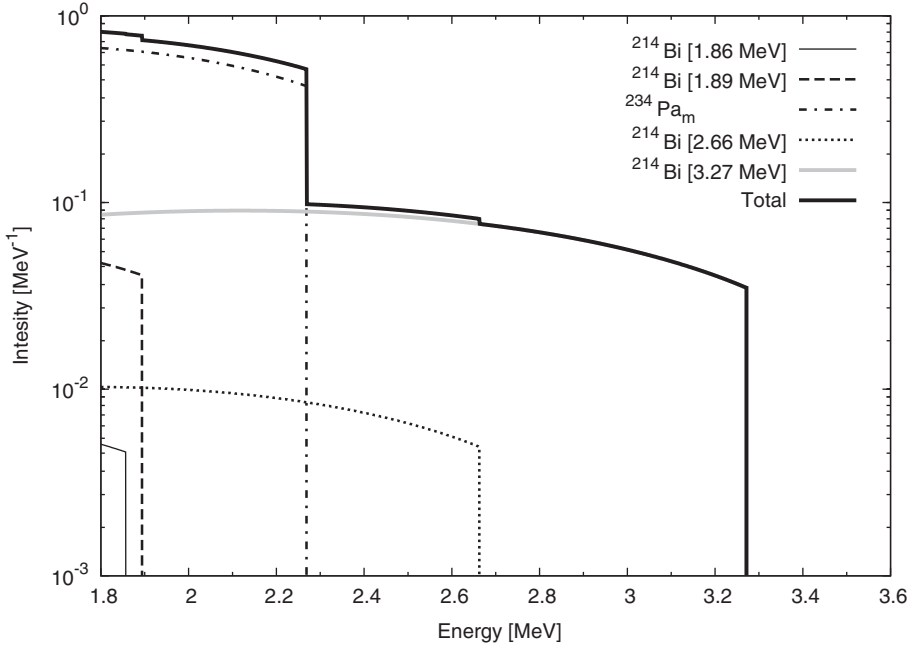
Fig. 3. Geo-neutrino spectra from the five main β decays of the ^{238}U chain. All spectra are normalized to one decay of the head element of the chain. Since the ^{238}U chain contains six β decays, the integral from zero to the end point of the total spectrum is 6. Note that only 0.38 neutrinos per chain are above thresholds.

2.4. From cross sections to event rates

As already mentioned, the classical process for detection of low energy antineutrinos is the inverse beta decay on free protons

$$\bar{\nu}_e + p \rightarrow e^+ + n. \tag{18}$$

The threshold of the reaction is

$$E_\nu^{\text{thr}} = \frac{(M_n + m_e)^2 - M_p^2}{2M_p} c^2 = 1.806 \,\text{MeV}. \tag{19}$$

The total cross section, neglecting terms of order E_e/M_p, is given by the standard formula

$$\sigma = 0.0952 \times \left(\frac{E_e p_e c}{\text{MeV}^2} \right) \times 10^{-42} \,\text{cm}^2, \tag{20}$$

where $E_e = E_{\bar{\nu}} - (M_n - M_p)c^2$ is the positron energy, when the (small) neutron recoil is neglected, and p_e is the corresponding momentum. The numerical factor in Eq. (20) is tied directly, see (Bemporad et al., 2002), to the neutron lifetime, known to 0.1% (Yao and et al., 2006). This expression of the total cross section is shown in Fig. 8.

Corrections to the cross section of order E_e/M_p, which are negligible for geo-neutrinos whereas should be considered at reactor energies, and the angular distribution of the positrons are described by Vogel and Beacom (1999); see also Bemporad et al. (2002).

A more general discussion of the neutrino/nucleon cross section for energies from threshold up to several hundred MeV can be found in Strumia and Vissani (2003); in the same paper Strumia and Vissani give a simple approximation which agrees with their full result within few per-mille for $E_\nu \lesssim 300$ MeV,

$$\sigma(\bar{\nu}_e p) \approx 10^{-43} \,[\text{cm}^2] p_e E_e E_\nu^{-0.07056 + 0.02018 \ln E_\nu - 0.001953 \ln^3 E_\nu}, \quad E_e = E_\nu - \Delta, \tag{21}$$
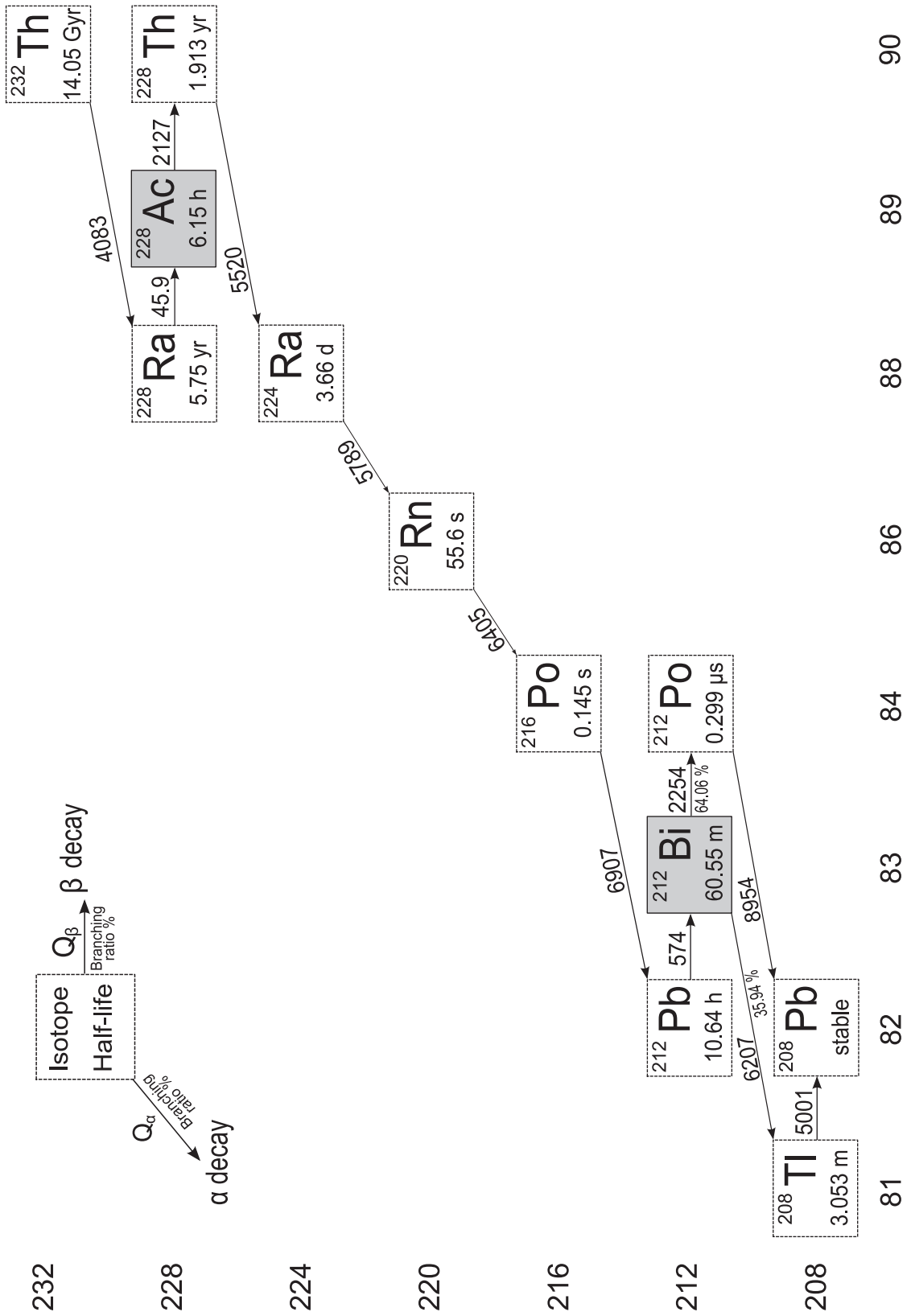
Fig. 4. The ^{232}Th decay chain. The two nuclides inside the grey boxes (^{228}Ac and ^{212}Bi) are the main sources of geo-neutrinos.

Table 4
Beta decays in the ^{232}Th chain. For each decay we present the probability, the maximal antineutrino energy and the number of effective transitions, defined as those producing antineutrinos with $E > 1806$ keV

$i \rightarrow j$	$R_{i,j}$	E_{max} (keV)	Effective transitions
^{228}Ra$\rightarrow$^{228}Ac	1.0000	39.62	0
^{228}Ac$\rightarrow$^{228}Th	1.0000	2069.24	2
^{212}Pb$\rightarrow$^{214}Bi	1.0000	573.8	0
^{212}Bi$\rightarrow$^{212}Po	0.6406	2254	1
^{208}Tl$\rightarrow$^{208}Pb	0.3594	1803.26	0

Table 5
Effective transitions in the ^{232}Th chain

$i \rightarrow j$	$R_{i,j}$	E_{max} (keV)	I_k	ΔI_k	Type (%)	S_{Th} (%)	S_{tot}
^{212}Bi$\rightarrow$^{212}Po	0.6406	2254	0.8658	0.0016	1st forbidden $1^{(-)} \rightarrow 0^+$	94.15	20.00
^{228}Ac$\rightarrow$^{228}Th	1.0000	2069.24	0.08	0.06	Allowed $3^+ \rightarrow 2^+$	5.66	1.21
		1940.18	0.008	0.006	Allowed $3^+ \rightarrow 4^+$	0.19	0.04

In addition to quantities defined in Table 4 we present the intensity I_k, its error ΔI_k, type and percentage contributions to the thorium geo-neutrino signal, and to the total (U + Th) geo-neutrino signal. For this last column we assume the chondritic ratio for the masses (Th/U = 3.9), which implies that 21% of the geo-neutrino signal comes from thorium.
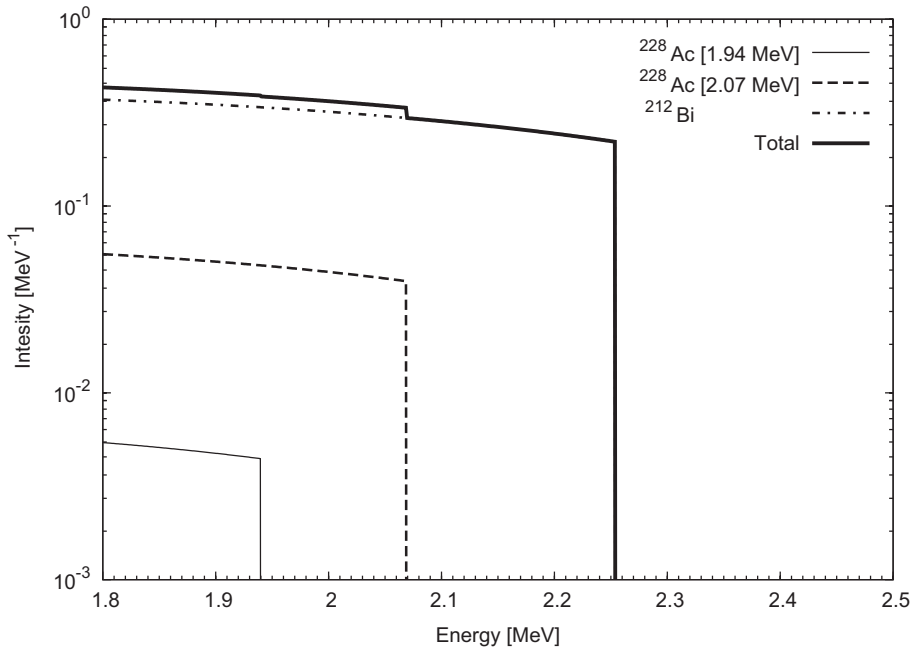

Fig. 5. Geo-neutrino spectra from the three main β decays of the ^{232}Th chain. All spectra are normalized to one decay of the head element of the chain. Since the ^{232}Th chain contains four β decays, the integral from zero to the end point of the total spectrum is 4. Note that only 0.15 neutrinos per chain are above thresholds.

where Δ is the neutron–proton mass difference and all energies are in MeV. They conservatively estimate an overall uncertainty of the cross section at low energy of 0.4%. At the energy relevant for geo-neutrinos ($\leqslant 3.27$ MeV) Eq. (20) overestimates the full result of Strumia and Vissani by less than 1% and it is already identical at about 2 MeV.
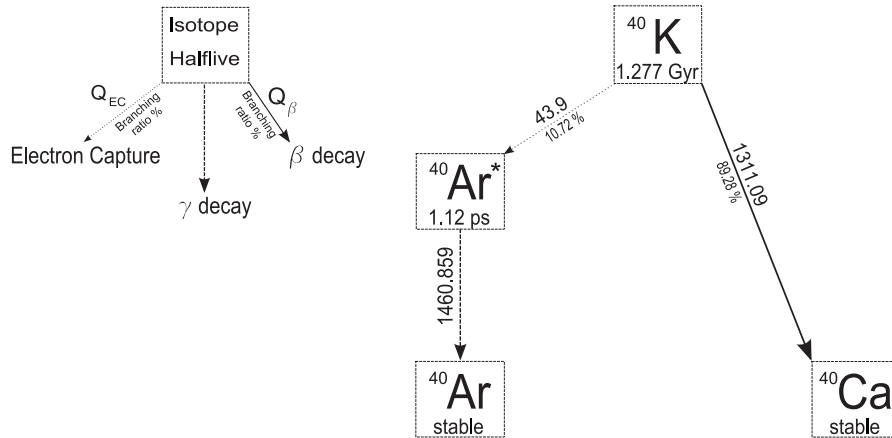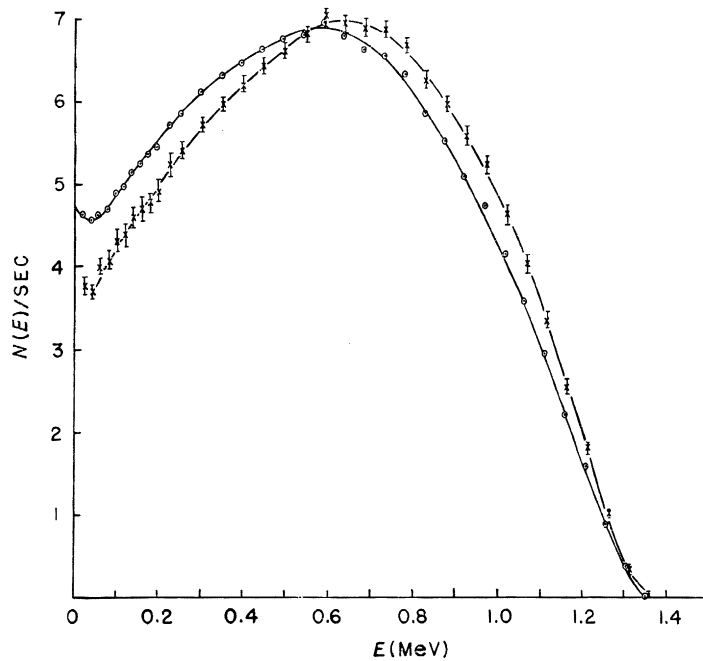
Fig. 6. Simplified decay scheme for ^{40}K.

Table 6
Decays of ^{40}K. For each decay we show the maximal antineutrino/neutrino energy, the intensity and the type of transition

$i \rightarrow j$	$E_{\max}$ (keV)	I_k	Type
$^{40}\text{K} \rightarrow {}^{40}\text{Ca} + e^- + \bar{\nu}$	1311.09	0.8928	3rd Forbidden $4^- \rightarrow 0^+$
$e^- + {}^{40}\text{K} \rightarrow {}^{40}\text{Ar}^* + \nu$	44.04	0.1067	1st Forbidden $4^- \rightarrow 2^+$
$e^- + {}^{40}\text{K} \rightarrow {}^{40}\text{Ar} + \nu$	1504.9	0.00047	3rd Forbidden $4^- \rightarrow 0^+$
$^{40}\text{K} \rightarrow {}^{40}\text{Ar} + e^+ + \nu$	482.9	0.00001	3rd Forbidden $4^- \rightarrow 0^+$

Fig. 7. Experimental spectrum of electron kinetic energy for the decay of ^{40}K into ^{40}Ca, from Kelley et al. (1959). The circles show the measured spectrum including background, 1.46 MeV gamma and finite resolution corrections. The x–s show the spectrum after the electron escape corrections. The flags represent total estimated error at each point, due to the uncertainty in the electron escape correction.
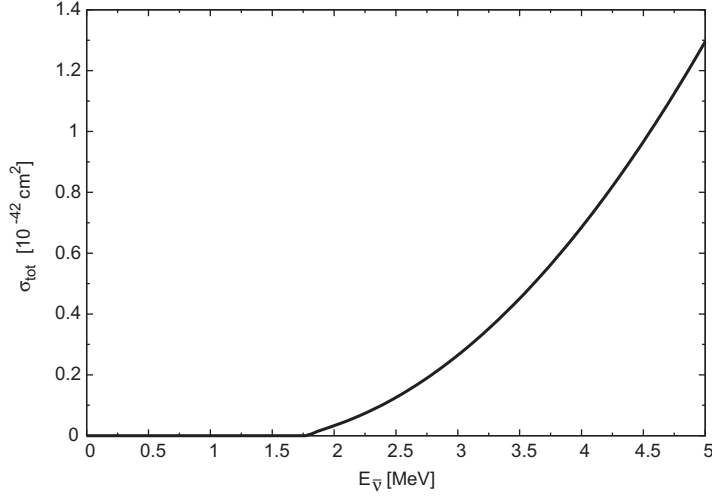
Fig. 8. Total cross section for $\bar{\nu}_e + p \rightarrow e^+ + n$ as a function of the antineutrino energy, Eq. (20).

The geo-neutrino event rate from the decay chain of element X $= {}^{238}$U or ^{232}Th is

$$S(X) = N_p \int dE_{\bar{\nu}} \varepsilon(E_{\bar{\nu}}) \sigma(E_{\bar{\nu}}) \phi_X^{(\text{arr})}(E_{\bar{\nu}}), \tag{22}$$

where N_p is the number of free protons in the target, ε is the detection efficiency, $\sigma(E_{\bar{\nu}})$ is the cross section for reaction (18), and:

$$\phi_X^{(\text{arr})}(E_{\bar{\nu}}) = \int_{V_\oplus} d\vec{r} \frac{\rho(\vec{r})}{4\pi|\vec{R} - \vec{r}|^2} \frac{a_X(r) C_X}{\tau_X m_X} f_X(E_{\bar{\nu}}) p(E_{\bar{\nu}}, |\vec{R} - \vec{r}|) \tag{23}$$

is the differential flux of antineutrinos from ^{238}U or ^{232}Th arriving into the detector, ρ is the density, a_X is the elemental mass abundance, C_X, τ_X, and m_X are the isotopic concentration, lifetime and mass of nucleus X. The energy distribution of antineutrinos $f_X(E_{\bar{\nu}})$ is normalized to the number of antineutrinos n_X emitted per decay chain:

$$n_X = \int dE_{\bar{\nu}} f_X(E_{\bar{\nu}}); \tag{24}$$

$p(E_{\bar{\nu}}, |\vec{R} - \vec{r}|)$ is the survival probability for $\bar{\nu}$ with energy $E_{\bar{\nu}}$ produced at $\vec{r}$ to reach the detector at $\vec{R}$.

In view of the values of the oscillation length one can average the survival probability over a short distance, see Mantovani et al. (2004), and bring out of the integral the averaged survival probability:

$$\langle P_{ee} \rangle = 1 - \frac{1}{2}\sin^2 2\theta = \frac{1 + \tan^4\theta}{(1 + \tan^2\theta)^2}. \tag{25}$$

In this way we are left with

$$S(X) = N_p \langle P_{ee} \rangle \int dE_{\bar{\nu}} \varepsilon(E_{\bar{\nu}}) \sigma(E_{\bar{\nu}}) f_X(E_{\bar{\nu}}) \int_{V_\oplus} d\vec{r} \frac{\rho(\vec{r})}{4\pi|\vec{R} - \vec{r}|^2} \frac{a_X(r) C_X}{\tau_X m_X}. \tag{26}$$

The second integral is proportional to the (angle integrated) produced flux of anti-neutrinos

$$\Phi(X) = \frac{n_X C_X}{4\pi \tau_X m_X} \int_{V_\oplus} d\vec{r} \frac{\rho(\vec{r}) a_X(r)}{|\vec{R} - \vec{r}|^2}. \tag{27}$$

Note that this quantity is different from the flux normal to earth surface. Note also that "produced" essentially means the flux which one would observe in the absence of oscillations.
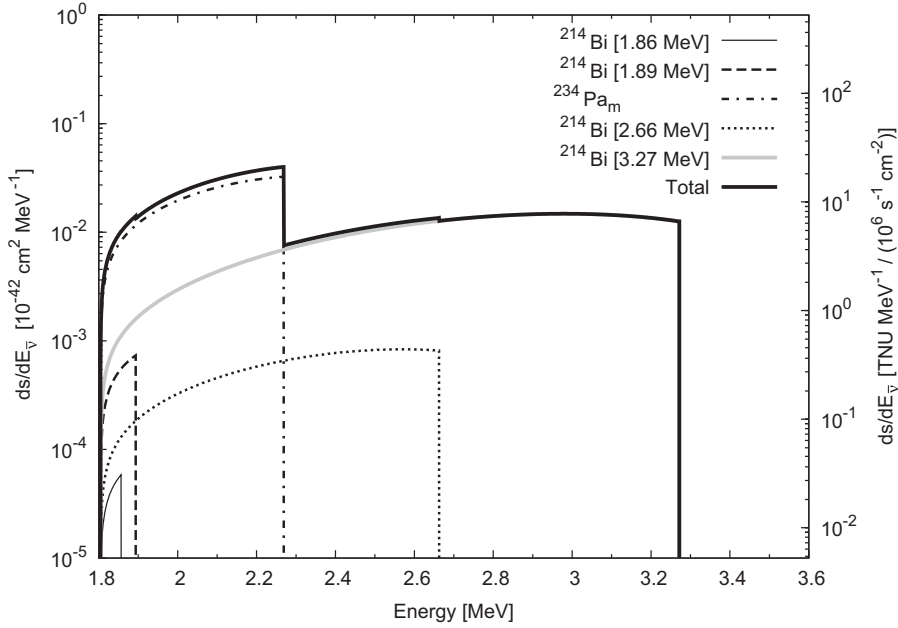
Fig. 9. Geo-neutrino differential signal per unit flux from the five main β decays of the ^{238}U chain, see Eq. (33).

One can also assume the detection efficiency as approximately constant over the small (< 2 MeV) energy integration region. Then Eq. (26) becomes

$$S(X) = N_p \langle P_{ee} \rangle \varepsilon \Phi(X) \int dE_{\bar{v}} \frac{\sigma(E_{\bar{v}}) f_X(E_{\bar{v}})}{n_X}. \tag{28}$$

It can be useful to introduce an average cross section:

$$\langle \sigma \rangle_X = \int dE_{\bar{v}} \sigma(E_{\bar{v}}) f_X(E_{\bar{v}}) \bigg/ \int dE_{\bar{v}} f_X(E_{\bar{v}}). \tag{29}$$

This is computed by using Eq. (20) for the cross section $\sigma(E_{\bar{v}})$ and the spectrum $f_X(E_{\bar{v}})$ obtained in the previous section. Thus one finds $\langle \sigma \rangle_{238_U} = 0.404 \times 10^{-44} \text{cm}^2$ and $\langle \sigma \rangle_{232_{Th}} = 0.127 \times 10^{-44} \text{cm}^2$.

The event number can thus be written as the product of a few terms:

$$S(X) = N_p \langle P_{ee} \rangle \varepsilon \Phi(X) \langle \sigma \rangle_X. \tag{30}$$

The result is

$$S(^{238}U) = 4.04 \times 10^{-7} \, \text{s}^{-1} \times \langle P_{ee} \rangle \varepsilon \left(\frac{N_p}{10^{32}} \right) \left(\frac{\Phi(^{238}U)}{10^6 \, \text{cm}^{-2} \, \text{s}^{-1}} \right), \tag{31}$$

$$S(^{232}Th) = 1.27 \times 10^{-7} \, \text{s}^{-1} \times \langle P_{ee} \rangle \varepsilon \left(\frac{N_p}{10^{32}} \right) \left(\frac{\Phi(^{232}Th)}{10^6 \, \text{cm}^{-2} \, \text{s}^{-1}} \right). \tag{32}$$

This is the way in which Eqs. (8) and (9) were derived. Our goal in the rest of the paper will be to provide calculations of the produced fluxes based on geological models.

It is interesting to examine the differential geo-neutrino signal per unit flux as a function of the energy:

$$\frac{ds_X}{dE_{\bar{v}}} = \sigma(E_{\bar{v}}) f_X(E_{\bar{v}}) \bigg/ \int dE_{\bar{v}} f_X(E_{\bar{v}}) . \tag{33}$$

This quantity is shown in Figs. 9 and 10 for uranium and thorium, respectively. Note that most of the geo-neutrino flux originates from very few transitions.
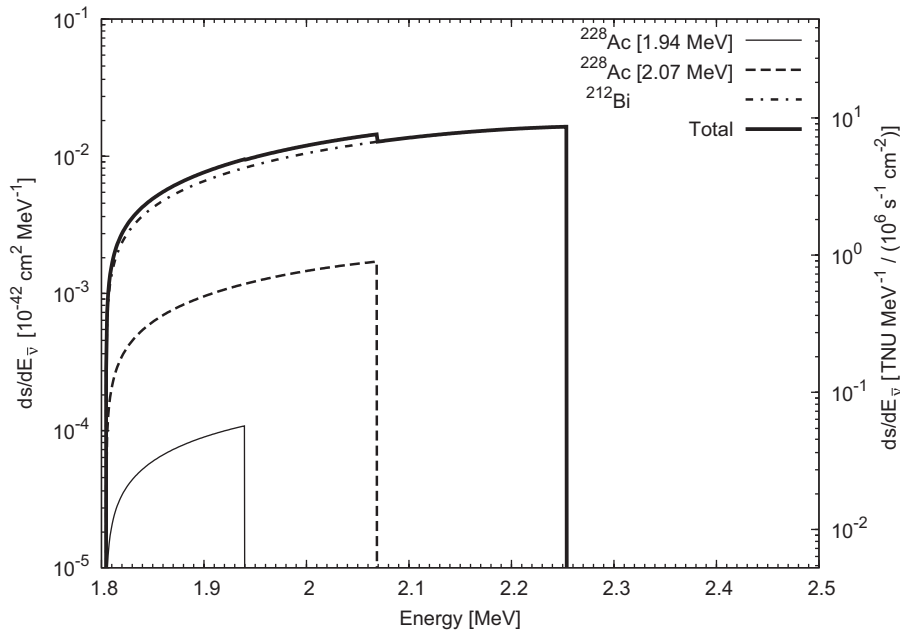
Fig. 10. Geo-neutrino differential signal per unit flux from the three main β decays of the ^{232}Th chain, see Eq. (33).

3. A historical perspective

Geo-neutrinos have been conceived during the very first attempts of neutrino detection, performed at the Hanford nuclear reactor by Reines and Cowan in 1953. Experimental results showed an unexpected and unexplained background.[16] While on board of the Santa Fe Chief Train, Georg Gamow wrote to Fred Reines (see Fig. 11):

> It just occurred to me that your background may just be coming from high energy beta-decaying members of U and Th families in the crust of the Earth.

The first estimate of geo-neutrino flux was given in a teletype message by Reines (Fig. 12) in response to the letter of Gamow:

> Heat loss from Earth's surface is 50 erg cm^{-2} s^{-1}. If assume all due to beta decay than have only enough energy for about 10^8 one-MeV neutrinos cm^{-2} and s.

In the scientific literature, geo-neutrinos were introduced by Eder (1966) in the 1960s and Marx (1969) soon realized their relevance. In the 1980s Krauss et al.discussed their potential as probes of the Earth's interior in an extensive publication (Krauss et al., 1984). In the 1990s the first paper on a geophysical journal was published by Kobayashi and Fukao (1991). Of particular interest, in 1998, Raghavan et al. (1998) and Rothschild et al. (1998) pointed out the potential of KamLAND and Borexino for geo-neutrino detection.

In the last few years more papers appeared than in the previous decades: in a series of papers (Fiorentini et al., 2003a,b,2004,2005b,c,d; Mantovani et al., 2004) Fiorentini et al. discussed the role of geo-neutrinos for determining the radiogenic contribution to the terrestrial heat flow and for discriminating among different models of Earth's composition and origin. A reference model for geo-neutrino production, based on a compositional map of the Earth's crust and on geochemical modeling of the mantle, was presented in Mantovani et al. (2004). Similar calculations were performed by Enomoto et al. (2005) and by Fogli et al. (2006). The claim (Eguchi et al., 2003 of an indication of geo-neutrino events in the first data release of KamLAND stimulated several theoretical investigations (Domogatsky et al., 2006;

---

[16] Actually the background was due to cosmic radiation.

Fig. 11. The message from Georg Gamow to Fred Reines.

TO: DR. GEORGE GAMOW
               THE UNION
               UNIVERSITY OF MICHIGAN
               ANN ARBOR, MICHIGAN

MESSAGE:

FROM NUMBERS IN UREY BOOK ON THE PLANETS, EQUILIBRIUM HEAT LOSS FROM EARTH'S SURFACE IS 50 ERGS/CM^{2}SEC. IF ASSUME ALL DUE TO BETA DECAY THEN HAVE ONLY ENOUGH ENERGY FOR ABOUT 10^8, 1 Mev NEUTRINOS PER CM^2 AND SEC. THIS IS LOW BY 10^5 OR SO. SHORT HALF LIVES WOULD BE MADE BY COSMIC RAYS OR NEUTRONS IN EARTH. IN VIEW OF RARITY OF COSMIC RAYS: I.E. ABOUT EQUAL TO ENERGY OF STARLIGHT AND OF NEUTRONS IN EARTH THIS SOURCE OF NEUTRONS SEEMS EVEN LESS LIKELY AS A SOURCE OF OUR SIGNAL.

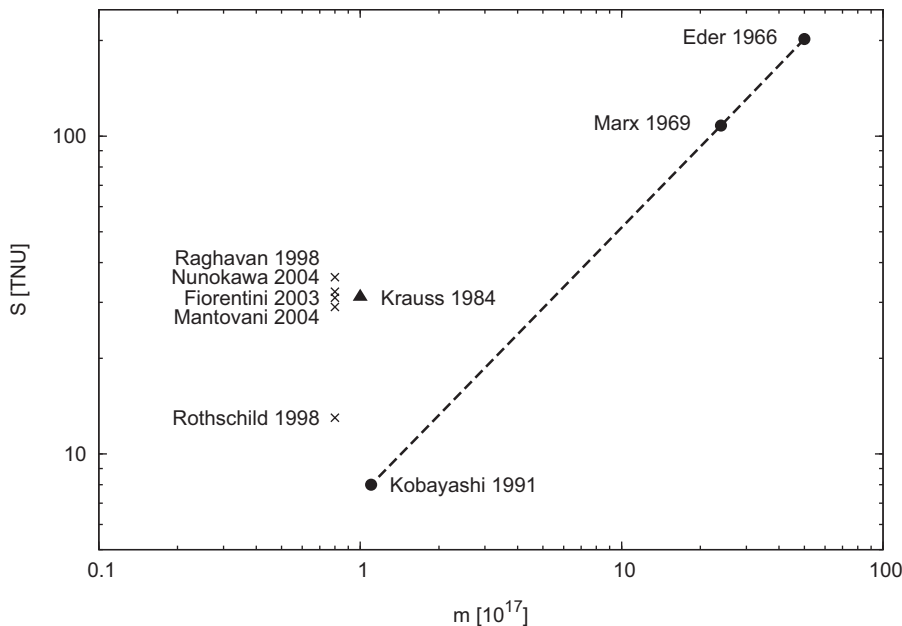Fig. 12. The teletype message from Reines to Gamow.

Fig. 13. Previous estimates of the geo-neutrino signal S, renormalized to the average survival probability $\langle P_{ee} \rangle = 0.59$, and the corresponding estimated uranium mass m. The signal is in Terrestrial Neutrino Units (1 TNU = 1 event/year/10^{32} proton). From Fiorentini et al. (2005d).

Eguchi et al., 2003; Fields and Hochmuth, 2006; Fiorentini et al., 2005a; Fogli et al., 2005; McKeown and Vogel, 2004; Miramonti, 2003; Nunokawa et al., 2003). A summary of the theoretical predictions is presented in Fig. 13. Early models (Eder, 1966; Kobayashi and Fukao, 1991; Marx, 1969) (full circles) assumed a uniform uranium distribution in the Earth and different values of the uranium mass. In fact these predictions are almost proportional to the estimated mass of heat generating elements. The huge signals predicted by Eder and by Marx were obtained by assuming that the uranium density in the whole Earth is about the same as that observed in the continental crust; Marx (Eder) assumed thus an uranium mass 30 (60) times larger than that estimated within the BSE model (see Section 5.3).

Krauss et al. (1984) distributed about 10^{17} kg of uranium uniformly over a 30 km crust. The other estimates (crosses) are all obtained by using the BSE value for the uranium mass ($\approx 10^{17}$ kg) as an input and different models for distributing the uranium content between crust and mantle. In this class, Rothschild et al. (1998) obtained the minimal prediction by assuming for the crust a very small uranium abundance, definitely lower than the values reported in more recent and detailed estimates.

In July 2005 the KamLAND collaboration presented the first evidence of a signal truly originating from geo-neutrinos, showing that the technology for geo-neutrino detection is now available. KamLAND reported (Araki et al., 2005a) data from an exposure of $N_p = (0.346 \pm 0.017) \times 10^{32}$ free protons over a time of 749 days. In the energy region where geo-neutrinos are expected, there are 152 counts. After subtracting several backgrounds, there remain about 25 true geo-neutrino events. This indicates the difficulties of this experiment: a signal rate of one geo-neutrino event per month, to be distinguished over a five times larger background, mostly originating from the surrounding nuclear power plants. The implication of KamLAND result on radiogenic terrestrial heat have been discussed in Fiorentini et al. (2005a).

Following the important KamLAND result, a meeting specifically devoted to study the potential of geo-neutrinos in Earth's science was gathered at Hawaii in December 2005 (Learned et al., 2006). It provided a first opportunity for a joint discussion between the communities of particle physics and of geo-science.

In a few years KamLAND should provide definite evidence of the geo-neutrino signal, after accumulating a much larger statistics and reducing background. In the meanwhile other projects for geo-neutrino detection are being developed. Borexino at Gran Sasso, which is expected to take data soon, will benefit from the absence of nearby reactors. Domogatsky et al. (2006) are proposing a one-kton scintillator detector in Baksan, again very far from nuclear reactors. A group at the Sudbury Neutrino Observatory in Canada is studying the possibility of using liquid scintillator after the physics program with heavy water is completed (Chen, 2006). The LENA proposal envisages a 30-kton liquid

scintillator detector at the Center for Underground Physics in the Pyhasalmi mine (Finland) (Undagoitia et al., 2006). Due to the huge mass, it should collect several hundreds of events per year. The proposal of a geo-neutrino directional detector at Curacao has been advanced (de Meijer et al., 2006). The possibility of a detector located at Hawaii islands has been presented by Dye et al. (2006). In conclusion, one can expect that within 10 years the geo-neutrino signal from uranium and thorium will be measured at a few points on the globe.

4. Radioactivity in the earth

4.1. A first look at Earth's interior

A global look at Earth's interior is useful before entering a detailed discussion on the element distributions. The amount of information which we (assume to) have on Earth's interior is somehow surprising, if one considers that the deepest hole which has ever been dug is only about twelve kilometers deep.

Seismology has shown that Earth is divided into several layers, which can be distinguished from discontinuities in the sound speed, see Figs. 14 and 15. The outer layer is the relatively thin crust which accounts for 0.47% of the Earth mass; it is divided in two types, continental crust (CC) and oceanic crust (OC). The former averages 38 km in thickness, varying around the globe from 20 to 70 km, and it is made primarily of light elements such as potassium, sodium, silicon, calcium, and aluminum silicates. The oceanic crust is much thinner, from about 6 to 8 km.

Inside this crustal skin is Earth's mantle which is 2900 km deep over all. Largely made up of iron and magnesium silicates, the mantle as a whole accounts for about 68% of Earth's mass. One distinguishes the upper mantle (UM) from the lower mantle (LM), however, the seismic discontinuities between the two parts do not necessarily divide the mantle into layers. The main questions about the mantle are: does it move as a single layer or as multiple layers? Is it homogeneous in composition or heterogeneous? How does it convect? These questions sound simple, but the answers are complex, possibly leading to more questions, see Davies et al. (2002).

Inside the mantle is Earth's core, which accounts for about 32% of Earth's mass. Based on comparison with the behavior of iron at high pressures and temperatures in laboratory experiments, on the seismic properties of the core, and on the fact that iron is the only sufficiently abundant heavy element in the universe, the core is generally believed to be made primarily of iron with small amounts of nickel and other elements. Over thirty years ago, however, it was suggested that a significant amount of potassium could be hidden in Earth's core, thus providing a large fraction of the terrestrial heat flow through ^{40}K decay. This controversial possibility has been revived recently in Rama Murthy et al. (2003), see, however, Corgne et al. (2007).
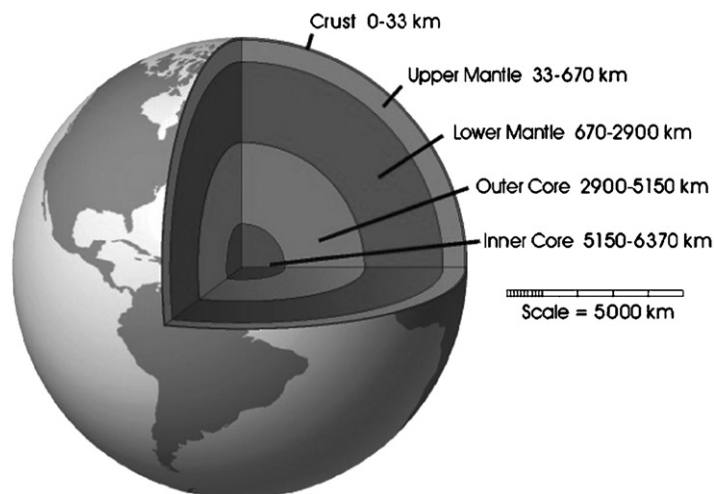

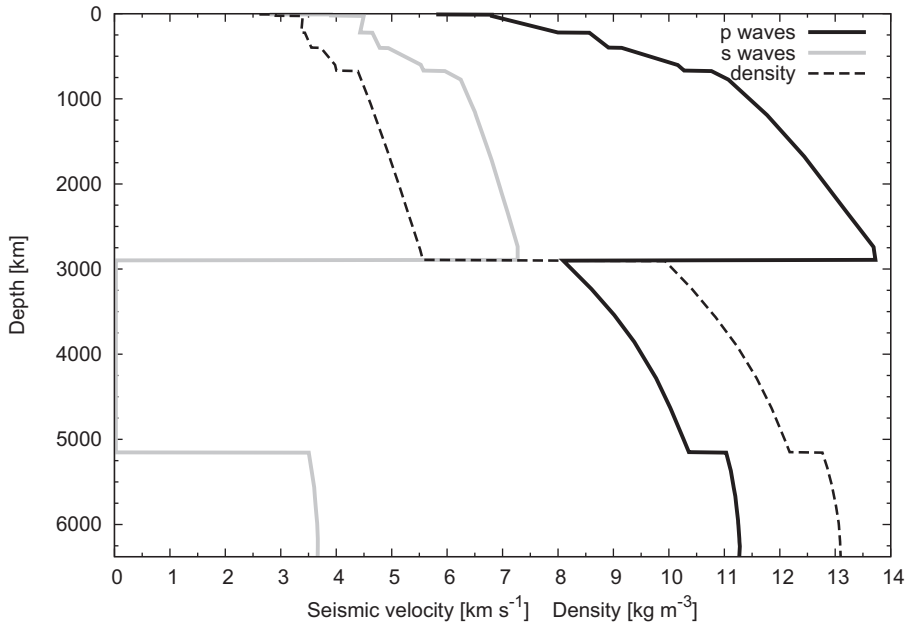Fig. 14. A sketch of the Earth's interior.

Fig. 15. PREM (Preliminary Reference Earth Model) (Dziewonski and Anderson, 1981) velocity structure through the Earth: $\rho = $ density, $\alpha = $ seismic P-waves velocity, $\beta = $ S-waves velocities. Figure taken from http://shadow.eas.gatech.edu/~anewman/classes/geodynamics/random/prem_earth.pdf.

Concerning the density profile of our planet, a classical reference is the Preliminary Reference Earth Model (PREM) of Dziewonski and Anderson (1981). This one-dimensional spherically symmetric model is at the basis of all calculations for geo-neutrino production from the mantle. In the last twenty years seismic tomography has progressed so as to provide three dimensional views of the mantle. Density differences with respect to the one-dimensional model (typically of order of few percent) are most important for understanding mass circulation inside the mantle; however, they are too small in order to affect significantly the calculated geo-neutrino production.

From seismic studies one can derive the density profile of our planet and the aggregation state of the different layers; however, one cannot reconstruct its composition.

Earth global composition is generally estimated from that of CI chondritic meteorites by using geochemical arguments which account for loss and fractionation during planet formation. Along these lines the BSE model is built, which describes the element composition of the "primitive mantle", i.e. the outer portion of the Earth after core separation and before the differentiation between crust and mantle, see Table 7. The model is believed to describe the present crust plus mantle system. It provides the total amounts of U, Th, and K in the Earth, as these lithophile elements should be absent in the core. Estimates from different authors (McDonough, 2003) are concordant within 10–15%, extensive reviews being provided in McDonough and Sun (1995), Palme and O'Neill (2003). From the mass, the present radiogenic heat production rate and neutrino luminosity can be immediately calculated by means of Eqs. (4), (2), (3) and (1), and are shown in Table 8.

The BSE is a fundamental geochemical paradigm. It is consistent with most observations, which however regard the crust and the uppermost portion of the mantle only. Its prediction for the present radiogenic production is 19 TW.

Concerning the distribution of heat generating elements, estimates for uranium in the (continental) crust based on observational data are in the range:

$$m_C(U) = (0.3\text{–}0.4) \times 10^{17} \, \text{kg}. \tag{34}$$

The crust—really a tiny envelope—should thus contain about one half of uranium in the Earth. For the mantle, observational data are scarce and restricted to the uppermost part, so the best estimate for its uranium content $m_M(U)$ is obtained by subtracting the crust contribution from the BSE estimate:

$$m_M(U) = m_{\text{BSE}}(U) - m_C(U). \tag{35}$$

Table 7

The composition of the silicate Earth. Abundances are given in $\mu g\,g^{-1}$ (ppm), unless stated as "%" which are given in weight percentage. Data from McDonough (2003)

H	100	Zn	55	Pr	l0.25
Li	1.6	Ga	4	Nd	1.25
Be	0.07	Ge	1.1	Sm	0.41
B	0.3	As	0.05	Eu	0.15
C	120	Se	0.075	Gd	0.54
N	2	Br	0.05	Th	0.1
O (%)	44	Rb	0.6	Dy	0.67
F	15	Sr	20	Ho	0.15
Na (%)	0.27	Y	4.3	Er	0.44
Mg (%)	22.8	Zr	10.5	Tm	0.068
Al (%)	2.35	Nb	0.66	Yb	0.44
Si (%)	21	Mo	0.05	Lu	0.068
P	90	Ru	0.005	Hf	0.28
S	250	Rh	0.001	Ta	0.037
Cl	17	Pd	0.004	W	0.029
K	240	Ag	0.008	Re	0.0003
Ca (%)	2.53	Cd	0.04	Os	0.003
Sc	16	In	0.01	Ir	0.003
Ti	1200	Sn	0.13	Pt	0.007
V	82	Sb	0.006	Au	0.001
Cr	2625	Te	0.012	Hg	0.01
Mn	1045	I	0.01	Tl	0.004
Fe (%)	6.26	Cs	0.021	Pb	0.15
Co	105	Ba	6.6	Bi	0.003
Ni	1960	La	0.65	Th	0.08
Cu	30	Ce	1.68	U	0.02

Table 8

Mass, heat production, and geo-neutrino luminosity of U, Th, ^{40}K according to BSE

	m $(10^{17}\,\text{kg})$	H_R $(10^{12}\,2)$	$L_{\bar{\nu}}$ $(10^{24}\,\text{s}^{-1})$
U	0.8	8.0	6.2
Th	3.2	8.7	5.3
^{40}K	1.1	3.6	26.5

We remark that this estimate is essentially based on a cosmo-chemical argument and there is no direct observation capable of telling how much uranium is in the mantle, and thus on the whole Earth.

Similar considerations hold for thorium and potassium, the relative mass abundance with respect to uranium being globally estimated as $a(\text{Th}) : a(\text{U}) : a(\text{K}) \approx 4 : 1 : 12000$. Geochemical arguments are against the presence of radioactive elements in the (completely unexplored) core, as discussed by McDonough in an excellent review of compositional models of the Earth (McDonough, 2003).

A comprehensive review about the knowledge of Earth's interior is given in volumes 2 and 3 of Holland and Turekian (2003).

The following subsections are devoted to present, in some more detail, the available information on the amounts of heat generating elements in the whole Earth and within its separate layers.

4.2. The BSE model and heat generating elements in the interior of the Earth

In the BSE frame, the amount of heat/neutrino generating material inside Earth is determined through the following steps:

(a) From the compositional study of selected samples emerging from the mantle, after correcting for the effects of partial melting, one establishes the absolute primitive abundances in major elements with refractory and lithophile

character, i.e. elements with high condensation temperature (so that they do not escape in the processes leading to Earth formation) and which do not enter the metallic core. In this way primitive absolute abundances of elements such as Al, Ca and Ti are determined, a factor about 2.8 times CI chondritic abundances.

(b) It is believed, and supported by studies of mantle samples, that refractory lithophile elements inside Earth are in the same proportion as in chondritic meteorites. In this way, primitive abundances of Th and U can be derived by rescaling the chondritic values.

(c) Potassium, being a moderately volatile elements, could have escaped in the planetesimal formation phase. Its absolute abundance is best derived from the practically constant mass ratio with respect to uranium observed in crustal and mantle derived rocks.

There are several calculations of element abundances in the BSE model, all consistent with each other to the level of 10%. By taking the average of results present in the literature, in Mantovani et al. (2004) the following values were adopted[17]: for the uranium abundance $a_{BSE}(U) = 2 \times 10^{-8}$, for the ratio of elemental abundances $Th/U \equiv a_{BSE}(Th)/a_{BSE}(U) = 3.9$, and $K/U \equiv a_{BSE}(K)/a_{BSE}(U) = 1.14 \times 10^4$. For a comparison, a recent review (Palme and O'Neill, 2003)—subsequent to Mantovani et al. (2004)—gives $a_{BSE}(U) = 2.18 \times 10^{-8}$, $Th/U = 3.83$, and $K/U = 1.2 \times 10^4$.

4.3. The crust

Earth is the only planet, in our solar system, that has both liquid water and a topographically bimodal crust, consisting of low-lying higher-density basaltic oceanic crust (OC) and high-standing lower-density andesitic continental crust (CC) (Rudnick and Fountain, 1995).

Although the continental crust is insignificant in terms of mass (about half of a percent of the total Earth), it forms an important reservoir for many of the trace elements on our planet, including the heat producing elements. It also provides us with a rich geologic history: the oldest dated crustal rocks formed within 500 Ma (million years) of Earth accretion, whereas the oceanic crust records only the last 200 Ma of Earth history.

The crust extends vertically from the Earth's surface to the Mohorovicic (Moho) discontinuity, a jump in compressional wave speeds from ≈ 7 to ≈ 8 km/s which occurs, on the average, at a depth of ≈ 40 km for the continental crust and at a depth of about 8 km for the oceanic crust.

The Conrad discontinuity separates the continental crust into two parts. Actually, based on additional seismic information several authors, e.g., Rudnick and Fountain (1995), identify three components in the crust, the upper-, middle-, and lower-crustal layers (which we shall refer to as UC, MC and LC, respectively). The upper crust is readily accessible to sampling and robust estimates of its composition are available for most elements, whereas the deeper reaches of the crust are more difficult to study, so that the estimated elemental abundances are more uncertain. The observations show that the crust becomes more mafic[18] with depth and the concentration of heat producing elements drops rapidly from the surface downwards. Not only the crust is vertically stratified in terms of its chemical composition, but it is also heterogeneous from place to place. This makes it difficult to determine the average composition of such a heterogeneous mass.

4.3.1. Abundances of heat generating elements

For each component of the crust, one has to adopt a value for the abundances[19] $a(U)$, $a(Th)$, and $a(K)$ and to associate it with an uncertainty. In the literature of the last twenty years one can find many estimates of abundances for the various components of the crust (upper, middle, lower crust = UC, MC, LC and oceanic crust = OC), generally without an error value, two classical reviews being (Taylor and McLennan, 1995; Wedepohl, 1995). Average elemental abundances in the continental crust, and their vertical distribution in the three main identifiable layers have been presented in a recent comprehensive review (Rudnick and Gao, 2003), together with a wealth of data and with a critical

---

[17] We shall always refer to element abundances in mass and we remind the reader that the natural isotopic composition is $^{238}U/U = 0.993$, $^{232}Th/Th = 1$, and $^{40}K/K = 1.2 \times 10^{-4}$.

[18] Mafic is used for silicate minerals, magmas, and rocks which are relatively high in the heavier elements. The term is derived from "magnesium" and "ferrum" (Latin for iron), but mafic magmas are also relatively enriched in calcium and sodium.

[19] Throughout the paper the term abundance refers to abundance in mass.

Table 9
Uranium mass abundances in the Earth's reservoirs and in the silicate Earth (BSE) used in recent geo-neutrino studies. Units are $\mu g\,g^{-1}$ (ppm) for the crust, $ng\,g^{-1}$ (ppb) otherwise

Reservoir	Units	Mantovani et al. (2004)		σ	Fogli et al. (2005)	σ	Enomoto (2005)
		Adopted value	$\dfrac{(a_{max} - a_{min})}{2}$		Adopted value		Adopted value
UC	ppm	2.5	0.3	0.13	2.7	0.6	2.8
MC	ppm	1.6	–	–	1.3	0.4	1.6
LC	ppm	0.63	0.45	0.23	0.2	0.08	0.2
OC	ppm	0.1	–	–	0.1	0.03	0.1
UM	ppb	6.5	1.5	1.5	3.95	1.2	12
BSE	ppb	20	2.5	1.0	17.3	4.7	20

survey of earlier literature on the subject. A most useful and continuously updated source is provided by the GERM Reservoir database. Table 9 presents the uranium abundances used for geo-neutrino calculation in a few studies.

Earlier paper on geo-neutrinos adopted abundances from some review papers, without tackling the problem of the associated uncertainties. A similar approach is taken in the recent paper by Enomoto et al. (2005) where the values from (Rudnick and Fountain, 1995) are used directly, without any estimate of the associated uncertainties.

Our group adopted as reference values for the abundances the average $\langle a \rangle$ of values which were available in the GERM database[20] in 2003, considering the spread of the reported abundances $(a_{max} - a_{min})/2$ as indication of the corresponding uncertainty. In Table 9 we also presents the standard deviation of the average:

$$\sigma = \sqrt{\frac{1}{N(N-1)} \sum_{i=1}^{N} (a_i - \langle a \rangle)^2}. \tag{36}$$

Fogli et al. (2005) basically adopt the results of a recent and comprehensive review (Rudnick and Gao, 2003) for the UC, MC, LC abundances of (U, Th, K) and the uncertainties quoted in that paper. Since no error estimates are given in (Rudnick and Gao, 2003) for the LC, Fogli et al. assume a fractional 1σ errors of 40%. A more extensive comment on uncertainties can be found in Appendix C.

From the table one sees that the values adopted by different groups are generally in agreement within the quoted uncertainties, however with the following remarks:

- A major difference lies in the abundance for the (poorly constrained) lower portion of the crust. In the literature, values as low as 0.2 ppm and as high as 1.1 ppm have been reported, as a consequence of different assumptions for the fraction of (uranium poor) metaigneous rocks and (uranium rich) metapelitic rocks.
- Concerning the upper crust, the values quoted by different authors using different methods (surface exposure data, sedimentary data and loess correlations with La) are consistent within about 10%. From a study of loess[21] correlations with La, in Rudnick and Gao (2003) a concordant average value has being obtained, however with a 1σ uncertainty of 21% mainly due to the variability of the U/La correlation.

From the table, it emerges that the contributions to geo-neutrino production from different portions of the Earth's crust are markedly different, the continental crust being an order of magnitude richer in heat generating material than the oceanic part. Relative uncertainties, as natural, increase with depth and their assessment is at the moment somehow tentative.

4.3.2. The distribution of heat generating elements
The earlier geo-neutrino studies considered the distribution of heat generating elements as spherically symmetrical over the Earth's crust. Actually one has to distinguish between continental and oceanic crust since they have quite

---

[20] Geochemical Earth Reference Model (GERM) available online at http://earthref.org/GERM/.
[21] Loess is a deposit of silt (sediment with particles 2–64 μm in diameter) that have been laid down by wind action.

different contents of heat generating elements. In addition the thickness of the crust significantly differs from place to place. More recent studies, since Rothschild et al. (1998), take into account the actual inhomogeneity of Earth crust.

A global crustal model on a $2° \times 2°$ degree grid, available in Laske et al. (2001), has been widely used in recent years. Data gathered from seismic experiments were averaged globally for similar geological and tectonic settings (such as Archean, early Proterozoic, rifts, etc.). The sedimentary thickness is based on the recent compilation by Bassin et al. (2000), Laske et al. (2001). Bathymetry and topography is that of ETOPO5.

Within each $2° \times 2°$ degree tile, one distinguishes oceans and seawater, the continental crust, subdivided into three sub-layers (upper, middle, and lower), sediments and oceanic crust. For all these layers values of density and depth are given over the globe.[22]

4.4. The mantle: data, models and debate

Sandwiched between Earth's crust and metallic core, the mantle is a 2900 km layer of pressurized rock at high temperature. As reviewed by Hofmann (1997, 2003), mantle models can be divided into two broad classes, essentially corresponding to the presently contradictory geochemical and geophysical evidence of Earth's interior.

4.4.1. Geochemical and geophysical evidences

Geochemists have long insisted on a two-layer model, in which the mantle consists of a relatively primitive layer below a depth of about 670 km and an upper layer that is highly depleted of heat producing elements (panel (a) in Fig. 16). The two layers are viewed as separate sources of the Mid-Ocean-Ridge Basalts (MORB), which come from mantle regions that have been already depleted in incompatible elements by extraction of the continental crust, and of Ocean Island Basalts (OIB), which form by melting of deeper, less depleted or even enriched mantle sectors. Also, a more primitive deep layer is needed from global constraints, otherwise the amount of radiogenic elements inside Earth is much too small with respect to that estimated within BSE paradigm.

On the other hand, over the past several years seismic tomography has provided increasingly detailed images of apparently cold slab descending into the deep mantle, below the 670 km boundary. If cold slabs descend into the deep mantle, there must be a corresponding upward flow of deep-mantle material to shallow levels (panel (b) in Fig. 16). If this circulation reaches the bottom of the mantle (whole mantle convection), it would destroy any compositional layering below the crust in a few hundred million years (at a typical speed of $3 \, \text{cm yr}^{-1}$ it takes about 10^8 yr to move down to 2900 km).

In brief, the composition and circulation inside Earth's mantle is the subject of a strong and so far unresolved debate between geochemists and geophysicists. Geochemical evidence has been used to support the existence of two compositionally distinct reservoirs in the mantle, the borders between them being usually placed at a depth near $h_0 = 670 \, \text{km}$, whereas geophysics presents evidence of mantle convection extending well beyond this depth. If this convection involves the whole mantle, it would have destroyed any pre-existing layering, in conflict with geochemical evidence.

When building their respective reference models for geo-neutrino production, our group in Mantovani et al. (2004), as well as Fogli et al. (2005), used a two-reservoir mantle model. Observational values are adopted for the upper mantle whereas the lower mantle abundances are inferred from the BSE mass balance constraint. On the other hand, Enomoto et al. (2005) prefer a wholly mixed mantle, with uniform abundance within it derived from the BSE constraint, see Table 9.

4.4.2. A class of two-reservoir models

More generally, new views on mantle convection models overcome the widely diffused model of two-layer mantle convection, namely an outgassed and depleted upper layer overlying a deeper, relatively primordial and undegassed mantle layer. The ensemble of geochemical and geophysical evidence along with terrestrial heat flow-heat production balance argues against both whole mantle convection and layering at 670 km depth models, suggesting the existence of a transition between the two reservoirs (outgassed and depleted—degassed and primordial) at 1600–2000 km depth (Albarède and van der Hilst, 1999; van der Hilst and Karason, 1999; Kellogg et al., 1999). In the numerical simulation of their mantle convection model, Kellogg et al. (1999) located this boundary at a depth of about 1600 km.

---

[22] Note that additional useful databases are available at http://mahi.ucsd.edu/Gabi/rem.html.
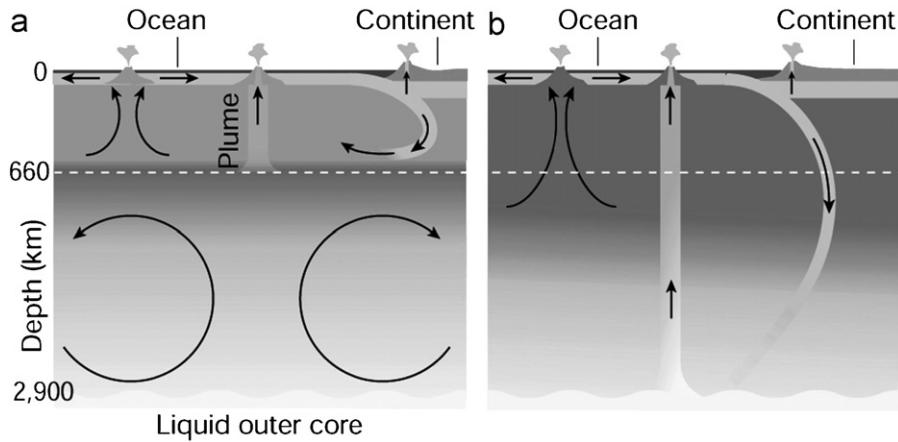
Fig. 16. Models of mantle circulation, adapted from Hofmann (2003): (a) is the traditional two-layer model with demarcation at 670 km and nearly complete isolation between upper and lower layers; (b) is a fully mixed model.
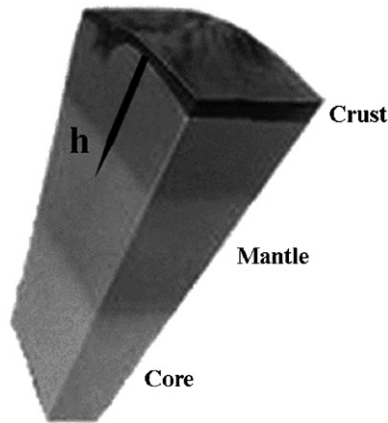

Fig. 17. Generic two-reservoir mantle model: the critical depth h is a free parameter.

In order to consider the implications of the present debate on mantle circulation and composition on the predicted geo-neutrino fluxes, our group has also considered (Fiorentini et al., 2005c) the uranium distribution in a wider class of models, including the extreme geochemical and geophysical models, in terms of just one free parameter, the depth h marking the borders between the two hypothetical reservoirs (see Fig. 17):

(i) above h one assumes uniform uranium abundance in the range from 2 to 7.1 ppb, as deduced from measures of the depleted upper mantle.
(ii) Below h one assumes an uniform abundance, determined by requiring mass balance for the whole Earth. This means that uranium mass below the critical depth, $m_{>h}$, is obtained by subtracting from the total BSE estimated mass (m_{BSE}) the quantity observationally determined in the crust (m_C) and that contained in the mantle above h ($m_{<h}$):

$$m_{>h} = m_{BSE} - m_C - m_{<h}. \tag{37}$$

For each model, the calculated uranium abundance in the lower portion of the mantle is shown in Fig. 18.

This class of models includes a fully mixed mantle (MIX), which is obtained for $h = 25$ km (i.e. just below a mean crust thickness obtained averaging the vales for continental and oceanic crust) so that the strongly impoverished mantle has a negligible thickness. The traditional geochemical model (REF) corresponds to $h = h_0$. As h increases, the depleted
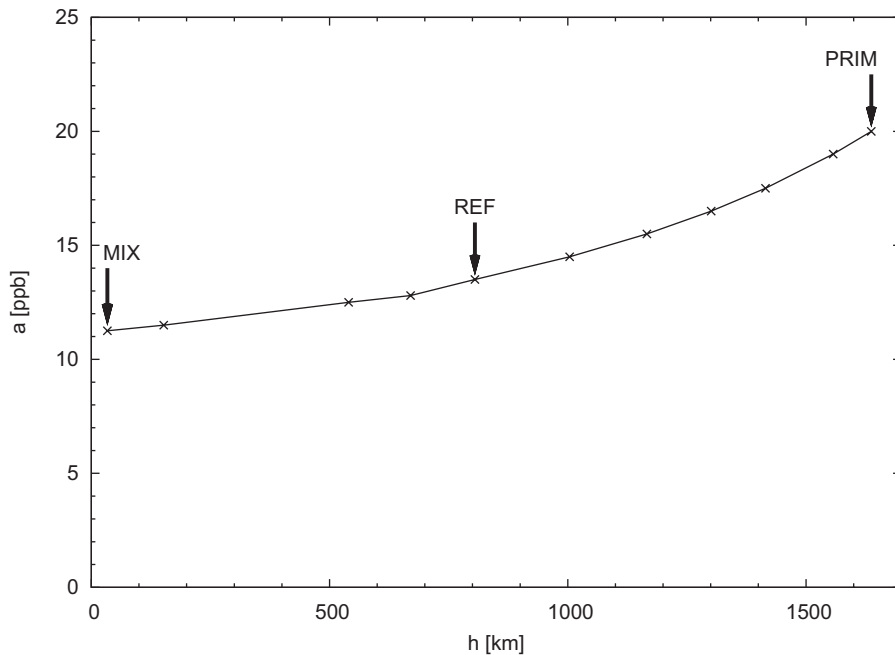
Fig. 18. Uranium abundance in the lower part of the mantle as a function of the critical depth h from Earth's surface, from Fiorentini et al. (2005c).

region extends deeper inside the Earth and—due to mass balance—the innermost part of the mantle becomes richer and closer in composition to the primitive mantle.

Among all possible models, the case $h = 1630\,\text{km}$ is particularly interesting. Below this depth the resulting uranium abundance is 20 ppb, corresponding to the BSE estimate. The innermost part of the mantle is thus primitive in its trace element composition and the crust enrichment is obtained at expenses of the mantle content above h. Again following Fiorentini et al. (2005c), we shall refer to this model as PRIM.

Concerning geo-neutrino fluxes from the mantle, all the models proposed above have the same amount of heat/anti-neutrino sources and only the geometrical distribution is varied. The largest flux corresponds to the model with sources closest to the surface, i.e. to the MIX model. On the other hand, the minimal prediction is obtained when the sources are concentrated at larger depth, which corresponds to the PRIM case.[23]

5. Terrestrial heat

Earth emits a tiny heat flux with an average value $q \approx (60\text{–}90)\,\text{mW}\,\text{m}^{-2}$, definitely smaller than the radiation coming from the Sun, $1.4\,\text{kW}\,\text{m}^{-2}$, larger, however, than the energy deposited by cosmic rays, about $10^{-8}\,\text{W}\,\text{m}^{-2}$. When integrated over the Earth's surface, the tiny flux translates into a huge heat flow, $H \approx (30\text{–}45)$ TW, the equivalent of ten thousand nuclear power plants. In this section we briefly review the estimates of terrestrial heat flow and discuss the sources which can sustain it.

5.1. Heat flow from the Earth: data and models

A frequently quoted value for the total heat release from Earth's surface is the estimate by Pollack et al. (1993), $H = 44.2 \pm 1.0$ TW. In spite of the small quoted error, uncertainties seem to be much bigger: a recent revisitation of the problem by Hofmeister and Criss (2005a) yields 31 ± 1 TW with a central value close to that quoted in the seventies.

The heat flux q is determined by using the conduction law (if one assumes that conduction is the main mechanism for heat transport): one measures the temperature gradient ∇T in near-surface rocks and their thermal

---

[23] This is a part of the *proximity argument*, which we shall exploit extensively later, see Section 8.

conductivity k, and derives:

$$q = -k\nabla T. \tag{38}$$

In this way one obtains a mean heat flux of $65\,\text{mW}\,\text{m}^{-2}$ from the continents. This commonly agreed value yields a continental contribution to terrestrial heat flow of 13 TW. Direct measurements from the oceanic crust give comparable values for the flux, so that, when weighted with the surface, the oceanic contribution would be about 20 TW. By summing these contributions one finds a total heat flow of about 30 TW, a value commonly found in the *old* literature.

However, the estimate of the actual heat flow for the ocean is more difficult and controversial. The point is that the heat flow determined from Eq. (38) is a lower bound for its actual value, since in porous and permeable rocks heat may be also carried out by convective flow of interstitial fluid (water). This convection lowers the temperature gradient below the value it would have if the rocks were dry or impervious to water. On these grounds, other attempts have been developed for estimating the oceanic heat flow.

Instead of using the distribution of conductive heat measurements, Pollack et al. have based the estimate of the heat flux from the oceanic crust on theoretical *thermal models*, such as the Half Space Cooling (HSC) model and its variants. The models aim at a description of both ocean depths and heat flow versus age data. In the HSC model, as an example, depth and heat flow vary as the square root of age and the reciprocal of the square root of age, respectively. The models reproduce data at a semi-quantitative level; however, the predicted heat fluxes come out to be larger than those provided by the conductive heat measurements, particularly for very young ages. As a result, the mean heat flow from the oceans amounts to $101\,\text{mW}\,\text{m}^{-2}$, with the oceans giving a contribution to the terrestrial heat flow of about 31 TW, so that the total flow is near 45 TW.

Note that with respect to heat flow inferred from conductive heat measurements in the ocean, there is a difference of 11 TW which is attributed to hydrothermal flow. As already mentioned, however, this procedure has been criticized by Hofmeister and Criss, with their paper opening a debate, see von Herzen et al. (2005), Hofmeister and Criss (2005b).

In conclusion, it seems to us that for the global heat flow 30 TW is a sound lower limit based on direct observations, whereas 45 TW is a reasonable upper limit, as it corresponds to the highest estimate available in the literature.

5.2. Energy sources

Coming to the sources of heat flow, the situation is even more complex. A comparison between the Sun and Earth energy inventories may be useful for illustrating the differences between the two cases and for appreciating the difficulties when discussing Earth's energetics. Clearly, a heat flow H can be sustained for a time t provided that an energy source of at least $U = H \times t$ is available. For the Sun $U_\odot = H_\odot t_\odot \approx 5 \times 10^{43}\,\text{J}$: clearly neither gravitation, $U_G \sim GM_\odot^2/R_\odot \approx 4 \times 10^{41}\,\text{J}$, nor chemical reactions, $U_{\text{chem}} \sim 0.1\,\text{eV} \times N_\odot \approx 2 \times 10^{37}\,\text{J}$ (where $N_\odot$ is the number of nucleons in the Sun) are sufficient; only nuclear energy, $U_{\text{nucl}} \sim 1\,\text{MeV} \times N_\odot \approx 2 \times 10^{44}\,\text{J}$, can sustain the solar luminosity over the solar age, as beautifully demonstrated by Gallium experiments in the previous decade (Abdurashitov et al., 2002; Altmann, 2000; Hampel et al., 1999). On the other hand, for the Earth one finds $U_G \approx 4 \times 10^{32}\,\text{J}$, $U_{\text{chem}} \approx 6 \times 10^{31}\,\text{J}$, and $U_{\text{nucl}} \approx 6 \times 10^{30}\,\text{J}$, (assuming that some 10^{-8} of Earth mass consists of radioactive nuclei), so that any of the previous mechanisms can sustain the present heat flow for the Earth's age: $U_\oplus = H_\oplus t_\oplus \approx 5 \times 10^{30}\,\text{J}$.

In order to understand the energetics of the Earth one has to clarify the roles of the different energy sources, their locations and when they have been at work. In 1980, at the end of a review on the Earth energy sources, Verhoogen (1980) summarized the situation with the following words:

> What emerges from this morass of fragmentary and uncertain data is that radioactivity by itself could plausibly account for at least 60%, if not 100%, of the Earth's heat output. If one adds the greater rate of radiogenic heat production in the past,… possible release of gravitational energy (original heat, separation of core, separation of inner core, tidal friction …meteoritic impact …), the total supply of energy may seem embarrassingly large. …Most, if not all of the figures mentioned above are uncertain by a factor of at least two, so that disentangling contributions from the several sources is not an easy problem.

Anderson (2005) opens a recent review, entitled "Energetics of the Earth and the Missing Heat Source Mistery", with the following words:

> Global heat flow estimates range from 30 to 44 TW. Estimates of the radiogenic contribution (from the decay of U, Th, and K in the mantle), based on cosmochemical considerations, vary from 19 to 31 TW. Thus, there is

Table 10
Sources of thermal energy in the Earth's interior, adapted from Anderson (2005)

Energy supply (potential contributions)	TW
Non radiogenic:	
Conducted from core	8.6
Mantle differentiation	0.6
Thermal contraction	2.1
Earthquake induced gravitational energy	2
Radiated seismic energy	0.3
Tidal friction	1–2
Total (nonradiogenic)	**15–16**
Radiogenic:	
Present radiogenic	19–31
Delayed radiogenic	
(1–2 Ga delay between production and arrival at surface)	5
Total (radiogenic)	**24–36**
Secular cooling (0–100 K Ga^{-1})	**0–14**
Total input	**39–66**

> either a good balance between current input and output, …or there is a serious missing heat source problem, up to a deficit of 25 TW.

Anderson summarizes in Table 10 the potential contributions to the terrestrial energy budget. Similar to Verhoogen, he notes that the potential supply from radiogenic and non radiogenic sources, up to 66 TW, can even exceed the observed heat flow, so that *paradoxes such as the missing heat source problem can be traced to non-realistic assumptions and initial and boundary conditions* and *The bottom line is that there appears to be no mismatch between observed heat flow and plausible sources of heating*. He also notes, and we agree, that uncertainties on the different ingredients of the energy balance (total outflow, amounts of radiogenic material in the Earth, …) are much larger than it was estimated in the past.

5.3. Radiogenic heat: the BSE, unorthodox and even heretical Earth models

We recall that the canonical BSE model predicts a present radiogenic heat production of 20 TW. The BSE is a fundamental geochemical paradigm: it is consistent with most observations, which however regard the crust and the uppermost portion of the mantle only. On the grounds of available geochemical and/or geophysical data, however, one cannot exclude that radioactivity in the present Earth provides a larger contribution to the terrestrial heat flow, sufficient to account for even the highest estimate of terrestrial heat flow.

For a comparison, let us summarize some—less orthodox or even heretical—alternatives to the BSE.

(a) It is conceivable that the original material from which the Earth formed is not exactly the same as inferred from CI-chondrites. A model with initial composition as that of enstatite chondrites could account for a present production of some 30 TW (Hofmeister and Criss, 2005a; Javoy, 1995).

(b) A model where the BSE abundances of U, Th, and K are proportionally rescaled by a factor of 2.2 cannot be excluded by the observational data, if one assumes that the missing radiogenic material is hidden below the upper mantle. This model gives a present radiogenic heat production of 44 TW, which matches the highest estimate of the present heat flow.

(c) Starting with Hall and Rama Murthy (1971), and Lewis (1971), several authors have been considering the possibility that a large amount of potassium is sequestered into the Earth's core, where it could provide the light element that accounts for the right core density, the energy source for driving the terrestrial dynamo, and—more generally—an additional contribution to Earth energy budget. This possibility has been recently revived in Rama Murthy et al. (2003), where from high-pressure and high-temperature data it was shown that potassium can enter iron sulphide melts in a strongly temperature-dependent fashion so that ^{40}K could be as a substantial heat source in the core of the Earth.

(d) Herndon (2003) has proposed that a large drop of uranium has been collected at the center of the Earth, forming a natural 3–6 TW breeder reactor, see also Raghavan (2002). In this case nuclear fission should provide the energy source for terrestrial magnetic field, a contribution to missing heat, and the source of the anomalous ^{3}He/^{4}He flow from Earth.

In summary, an unambiguous and observationally based determination of the radiogenic heat production would provide an important contribution for understanding Earth's energetics. It requires to determine how much uranium, thorium and potassium are on the Earth, quantities which are strictly related to the anti-neutrino luminosities from these elements.

6. The reference model

A reference model for geo-neutrino production is a necessary starting point for studying the potential and expectations of detectors at different locations.

By definition, it should incorporate the best available geochemical and geophysical information on our planet. In practice, it has to be *based on selected geophysical and geochemical data and models* (*when available*), *on plausible hypotheses* (*when possible*), *and admittedly on arbitrary assumptions* (*when unavoidable*). These duly cautious words from Fogli et al. (2005) explain the difficulties and to some extent the arbitrariness when building such models. They also mean that estimates of uncertainties on the predicted geo-neutrino fluxes are at least as important as the predicted values.

6.1. Comparison among different calculations

Recently a few such models have been presented in the literature (Enomoto et al., 2005; Fogli et al., 2005; Mantovani et al., 2004). Predictions by different authors for a few locations are compared in Table 11.

All these models rely on the geophysical $2° \times 2°$ crustal map of Bassin et al. (2000), Laske et al. (2001) and on the density profile of the mantle as given by PREM (Dziewonski and Anderson, 1981).

Concerning the adopted abundances in the crust layers, Mantovani et al. (2004) use average values from results available in the literature in 2002, Fogli et al. (2005) refer to the values of the recent review by Rudnick and Gao (2003), whereas Enomoto et al. (2005) adopt the values reported in the 1995 review by Rudnick and Fountain (1995). Mantovani et al. and Fogli et al. assume a chemically layered mantle, with abundances in the upper mantle from Jochum et al. (1983), Zartman and Haines (1988), Salter and Stracke (2004), and Workman and Hart (2005), respectively; whereas Enomoto et al. consider a chemically homogeneous mantle. The adopted uranium abundances in the various reservoirs are compared in Table 9. All papers use the BSE mass constraint in order to determine the adopted abundances in the lower portion of the mantle.

Concerning uncertainties on the abundances in the crust and in the upper mantle, Mantovani et al. (2004) estimate them from the spread of published values, whereas Fogli et al. (2005) use the errors quoted by Rudnick and Gao (2003), where available, see Table 9. The uncertainties of the abundances in the lower mantle are obtained by Fogli et al. by propagating in the mass constrain also the uncertainties estimated for the BSE. Mantovani et al. release the BSE constraint and take a more conservative attitude, including as extreme values the possibility that the lower mantle has the same small abundances observed in the upper mantle and, on the other side, the possibilities that the amount of heat generating elements can sustain a fully radiogenic 44 TW heat flow, with most of the material being hidden in the unexplored lower mantle. The BSE mass constraint used by Fogli et al. fixes the total amount of heat generating elements to the level of $\pm 14\%$ (1σ), whereas the range considered in Mantovanti et al. is much wider. This is at the origin of the differences in the uncertainties quoted in Table 11. Indeed, if the calculation of Mantovani et al. is restricted to the BSE range, the uncertainties become comparable to those of Fogli et al.

One has to remark[24] that Fogli et al. also present a systematic approach to the ubiquitous issue of covariances in geo-neutrino analyses. In fact, for the only (at the moment) relevant case, the correlation between U and Th, they use the value $\rho = 0.94$, estimated by the errors on the U/Th ratio, very close to $\rho = 1$, which was used in Mantovani et al. (2004).

---

[24] A more extensive comment on the treatment of uncertainties is presented in Appendix C.

Table 11
Predicted geo-neutrino rate from U + Th at various locations. Rates are in TNU. All calculations are normalized to a survival probability $\langle P_{ee}\rangle = 0.57$. For Mantovani et al. the uncertainties are estimated as $(N_{high} - N_{low})/6$, see Table 12 of Mantovani et al. (2004)

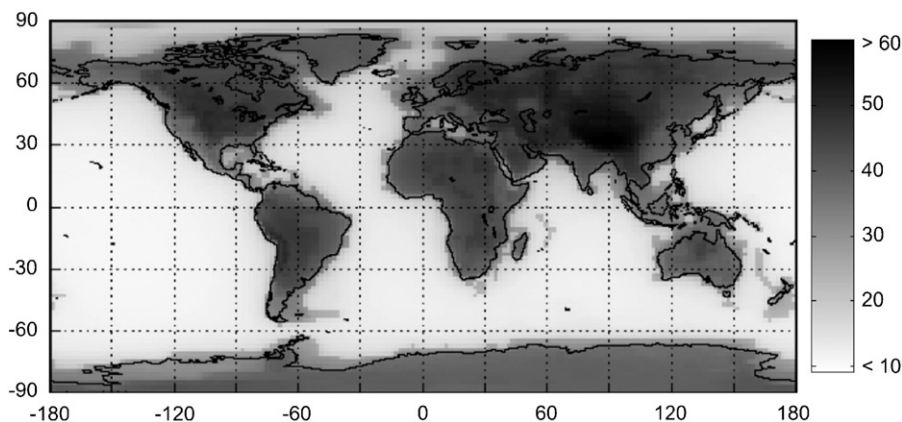| Location	Mantovani et al. (2004)	Fogli et al. (2005)	Enomoto[a]
Hawaii	12.5 ± 3.6	13.4 ± 2.2	13.4
Kamioka	34.8 ± 5.9	31.6 ± 2.5	36.5
Gran Sasso	40.5 ± 6.5	40.5 ± 2.9	43.1
Sudbury	49.6 ± 7.3	47.9 ± 3.2	50.4
Phyasalami	52.4 ± 7.6	49.9 ± 3.4	52.4
Baksan	51.9 ± 7.6	50.7 ± 3.4	55.0

[a]Private communication.

Fig. 19. Predicted geo-neutrino events from uranium and thorium decay chains, normalized to 10^{32} proton yr and 100% efficiency, from Fiorentini et al. (2005c).

6.2. The contribution of the various reservoirs

The predicted signal all over the world is shown in Fig. 19, taken from Fiorentini et al. (2005c). It presents the Earth as it shines in geo-neutrinos. The more intense signals arise from regions with a thick continental crust, whereas over the oceans the signal essentially originates from the mantle.

The separate contributions of the different reservoirs to the produced flux of geo-neutrinos from the uranium decay chain are analyzed in Table 12, from Mantovani et al. (2004). At Himalaya, a site which maximizes the crust contribution, the prediction is $\Phi(U) = 6.7 \times 10^6 \, \text{cm}^{-2} \, \text{s}^{-1}$ whereas at Hawaii, a site which minimizes the crust contribution, the prediction is $\Phi(U) = 1.3 \times 10^6 \, \text{cm}^{-2} \, \text{s}^{-1}$, originated mainly from the mantle. For the Kamioka mine, where the KamLAND detector is in operation, the predicted uranium flux is $\Phi(U) = 3.7 \times 10^6 \, \text{cm}^{-2} \, \text{s}^{-1}$. Within the reference model, about 3/4 of the flux is generated from material in the crust and the rest mainly from the lower mantle. At Gran Sasso laboratory, where Borexino (Alimonti et al., 1998) is in preparation, the prediction is $\Phi(U) = 4.2 \times 10^6 \, \text{cm}^{-2} \, \text{s}^{-1}$, this larger flux arising from a bigger contribution of the surrounding continental crust. A similar calculation for Sudbury, the place which hosts the SNO detector, gives $\Phi(U) = 4.4 \times 10^6 \, \text{cm}^{-2} \, \text{s}^{-1}$. The crust contribution exceeds 80%.

The contribution to the signal as a function of the distance from the detector is shown in Fig. 20 from Mantovani et al. (2004) for the specific case of Kamioka. One notes that some 15% of the total signal originates from a region within 30 km from the detector, whereas half of the signal is generated within some 600 km. We remind the typical linear dimension of each tile in the $2° \times 2°$ crustal map is of order 200 km, so that any information on a smaller scale is lost. A better geological and geochemical description of the region surrounding the detector is needed for a more precise estimate of the geo-neutrino signal.

Table 12
Uranium: masses, radiogenic heat, and predicted fluxes

	$M(U)$	$H(U)$	Φ_U			
			Himalaya 33°N 85°E	Gran Sasso 42°N 14°E	Kamioka 36°N 137°E	Hawaii 20°N 156°W
Crust low	0.206[a]	1.960	3.337	1.913	1.594	0.218
Crust ref	**0.353**	**3.354**	**5.710**	**3.273**	**2.727**	**0.373**
Crust high	0.413	3.920	6.674	3.826	3.187	0.436
UM low	0.048	0.455	0.146	0.146	0.146	0.146
UM ref	**0.062**	**0.591**	**0.189**	**0.189**	**0.189**	**0.189**
UM high	0.077	0.727	0.233	0.233	0.233	0.233
LM low	0.147	1.399	0.288	0.288	0.288	0.288
LM ref	**0.389**	**3.695**	**0.760**	**0.760**	**0.760**	**0.760**
LM high	1.177	11.182	2.299	2.299	2.299	2.299
Total low	0.401	3.814	3.770	2.346	2.027	0.651
Total ref	**0.804**	**7.639**	**6.659**	**4.222**	**3.676**	**1.322**
Total high	1.666	15.828	9.206	6.358	5.720	2.968

Units are 10^{17} kg, TW and 10^6 cm^{-2} s^{-1}, respectively. The reference values, lower and upper limits are labeled as ref, low, and high, respectively. Crust summarizes CC and OC; UM (LM) denotes upper (lower) mantle. Data from Mantovani et al. (2004).

[a] This value corresponds to an uranium abundance in the continental crust equal to 0.91 ppm as estimated in Taylor and McLennan (1985). Starting from Fiorentini et al. (2004) we dismiss this estimate, since it is inconsistent with data from all other authors, and we use 0.3 as the lower limit for the uranium mass in the crust, see Fiorentini et al. (2004) for a discussion. The values of the fluxes from the crust corresponding to 0.3 are 4.92, 2.84, 2.35, and 0.33 for the four locations, respectively.
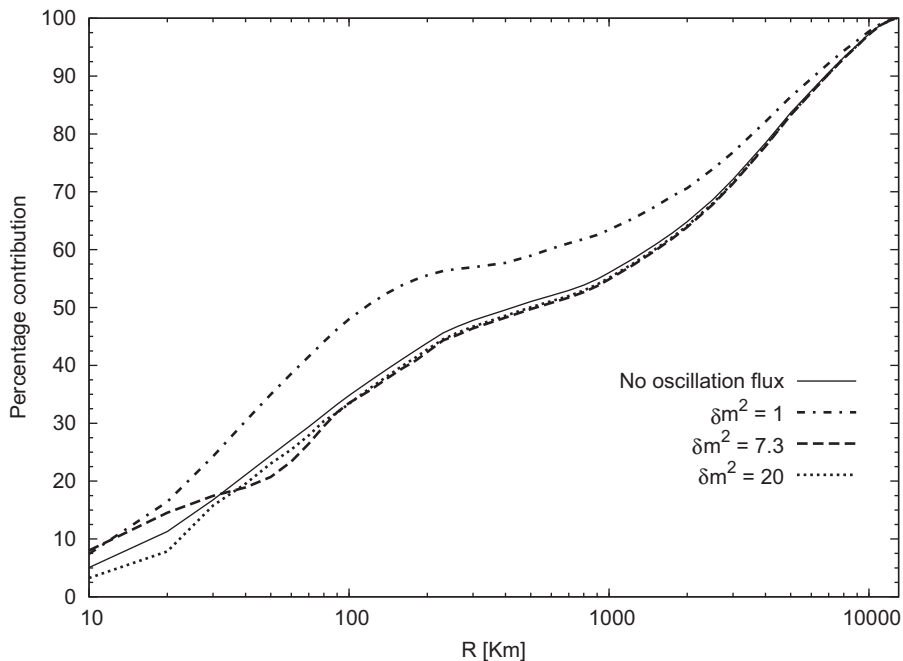

Fig. 20. Contributed signal as a function of distance. The percentage contribution to the event yield at Kamioka originating from sources within a distance R is shown for the indicated values of Δm^2 in units of 10^{-5} eV^2 at fixed $\sin^2 2\theta = 0.863$. The percentage contributed neutrino flux without oscillation is also shown for comparison. From Mantovani et al. (2004).

Table 13
Effect of the oscillation parameters on the predicted U + Th signal at Kamioka. The relative/absolute variation is computed with respect to the prediction for the best fit values ($\Delta m^2 = 8.0 \times 10^{-5}\,\mathrm{eV}^2$ and $\tan^2 \theta = 0.45$)

Parameter	Signal variation
$\Delta m^2 = 7.2 \times 10^{-5}\,\mathrm{eV}^2$	+0.11 TNU
$\Delta m^2 = 8.9 \times 10^{-5}\,\mathrm{eV}^2$	−0.09 TNU
$\tan^2 \theta = 0.61$	−7.5%
$\tan^2 \theta = 0.33$	+9.3%

6.3. The effect of uncertainties of the oscillation parameters

In this review we have fixed $\Delta m^2 = 8.0 \times 10^{-5}\,\mathrm{eV}^2$ and $\tan^2 \theta = 0.45$, which gives an asymptotical survival probability $\langle P_{ee} \rangle = 0.57$, following the best fit of Strumia and Vissani (2005). The same paper gives a 99% CL range $7.2 \times 10^{-5}\,\mathrm{eV}^2 < \Delta m^2 < 8.9 \times 10^{-5}\,\mathrm{eV}^2$ and $0.33 < \tan^2 \theta < 0.61$, with the corresponding range for the average survival probability $0.53 < \langle P_{ee} \rangle < 0.63$.

The effect of these uncertainties on the predicted signal is presented in Table 13.

The predicted signal is practically unaffected by the uncertainty on Δm^2: when this is varied within its 99% CL interval the signal changes by less than one tenth of TNU. This holds for any value of the total uranium and thorium mass, since the precise value of Δm^2 only matters in the region near the detector. In addition, we observe that the predictions computed for the best value ($\Delta m^2 = 8.0 \times 10^{-5}\,\mathrm{eV}^2$) and for the limit $\Delta m^2 = \infty$ differ by +0.3 TNU.

The uncertainty on the mixing angle is most important: at the 99% CL the relative error on the signal $\Delta S/S \approx 9\%$, somehow smaller (but not negligible) in comparison with the geological uncertainties.

7. Refinements of the reference model: the regional contribution

The geo-neutrino signal depends on the total amount of heat generating elements in the Earth and on the geochemical and geophysical properties of the region around the detector. For KamLAND, we estimated that about one half of the signal generated in the crust comes from a region within 200 km from the detector (half of the total signal is originated from within 600 km). This region, although containing a globally negligible amount of heat generating elements, produces a large contribution to the signal as a consequence of its proximity to the detector. This contribution has to be determined on the grounds of a detailed geochemical and geophysical study of the region.

The study of the region around Kamioka based on a detailed analysis of the six tiles depicted in Fig. 21, including the possible effects of the subducting plates below the Japan Arc and a discussion of the contribution from of the Japan Sea, has been presented in Fiorentini et al. (2005d) and in Enomoto (2005), and Enomoto et al. (2005). The result of Fiorentini et al. (2005d) for this regional contribution to the signal from uranium geo-neutrinos is

$$S_{\mathrm{reg}}(\mathrm{U}) = (15.41 \pm 3.07)\,\mathrm{TNU} \quad (3\sigma). \tag{39}$$

This result is obtained by including several effects, discussed in the next subsections. These refinements increase the signal by about 1 TNU. The global error is obtained by adding in quadrature the individual independent uncertainties.

The results of that paper, which only considered geo-neutrinos from uranium decay chains, have been extended to include geo-neutrinos from thorium.

7.1. The six tiles near Kamland

The depth distribution of the Conrad and Moho discontinuities beneath the whole of the Japan Islands are derived in Zhao et al. (1992), with an estimated standard error of ± 1 km over most of Japan territory. This allows distinguishing two layers in the crust: an upper crust extending down to the Conrad and a lower part down to the Moho discontinuity.

In Fiorentini et al. (2005d) a map of uranium abundance in the upper crust has been built, under the important assumption that the composition of the whole upper crust is the same as that inferred in Togashi et al. (2000) from the study of the exposed portion, see Fig. 21. There is no specific study of the lower part of the Japan crust, however, it
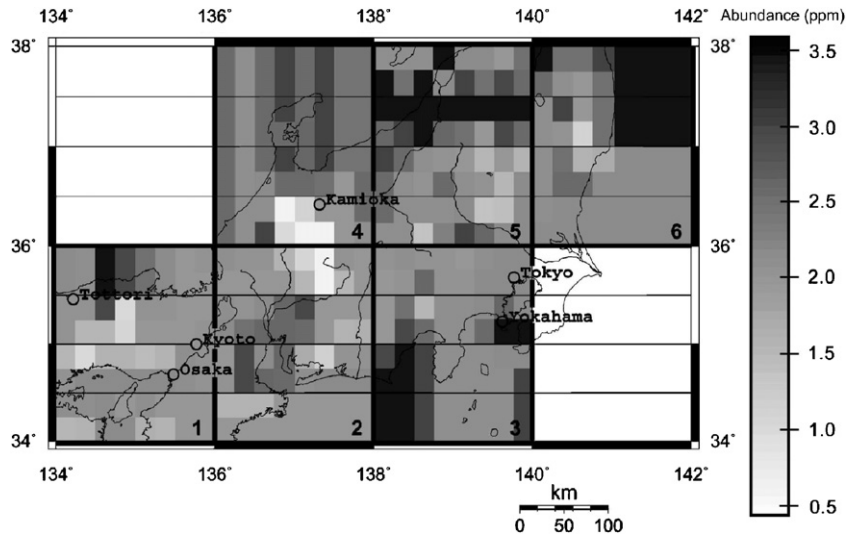
Fig. 21. Uranium abundance in the upper crust of Japan from Fiorentini et al. (2005d).

is well known that there are similarities between the composition of the Japanese crust and that of the Sino–Korean block. In an extensive compositional study of East China crust (Gao et al., 1998), the uranium abundance in the lower part is estimated between 0.63 and 1.08 ppm. On these grounds Fiorentini et al. (2005d) adopt for the abundance in the lower crust of Japan $a_{LC}(U) = (0.85 \pm 0.23)$ ppm.

We remind that for building the reference model, the entire Earth's crust was subdivided into $2° \times 2°$ tiles. In Fiorentini et al. (2005d) a more detailed grid was used where each tile is subdivided into 64 $(1/4)° \times (1/4)°$ cells, thus with a linear scale of about 20 km. This size is chosen since the sampling density for the study of the upper crust in the region near Kamioka is about one specimen per $400 \, km^2$ and also, concerning the vertical distribution of abundances in the crust, it is presently impossible to have information on the chemical composition on a scale smaller than the Conrad depth, generally lying at about 20 km.

The contributions from the six tiles to the uranium signal is $S_6(U) = 12.74$ TNU. The calculation for the same region within the reference model gave $S_6(U) = 14.10$ TNU. A similar reduction was also found in Enomoto (2005). The difference is understood in terms of the depletion of U concentration in the Japanese islands with respect to the average continental crust, already noted in Togashi et al. (2000).

With respect to the prediction of the reference model, the six tiles contribute 45% of the total signal. In more detail, the tile hosting Kamioka generates 30% of the total produced signal. Note that the uranium mass contained in the six tiles is about $m_6 = 3.3 \times 10^{13}$ kg, really negligible (less then 0.05%) with respect to that estimated for the whole Earth.

Fiorentini et al. (2005d) consider several sources of the uncertainties affecting this estimate: measurement errors of the chemical analysis, discretization of the upper crust, chemical composition of the lower crust and crustal depth. Their effects are summarized in Table 14.

7.2. Effect of the subducting slab beneath Japan

The Japan arc, at the crossing among the Eurasian, Philippine and Pacific plates, is the theater of important subduction processes. The Philippine plate is moving towards the Eurasia plate at about 40 mm yr^{-1} and is subducting beneath the southern part of Japan. The Pacific Plate is moving in roughly the same direction at about 80 mm yr^{-1} and is subducting beneath the northern half of Japan.

In order to estimate the effect of the subducting slab on geo-neutrino production, Fiorentini et al. (2005d) considered two extreme cases: (a) one assumes that the slab keeps its trace elements while subducting; (b) at the other extreme, it is possible that, as the slab advances, all uranium from the subducting crust is dissolved in fluids during dehydration reactions and accumulates in the lower part of the continental crust of Japan, thus strongly enriching it.

Table 14
Errors from the regional geophysical and geochemical uncertainties

Source	ΔS (TNU)	Remarks
Composition of upper-crust samples	0.96	3σ Error
Upper-crust discretization	1.68	
Lower-crust composition	0.82	Full range
Crustal depths	0.72	3σ Error
Subducting slab	2.10	Full range
Japan Sea	0.31	Full range
Total	3.07	

Table 15
The vertical extensions (km) of crustal layers in the Yamano basin (YB), Oki bank (OK), and Ulleung basin (UB) used for model (b)

	YB	OK	UB
Sediments	1.2	0.3	4
Upper	2.8	8.7	2
Lower	8.5	10.5	8

As there is no argument for deciding which of the extreme cases (a) or (b) is closer to reality and in order to encompass both of them, the contribution from the subducting slab was estimated in Fiorentini et al. (2005d) as[25]:

$$S_{\text{slab}}(U) = (2.3 \pm 2.1) \text{ TNU} \quad (3\sigma). \tag{40}$$

7.3. The crust below the Japan Sea

The morphology of the Japan Sea is characterized by three major basins (Japan, Yamato, and Ulleung Basins). The crust of the Japan basin is generally considered as oceanic, whereas the nature of other basins is controversial and debated. Again in Fiorentini et al. (2005d) two extreme models are considered:

(a) following Bassin et al. (2000), Laske et al. (2001) all the basins are formed with oceanic crust, extending down to 7 km below 1 km of sediments.
(b) Deeper crustal depths (up to 19 km for the Oki bank) and thicker sediments layers (up to 4 km for the Ulleung basin) are reported in the literature, see Table 15. By taking these values and assigning the abundances typical of continental crust, one maximizes geo-neutrino production.

In order to encompass these two extreme cases, Fiorentini et al. (2005d) fix the contribution to the signal from the Japan Sea as

$$S_{\text{JS}}(U) = (0.37 \pm 0.31) \text{ TNU} \quad (3\sigma). \tag{41}$$

7.4. Thorium contribution and the total geo-neutrino regional signal

By adding the above contributions, and summing in quadrature independent uncertainties one obtains equation (39). The same analysis repeated for Th gives a regional contribution:

$$S_{\text{reg}}(\text{Th}) = (3.66 \pm 0.68) \text{ TNU} \quad (3\sigma). \tag{42}$$

Assuming a complete correlation for the errors, one has

$$S_{\text{reg}}(\text{U} + \text{Th}) = (19.1 \pm 3.8) \text{ TNU} \quad (3\sigma). \tag{43}$$

---

[25] Enomoto et al. (2005) only consider case (a) and get a smaller correction.

8. Beyond the reference model

8.1. Overview

As discussed in the preceding sections, masses of heat generating elements in the Earth are estimated on the grounds of cosmochemical arguments, based on the compositional similarity between Earth and carbonaceous chondrites. Measurements of samples from the Earth's crust imply that the crust contains about one half of this global estimate, whereas the mantle—which should contain the rest—is practically unexplored in this respect. A direct determination of the mass of heat generating elements in the globe is clearly an important test of the origins of the Earth and will fix the radiogenic contribution to the terrestrial heat flow, which is a presently a debated issue, see Section 5.

The geo-neutrino signal depends on the total mass of heat generating elements in the Earth and on the geochemical and geophysical properties of the region around the detector. The region close to the detector, although containing a globally negligible amount of uranium, produces a large contribution to the signal as a consequence of its proximity to the detector. This contribution has to be determined on the grounds of a detailed geochemical and geophysical study of the region, if one wants to extract from the total signal the remaining part which carries the relevant information on the mass of heat generating elements. Such a study of the region around Kamioka has been presented in the previous section.

The contribution to the geo-neutrino signal from the rest of the world depends on the total amount of heat generating elements *as well as on their distribution inside the Earth*, since the closer is the source to the detector the larger is its contribution to the signal. For each value of the total mass, we shall construct distributions of abundances which provide the maximal and minimal signals, under the condition that *they are consistent with geochemical and geophysical information on the globe*.

This will bring us beyond the reference model. Essentially, we shall build models of the Earth which respect the observational data available, concerning the abundances in the crust and the density profile of the Earth, and we shall release the BSE constraint on the global amounts of heat generating elements.

In practice, we shall keep the masses of heat generating elements in the unexplored lower mantle as free parameters. One can still vary the abundances along the mantle depth (which are generally believed to increase with increasing depth) and obtain different geo-neutrino signal for the same total amount of heat generating elements. The important point (Fiorentini et al., 2005d) is the following: the assumption that the abundances are spherically symmetrical and non-decreasing with depth will be enough to provide rather tight constraints on the mantle contribution to the geo-neutrino signal.

This has to be further combined with the contribution from the crust, which also can be maximized/minimized by varying the abundances in the range allowed by observational data.

The combination of this information with the regional study allows to find the connection between the geo-neutrino signal and the masses of heat generating elements in the Earth.

This relationship will be developed in the following subsections, where we elucidate the proximity argument and then we combine the regional contribution for Kamioka found in the previous section with that of the rest of the world.

In principle, this argument can be developed separately for uranium and thorium, i.e. connecting the geo-neutrino signals $S(U)$ and $S(Th)$ with the respective masses $m(U)$ and $m(Th)$ all over Earth.

The main result is shown in Fig. 22, which presents for Kamioka the connection among the uranium mass, heat generation, and geo-neutrino signal.

By assuming the BSE mass constraint, our prediction is

$$S(U) = (29.5 \pm 1.6) \text{ TNU} \quad (1\sigma, \text{ BSE}). \tag{44}$$

If the chondritic Th/U ratio is assumed, one finds

$$S(U + Th) = (32 \pm 2) \text{ TNU} \quad (1\sigma, \text{ BSE}). \tag{45}$$

However, if the BSE constraint is released we get

$$S(U + Th) = (32^{+8}_{-4}) \text{ TNU} \quad (1\sigma, \text{ noBSE}). \tag{46}$$
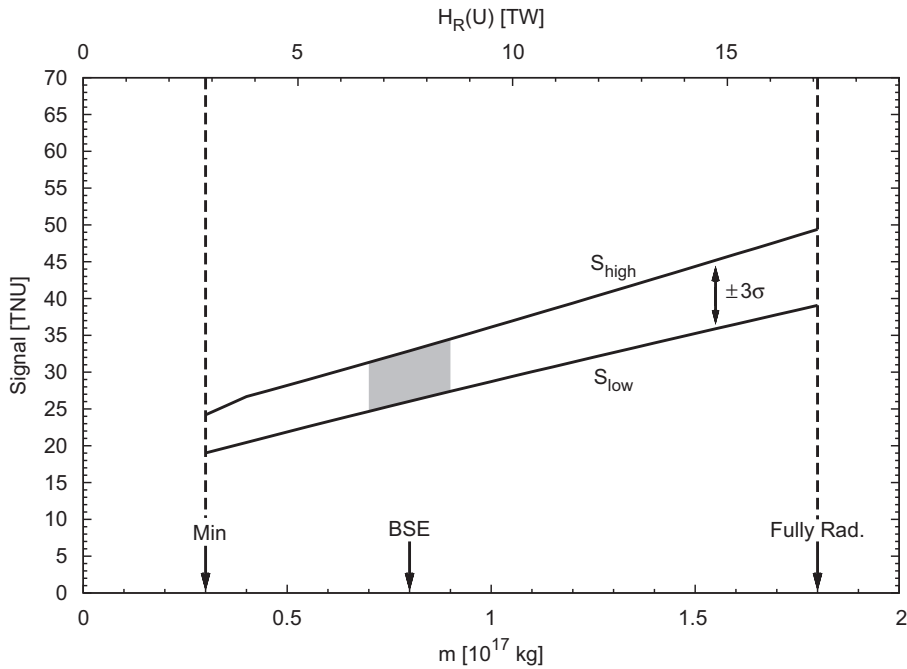
Fig. 22. The predicted signal from uranium geo-neutrinos at KamLAND, adapted from Fiorentini et al. (2005d).

8.2. The proximity argument

The main question is to build models which, for a given total uranium mass in the Earth, $m(U)$, provide the minimal and maximal signals, with the additional constraint that these models be consistent with available geochemical and geophysical observational data. This result can be accomplished by means of what we call the "proximity argument": *the minimal (maximal) contributed flux is obtained by placing heat radiogenic elements as far (close) as possible to the detector* (Fiorentini et al., 2004).

This argument can be used in several steps.

(i) For a place on or near the continental crust, since the continental crust lies on the average closer than the mantle to the detector the maximal (minimal) signal is obtained by putting as much (little) radiogenic material in the crust, as consistent with the observed values.[26] This determines the mass of uranium mass in the crust, $m_C(U)$, which is constrained by observational data to lie in the interval $(0.3–0.4) \times 10^{17}$ kg.

(ii) This leaves us with the problem of distributing the remaining mass, $m(U) - m_C(U)$, inside the mantle. Under the assumptions that the abundances in this reservoir are non-decreasing functions of the depth, the extreme predictions for the signal are obtained by: (a) placing heat generating elements in a thin layer at the bottom, or (b) distributing it with uniform abundance over the mantle.

(iii) One can then combine the extreme cases so as to obtain lower and upper limits to the global contribution to the signal.

8.3. The case of KamLAND

In the case of Kamioka, after excluding the region where a separate geo-chemical and geophysical investigation has been performed (see Section 7), the proximity argument provides for the signal from the rest of the world:

$$S_{RW}(U) = (2.25 + 14.76 \times m(U)) \pm (-0.55 + 2.61 \times m(U)), \qquad (47)$$

---

[26] The opposite holds for places very far from the continents as the Hawaii Islands, see Section 8.4.

where the signal is in TNU, the mass is in units of 10^{17} kg and the interval within the $\pm$ sign corresponds to the full range of models which have been considered.

By combining this results with the regional contribution, calculated in the previous section, $S_{\mathrm{reg}}(\mathrm{U}) = (15.41 \pm 3.07)$ TNU, we get the uranium geo-neutrino signal as a function of uranium mass in the Earth:

$$S(\mathrm{U}) = S_0(\mathrm{U}) \pm \Delta(\mathrm{U}), \tag{48}$$

where

$$S_0(\mathrm{U}) = 17.66 + 14.76 \times m(\mathrm{U}), \tag{49}$$

$$\Delta^2(\mathrm{U}) = (3.07)^2 + (2.61 \times m(\mathrm{U}) - 0.55)^2. \tag{50}$$

This error is obtained by combining in quadrature all geochemical and geophysical uncertainties discussed in the preceding paragraphs. All of them have been estimated so as to cover $\pm 3\sigma$ intervals of experimental measurements and total ranges of theoretical predictions.

However, this error does not account for present uncertainties on neutrino oscillation parameters. We remind (see Section 6.3) that the uncertainty on the mixing angle implies a 99% CL relative error on the signal $\Delta S/S \approx 9\%$, which is somehow smaller (but not negligible) in comparison with the geological uncertainties.

For the sake of discussing the potential of geo-neutrinos, we shall ignore in the following the error originating from uncertainties on the mixing parameter, which however should be measured more accurately.

The expected signal from uranium geo-neutrinos at KamLAND is presented as a function of the total uranium mass $m(\mathrm{U})$ in Fig. 22. The predicted signal as a function of $m(\mathrm{U})$ is between the two lines denoted as S_{high} and S_{low}, which correspond, respectively, to $S_0(\mathrm{U}) \pm \Delta(\mathrm{U})$.

We remark that the extremes of the band correspond to the whole range of uncertainty, which is estimated according to the following criteria:

(i) for statistical errors we consider a $\pm 3\sigma$ interval;
(ii) for systematic uncertainties of geochemical and geophysical parameters we determine an interval such as to cover all modern estimates which we found in the literature;
(iii) independent errors are combined in quadrature.

We remark that the "proximity argument", combining global mass balance with geometry, is very powerful in constraining the range of fluxes: in the allowed band are enclosed all the models consistent with geological data.

Since the minimal amount of uranium in the Earth is 0.3×10^{17} kg (corresponding to the minimal estimate for the crust and the assumption of negligible amount in the mantle), we expect $S(\mathrm{U})$ to be at least 19 TNU. On the other hand, the maximal amount of uranium tolerated by Earth's energetics,[27] 1.8×10^{17} kg, implies $S(\mathrm{U})$ not exceeding 49 TNU.

For the central value of the BSE model, $m(\mathrm{U}) = 0.8 \times 10^{17}$ kg, it was found in Fiorentini et al. (2005d) $S(\mathrm{U}) = 29.5 \pm 3.4$ TNU, i.e. with an accuracy of 12% at 3σ.

We remark that estimates by different authors for the uranium mass within the BSE are all between $(0.7–0.9) \times 10^{17}$ kg. This implies that the uranium signal has to be in the interval $(24.7–34.5)$ TNU. The measurement of geo-neutrinos can thus provide a direct test of an important geochemical paradigm.

We do not expect that the next generation of experiments can collect enough statistics so as to clearly separate the two components (U and Th) in the signal (see Section 2) and will have to rely on the chondritic estimate for the ratio for the global abundances of these two elements. On these grounds, we shall also assume this value of the ratio and rescale the results calculated for uranium to get the total signal as a function of the radiogenic heat from U + Th. In this way one gets Fig. 23.

---

[27] For an uranium mass $m(\mathrm{U}) = 1.8 \times 10^{17}$ kg and relative abundances as in Eq. (4), the present radiogenic heat production rate from U, Th, and K decays equals the maximal estimate for the present heat flow from Earth, $H_{\mathrm{max}} = 44$ TW (Pollack et al., 1993).
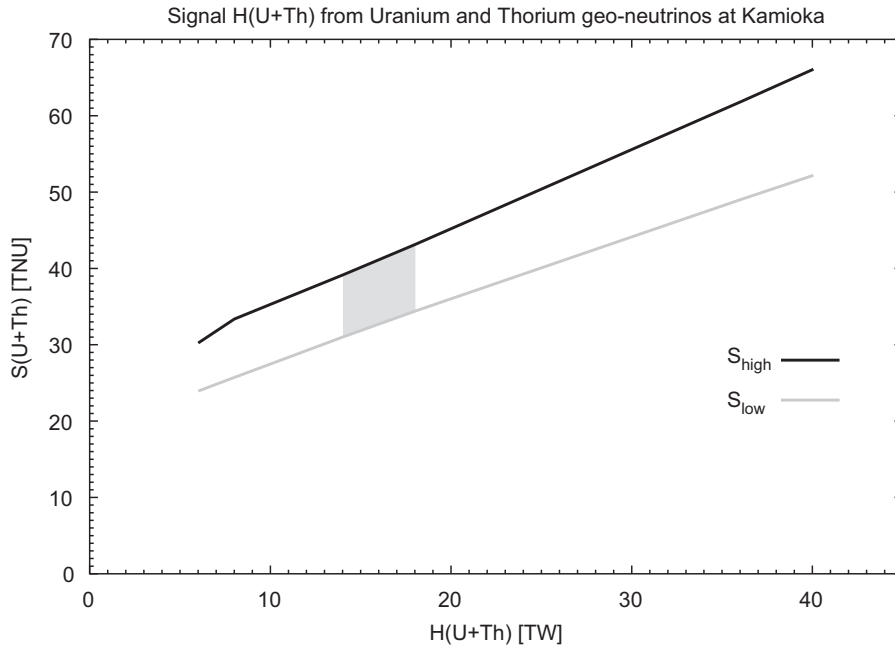
Fig. 23. Predictions on the combined signal $S(U + Th)$ from uranium and thorium geo-neutrinos at Kamioka as a function of the radiogenic heat production rate $H(U + Th)$. The area between the two lines (S_{high} and S_{low}) denotes the region allowed by geochemical and geophysical constraints. The shaded area denotes the region allowed by the BSE constraint. Earth energetics implies the signal does not exceed 62 TNU, and U and Th measured in the crust imply a signal of at least 24 TNU.

Table 16
The crust response coefficients α_i for a few locations

Site	α
Hawaii	8
Kamioka	57
Gran Sasso	69
Sudbury	93

8.4. Predictions at other locations

In order to understand the potential of detectors at other locations one should perform a study similar to the one just outlined for Kamioka. In the absence of a detailed geochemical and geophysical study of the region surrounding the detector, we can tentatively address the problem by using the prediction for the crust as derived by the $2° \times 2°$ crustal map.[28]

We resort again to the proximity argument, by making it more general, so as to cover also locations which lie far from the continents.

a. *Contribution from the crust*. The contribution, as a function of the uranium mass contained in the crust $m_C(U)$, can be obtained by rescaling the predictions of the reference model. This gives at the ith location:

$$S_C^i = \alpha_i \times m_C(U), \tag{51}$$

where the response coefficients α_i are presented in Table 16 for a few locations.

---

[28] We remind that for Kamioka the more detailed calculation changes the signal by just about 1 TNU; however the uncertainty of the regional contribution is about ± 3 TNU (at 3σ).
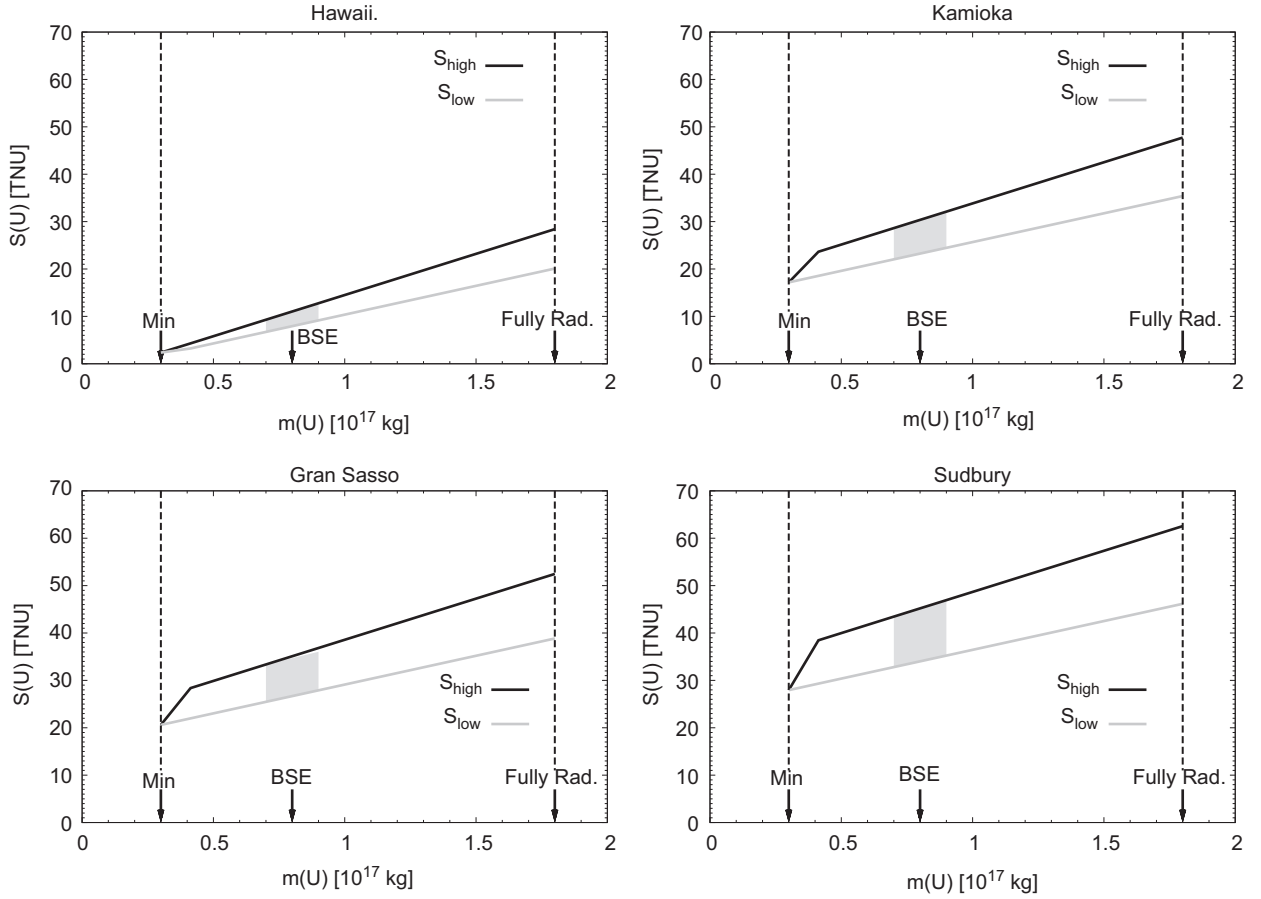
Fig. 24. The predicted signal from uranium geo-neutrinos at Hawaii (top-left), Kamioka (top-right), Gran Sasso (bottom-left), and Sudbury (bottom-right). The area between the black line (S_{high}) and the grey line (S_{low}) denotes the region allowed by geochemical and geophysical constraints.

b. *Contribution from the mantle*. We remind that, under the assumptions that the abundances in this reservoir are radial and nondecreasing function of the depth, the extreme predictions for the signal are obtained by:

(i) placing uranium in a thin layer at the bottom;
(ii) distributing it with uniform abundance over the mantle.

For a mass $m_M(U)$ in the mantle, the two cases give, respectively, and independently of the location:

$$S_{M,low}(U) = \beta_{low} \times m_M(U) \text{ TNU}, \tag{52}$$

$$S_{M,high}(U) = \beta_{high} \times m_M(U) \text{ TNU}, \tag{53}$$

with $\beta_{low} = 12.15$ TNU and $\beta_{high} = 17.37$ TNU when the mass, as here and in the following, is measured in units of 10^{17} kg.

c. *Combining mantle and crust*. At each location, the total uranium signal will be

$$S(U) = S_C(U) + S_M(U) = \alpha_i \times m_C(U) + \beta \times m_M(U) = (\alpha_i - \beta) \times m_C(U) + \beta \times m(U), \tag{54}$$

where the total uranium mass is $m(U) = m_C(U) + m_M(U)$.

If one wants the largest signal, obviously one has to put $\beta = \beta_{high}$ and, if $\alpha_i > \beta_{high}$, $m_C(U)$ has to be as large as possible, consistently with the observations of the crust, i.e. $m_C(U) = \min(m(U), 0.41)$. In the opposite case, $\alpha_i < \beta_{high}$,

one takes instead $m_C(U)$ as small as possible, i.e. $m_C(U) = 0.3$. Note that the first case is what occurs on or close to the continental crust, whereas the second case corresponds to locations far from the continents.

Similarly, for minimizing the signal one puts $\beta = \beta_{\text{low}}$ and then one takes $m_C(U) = 0.3$, if $\alpha_i > \beta_{\text{low}}$, or $m_C(U) = \min(m(U), 0.41)$ in the opposite case.

The results for the extreme cases, shown in Fig. 24, deserve the following comments. The band is most narrow for the Hawaii, as natural since this place, far from the continents, is most sensitive to the amount of radioactivity hidden in the mantle. On the other hand, it is more wide at Sudbury, where the signal is dominated from the contribution of the crust. Concerning Kamioka, the contour defined by this analysis are close (within four TNU or less) to those which were derived by adding the geological and geochemical information on the region, see Fig. 22. This gives us some confidence about the predictions for the other sites.

9. KamLAND results and their interpretation

9.1. Overview

KamLAND (Kamioka Liquid scintillator Anti-Neutrino Detector) is so far the largest low-energy antineutrino detector ever built and studies a wide range of science, spanning particle physics, geophysics and astrophysics.[29]

The KamLAND collaboration is made up of researchers from Japan, China, France and United States. The detector is situated in the same cavern used by the original Kamiokande experiment, where 2002 Nobel laureate Masatoshi Koshiba performed much of his ground-breaking research in neutrino physics.

Located on the island of Honshu in Japan, since 2002 KamLAND detects hundreds of anti-neutrinos per year from nuclear reactors hundreds of kilometers away, an enormous improvement over previous attempts with any other detector. KamLAND has observed an anti-neutrino deficit as well as energy spectral distortion confirming neutrino oscillations and hence non vanishing neutrino masses (Araki et al., 2005b; Eguchi et al., 2003). As a natural continuation of the scientific program, KamLAND aims now at the direct observation of ^{7}Be solar neutrinos by detecting recoil energy in neutrino-electron scattering processes.

KamLAND has also performed a geo-neutrino investigation. In 2005, the KamLAND collaboration has published (Araki et al., 2005a) experimental results, claiming some 28 geo-neutrino events from uranium and thorium decay chains in a two-year exposure. This important step shows that the technique for exploiting geo-neutrinos in the investigation of the Earth's interior is now available. From the KamLAND data, including new measurements of the ^{13}C$(\alpha, n)^{16}$O cross section, one finds $S(U + Th) = (63^{+28}_{-25})$ TNU, see Fiorentini et al. (2005a). The central value is close to the prediction of a maximal and fully radiogenic model (see Section 8.3), however the BSE prediction is within 1σ from it.

In the future, with more statistics KamLAND should be capable of providing a three-sigma evidence of geo-neutrinos, but discrimination between BSE and fully radiogenic models definitely requires new detectors, with class and size similar to that of KamLAND, far away from nuclear power plants.

In the next subsections we shall present KamLAND results on geo-neutrinos and discuss their implications on the terrestrial heat.

9.2. The KamLAND detector

Neutrinos are detected at KamLAND[30] by the inverse beta-decay reaction,

$$\bar{\nu}_e + p \rightarrow e^+ + n - 1.806 \, \text{MeV}, \tag{55}$$

with a large amount of organic liquid scintillator. The liquid scintillator essentially consists of hydrocarbons ($C_n H_{2n}$) which provide the hydrogen nuclei acting as the target for antineutrinos. We remind that the energy threshold of the reaction, 1.806 MeV, is low enough to detect a part of the U-series and Th-series geo-neutrinos.

The reaction produces two correlated signals. A prompt signal is given by the slowing down positron and by the two 0.51 MeV gamma rays from positron annihilation. The delayed signal consists of a 2.2 MeV gamma particle, which is emitted in the thermal neutron capture on proton. The thermalization and capture processes take place in about 200 μs,

---

[29] An overview of KamLAND science plan is found in Gratta (1999).

[30] An extensive description of the detector can be found in the Ph.D. Thesis of Enomoto (2005).
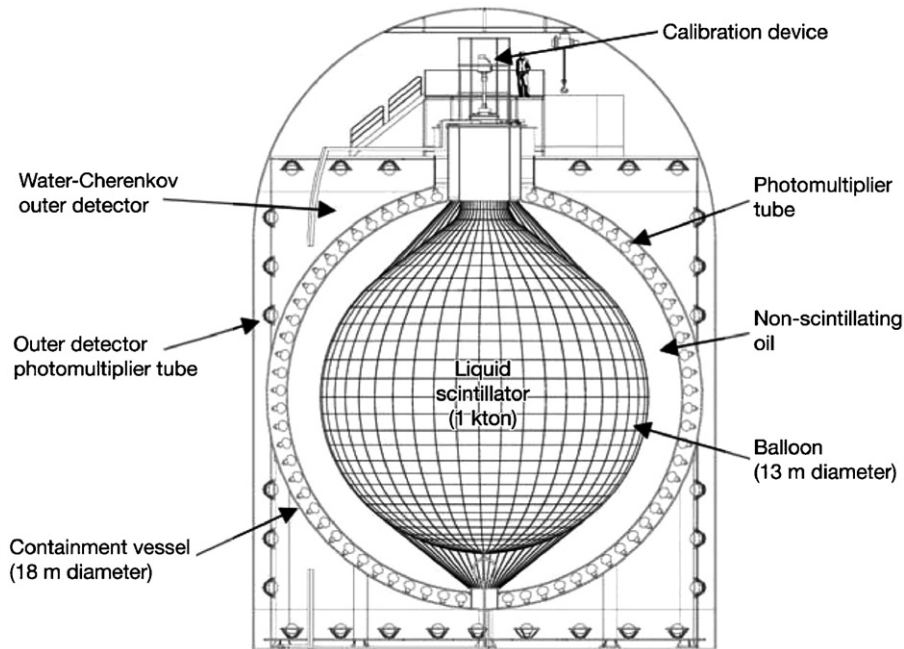
Fig. 25. An overview of the KamLAND detector from Enomoto (2005).

and neutron capture occurs typically 30–50 cm apart from the neutrino reaction vertex. The time and space correlations of the two signals are distinguishing characteristics of electron-type antineutrino events. The delayed coincidence of the two signals provides an effective way to select antineutrino events with excellent separation of background events.

The KamLAND detector basically consists of 1000 tons of ultra-pure liquid scintillator (LS) contained in a 6.5 m radius spherical balloon and of 1879 surrounding photomultiplier tubes (PMT) that cover 34% of the sphere. The detector is located 1000 m underground in the Kamioka mine, just beneath the Mt. Ikenoyama summit, Gifu, Japan (36.42°N, 137.31°E). The 2700 m water equivalent thickness of rock covering the detector sufficiently reduces cosmic muon flux, resulting in 0.34 Hz of muon event rate.

Fig. 25 illustrates the KamLAND detector. The LS, balloon and PMT's are contained in a 9 m radius spherical stainless steel vessel. PMT 17-in 1325 in number and 554 PMTs 20-in are mounted inside the stainless steel vessel viewing the center of the LS sphere. The 6.5 m radius LS-containing balloon is positioned at the center of the stainless steel vessel, being supported and constrained by a network of Kevlar ropes. Non-scintillating mineral oil (MO) is filled between the stainless steel vessel and the LS containing balloon, providing gravity/buoyancy balance to the LS sphere, and also acting as a buffer layer against radiations into the LS from the stainless steel vessel, PMT, and everything surrounding the vessel. The MO layer is further divided into two spherical shells by 8.25 m radius transparent acrylic wall, to isolate the balloon contacting MO from the PMT/vessel exposed MO and reduce radioactive contamination around the LS.

The inner part of the 9 m radius stainless vessel is called the inner detector (ID), whereas the portion outside of the 9 m radius vessel is called the outer detector (OD). The space between the vessel and the cave wall is filled with 3200 tons of pure water, and viewed by 225, 20 in PMTs. Cosmic muons passing through the OD are tagged by the OD PMTs, by detecting Cherenkov light.

9.3. KamLAND results on geo-neutrinos

The KamLAND collaboration has reported (Araki et al., 2005a) data from an exposure of $N_p = (0.346 \pm 0.017) \times 10^{32}$ free protons over a time $T = 749$ days with a detection efficiency $\varepsilon = 68.7\%$; the effective exposure is thus $\alpha = N_p \times T \times \varepsilon = (0.487 \pm 0.025) \times 10^{32}$ proton · yr.
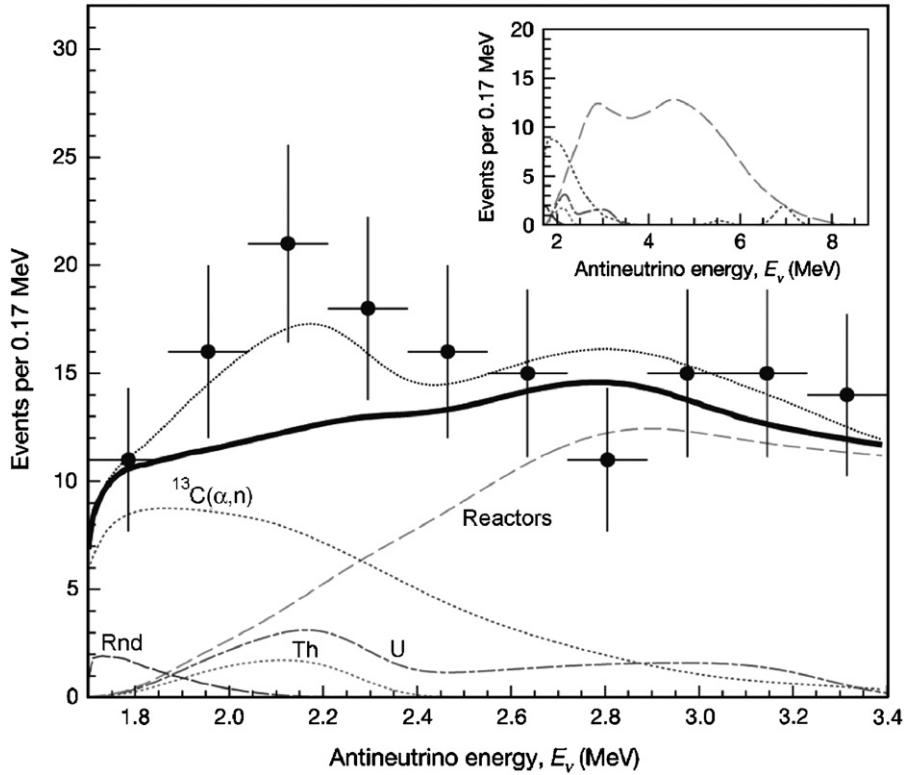
Fig. 26. The energy spectra in KamLAND, adapted from Araki et al. (2005a). Main panel, experimental points together with the total expectation (thin dotted black line). Also shown are the total expected spectrum excluding the geo-neutrino signal (thick solid black line), the expected signals from ^{238}U (dot–dashed line labeled U) and ^{232}Th (dotted line labeled Th) geo-neutrinos, and the backgrounds due to reactor antineutrinos (dashed line labeled Reactor), ^{13}C$(\alpha, n)^{16}$O reactions (dotted line labeled ^{13}C(α, n)), and random coincidences (dashed line labeled Rnd).

In the energy region where geo-neutrinos are expected, see Fig. 26, there are $C = 152$ counts, implying a statistical fluctuation[31] of ± 12.5. Of these counts, a number $R = 80.4 \pm 7.2$ are attributed to reactor events, based on an independent analysis of higher energy data. Fake geo-neutrino events,[32] originating from ^{13}C$(\alpha, n)^{16}$O reactions following the alpha decay of contaminant ^{210}Po, are estimated to be $F = 42 \pm 11$, where the error is due to a 20% uncertainty on the ^{13}C$(\alpha, n)^{16}$O cross section and a 14% uncertainty on the number of ^{210}Po decays in the detector. Other minor backgrounds account for $B = 4.6 \pm 0.2$ events.

A straight estimate by subtraction, $N(\text{U} + \text{Th}) = C - R - F - B$, with an uncertainty obtained by combining quadratically errors gives: $N(\text{U} + \text{Th}) = 25 \pm 18$.

KamLAND "rate only" analysis (Araki et al., 2005a), which includes detection systematic errors, partially correlated with background errors, gives $N(\text{U} + \text{Th}) = 25^{+19}_{-18}$; the corresponding geo-neutrino signal is thus $S(\text{U} + \text{Th}) = N(\text{U} + \text{Th})/\alpha = 51^{+39}_{-36}$ TNU.

This "rate only" study has been improved in Araki et al. (2005a) by exploiting the shape of the spectrum, with the ratio of events $N(\text{U})/N(\text{Th})$ being fixed at the chondritic (BSE) prediction. A likelihood analysis of the unbinned spectrum, see Fig. 27, yields $N(\text{U} + \text{Th}) = 28^{+16}_{-15}$ which implies $S(\text{U} + \text{Th}) = 57^{+33}_{-31}$ TNU.

As a curiosity, an analysis where both $N(\text{U})$ and $N(\text{Th})$ are left unconstrained yields as a best fit $N(\text{Th})/N(\text{U}) \approx 5.7$, which looks far from the *chondritic* value ≈ 0.25; however, both values are comfortably consistent with the data already at the 1σ level. In fact, the statistics is so poor that one cannot say anything from the KamLAND data concerning $N(\text{Th})/N(\text{U})$, see Fig. 28.

---

[31] In this section and in the following ones the quoted errors correspond to 1σ interval.

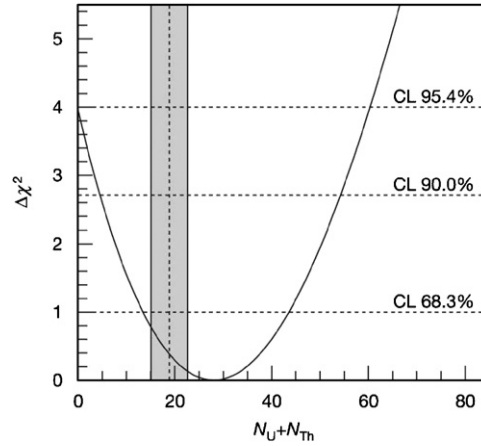[32] See Section 9.4 for a more detailed discussion of this point.

Fig. 27. Confidence intervals for the number of geo-neutrinos detected, from Araki et al. (2005a), assuming the mass ratio Th/U = 3.9. The shaded area represents the prediction of the reference model.
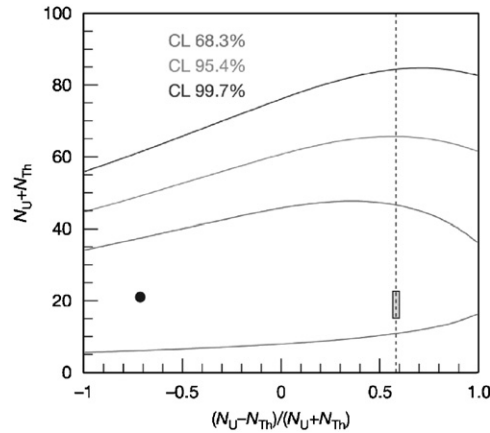

Fig. 28. Confidence intervals for the number of geo-neutrinos detected, from Araki et al. (2005a), when the mass ratio Th/U is left as free parameter. The shaded area represents the prediction of the reference model.

9.4. Fake antineutrinos and a refinement of the analysis

As a result of ^{222}Rn contamination, ^{210}Pb, which has half-life of 22 yr, is distributed throughout the detector. It produces (see Fig. 2) ^{210}Po which decays emitting α particles with a kinetic energy of 5.3 MeV. These act as a neutron source through ^{13}C$(\alpha, n)^{16}$O reactions occurring on the ^{13}C nuclei which are present in the organic scintillator. The neutrons in the ^{13}C$(\alpha, n)^{16}$O reaction are produced with kinetic energy up to 7.3 MeV. Owing to scintillation-light quenching for high-ionization density, only about one-third of this energy is converted into *visible* energy as the neutrons thermalize. The thermal neutrons are captured by protons with a mean capture time of 200 μs, producing a delayed signal identical to that from neutron inverse β-decay. In summary, one has a fake antineutrino signal.

In order to extract the true geo-neutrino signal one has to subtract these events. As already remarked, a major uncertainty originates from the ^{13}C$(\alpha, n)^{16}$O cross section.[33]

The number of ^{13}C nuclei in the fiducial volume is determined from the measured ^{13}C/^{12}C ratio in the KamLAND scintillator. On the basis of the ^{13}C$(\alpha, n)^{16}$O reaction cross-section, the α-particle energy loss in the scintillator, and

---

[33] In fact, the claim of 9 geo-neutrino events in Eguchi et al. (2003) should be dismissed: more than half of these events are to be considered as fake signals, produced from the ^{13}C$(\alpha, n)^{16}$O reaction.
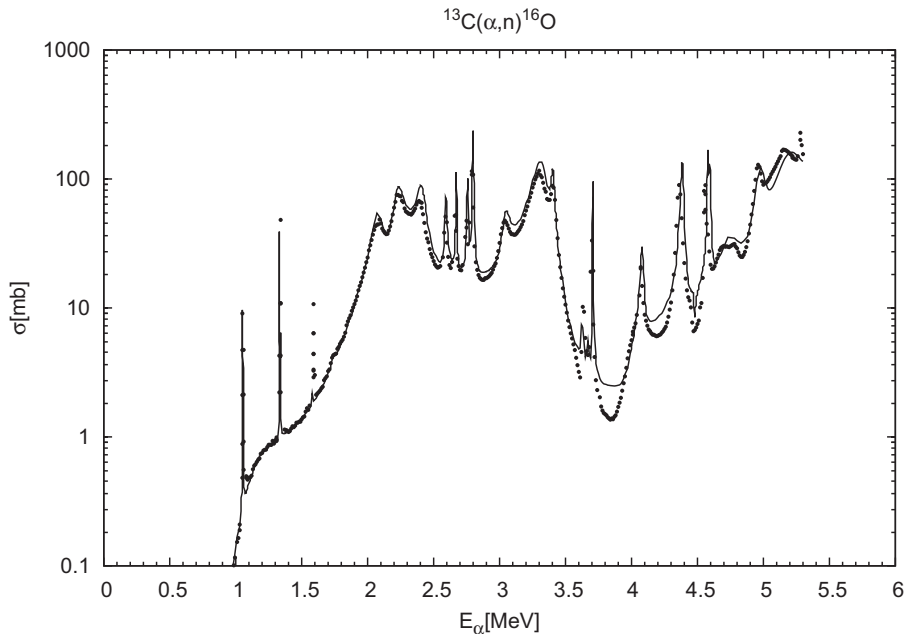
Fig. 29. Cross section of $^{13}C(\alpha, n)^{16}O$. The solid line corresponds to the JENDL compilation, dots are the experimental points from Harissopulos et al. (2005).

the number of ^{210}Po decays, the total number of neutrons produced is expected to be 93 ± 22. This error is dominated by the uncertainty in the total $^{13}C(\alpha, n)^{16}O$ reaction cross section. The values for the cross section used in Araki et al. (2005a) are taken from the JENDL (Shibata et al., 2002) compilation, which provides an R-matrix fit of relatively old data. A 20% overall uncertainty has been adopted in Araki et al. (2005a), corresponding to the accuracy claimed in the original experimental papers (see, e.g. (Shibata et al., 2002)).

Recently a series of high-precision measurements for this cross section has been performed (Harissopulos et al., 2005). In the relevant energy range (1–5.3) MeV, the absolute normalization has been determined with a 4% accuracy. The measured values are generally in very good agreement with those recommended in JENDL, see Fig. 29; however, it was found in Fiorentini et al. (2005a) that the neutron yield per α particle is 5% smaller. It follows that the number of fake geo-neutrinos is lower, $F = 40 \pm 5.8$, and geo-neutrino events obviously increase.[34]

The "rate only" analysis gives now 27^{+16}_{-15} geo-neutrino events (Fiorentini et al., 2005a), corresponding to $S(U + Th) = 55^{+33}_{-31}$ TNU. An analysis of the binned spectrum has also been performed in (Fiorentini et al., 2005a) with the result $N(U + Th) = 31^{+14}_{-13}$ counts, corresponding to $S(U + Th) = 63^{+28}_{-25}$ TNU.

These signals should be compared to $S(U + Th) = 51^{+39}_{-36}$ TNU and $S(U + Th) = 57^{+33}_{-31}$ TNU, respectively, which were obtained using the JENDL $^{13}C(\alpha, n)^{16}O$ cross section.

In summary, by using the new high-precision data on $^{13}C(\alpha, n)^{16}O$ one extracts from KamLAND data a larger geo-neutrino signal with a smaller error. This corroborates the evidence for geo-neutrinos in KamLAND data, which becomes close to 2.5σ.

9.5. Implications of KamLAND results

The geo-neutrino signal reported by KamLAND, $S(U + Th) = 57^{+33}_{-31}$ TNU, is well consistent with the BSE prediction, ≈ 37 TNU, as well as with the ≈ 56 TNU prediction of models for maximal and fully radiogenic heat flow, see Fig. 23.

---

[34] Indeed Araki et al. (2005a) mentions that an alternative analysis including the time structure of the scintillation light from different particles produced a slightly larger geo-neutrino signal, which is consistent with the result presented here.
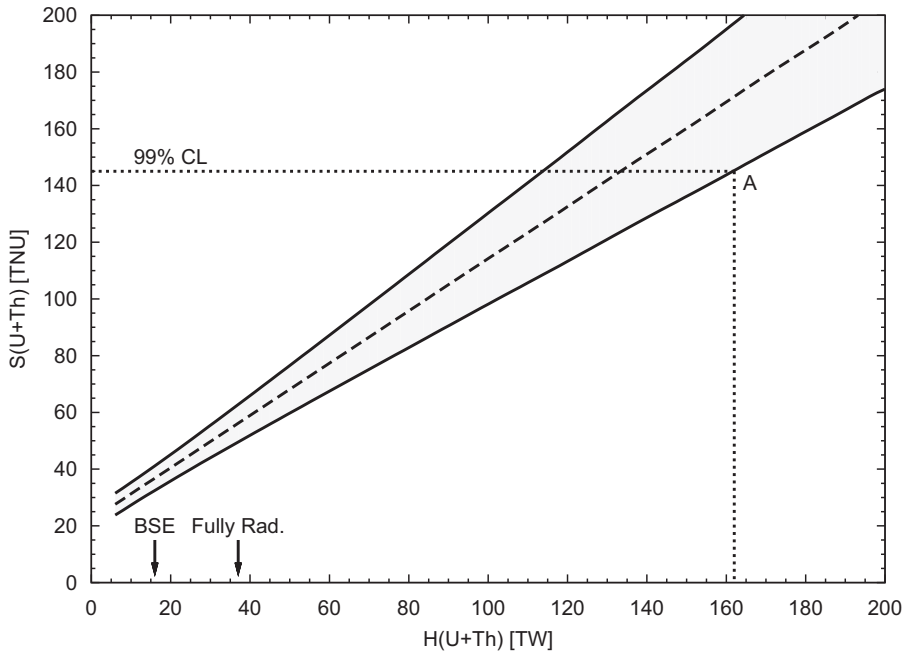
Fig. 30. The combined signal from uranium and thorium geo-neutrinos and the radiogenic heat production rate. The shaded area denotes the region allowed by geochemical and geophysical constraints. The dashed median line represents our best estimate for the relationship between signal and power.

In order to extract some more quantitative information from the data, we have to extend Fig. 23, including models which produce even larger heat and signal. These models have been built so that an arbitrary amount of uranium and thorium in the chondritic proportion is hidden in the mantle.[35] The allowed band in Fig. 30 is estimated by considering *rather extreme* models for the distributions of radioactive elements, chosen to maximize or minimize the signal for a given heat production rate (Fiorentini et al., 2005a). We also remark that, in comparison with the experimental error, the width of the allowed band is so narrow that we can limit the discussion to the median line in Fig. 30, which represents, according to Fiorentini et al. (2005a), the best estimate for the relationship between signal and power.

By considering only this median line in Fig. 30, the reported signal $S(U + Th) = 57^{+33}_{-31}$ TNU implies[36] $H(U + Th)$ $= 38^{+35}_{-33}$ TW (rate + spectrum) and the 99% confidence limit on the signal (145 TNU) corresponds to 133 TW. By including the uncertainty band of the theoretical models, one gets an upper bound of 162 TW, see point A in Fig. 30. This point corresponds to a model with a total uranium mass $m(U) = 8 \times 10^{17}$ kg, an uranium poor crust, $m_C(U) = 0.3 \times 10^{17}$ kg, the rest of the uranium being placed at the bottom of the mantle, and global chondritic thorium-to-uranium ratio.

This 162 TW upper bound is much higher than the 60 TW upper bound claimed in Araki et al. (2005a), which was obtained by using a family of geological models which are *too narrow* and are also *incompatible* with well-known geochemical and geophysical data, see the discussion in Fiorentini et al. (2005a).

We remark that the bound $H(U + Th) < 162$ TW does not add any significant information on Earth's interior, since anything exceeding $H(U + Th) = 37$ TW (i.e. $H(U + Th + K) = 44$ TW) is unrealistic. The upper limit simply reflects the large uncertainty in this pioneering experiment.

In summary, KamLAND has shown that the technology for geo-neutrino detection is now available; however, the determination of radiogenic heat power from geo-neutrino measurements is still affected by a 70% uncertainty.

---

[35] We note that models with $H(U + Th) > 37$ TW are essentially unrealistic; this portion of the graph is included just for discussing KamLAND results.

[36] By using the result from the analysis including the new values of $^{13}C(\alpha, n)^{16}O$, $S(U + Th) = 63^{+28}_{-25}$ TNU, one finds $H(U + Th) = 44^{+31}_{-27}$ TW.

An important quantity for deciding the potential of future experiments is the relationship between geo-neutrino signal and heat production. The basic parameter is the slope, dS/dH, which expresses how the experimental error translates into an uncertainty on the deduced heat production. For our models we find from Fig. 30 $dS/dH \approx 1$ TNU/TW. Discrimination between BSE, $H(U + Th) \approx 16$ TW, and fully radiogenic models $H(U + Th) \approx 37$ TW, requires a precision $\Delta H \approx 7$ TW, and thus an experiment with an accuracy $\Delta S \approx 7$ TNU.

10. Background from reactor antineutrinos

As first pointed out by Lagage (1985), antineutrinos form nuclear power plants can be a significant background for geo-neutrino detection.

An order of magnitude estimate of the flux of antineutrinos from reactor can be immediately found from the knowledge of the energy produced per fission ($E_{fis} \approx 200$ MeV) and the number of antineutrinos resulting form each fission ($N_{\bar{v}} \approx 6$). The flux at a detector lying a distance R from a reactor with thermal power W is thus

$$\Phi^{(arr)} = \langle P_{ee} \rangle \frac{N_{\bar{v}} W}{4\pi R^2 E_{fis}}. \tag{56}$$

For a typical value $W \approx 3$ GW at $R \approx 100$ km one has $\Phi^{(arr)} \approx 2.5 \times 10^5$ cm^{-2} s^{-1}. In a region where there many reactors, as near Kamioka (21 nuclear reactors already within 200 km) the signal of man-made antineutrinos exceeds that from natural radioactivity in the Earth.

In more detail, the four isotopes whose fission is the source of virtually all the reactor power are ^{235}U, ^{238}U, ^{239}Pu, and ^{241}Pu. Each isotope produces a unique neutrino spectrum through the decay of its fission fragments and their daughters. The instantaneous fission rates of the four isotopes are used as an input for the evaluation of the antineutrino spectrum. For all but ^{238}U, careful measurements of the (electron) spectrum from fission by thermal neutrons have been performed (Schreckenbach et al., 1985; Hahn et al., 1989). In Fig. 31 we show the differential antineutrino spectrum calculated assuming 10^{20} fissions s^{-1}, corresponding to about 3 GW, in a reactor 100 km from the detector. The spectrum was calculated assuming a fuel composition (0.568, 0.297, 0.078, 0.057) for (^{235}U, ^{239}Pu, ^{238}U, ^{241}Pu);
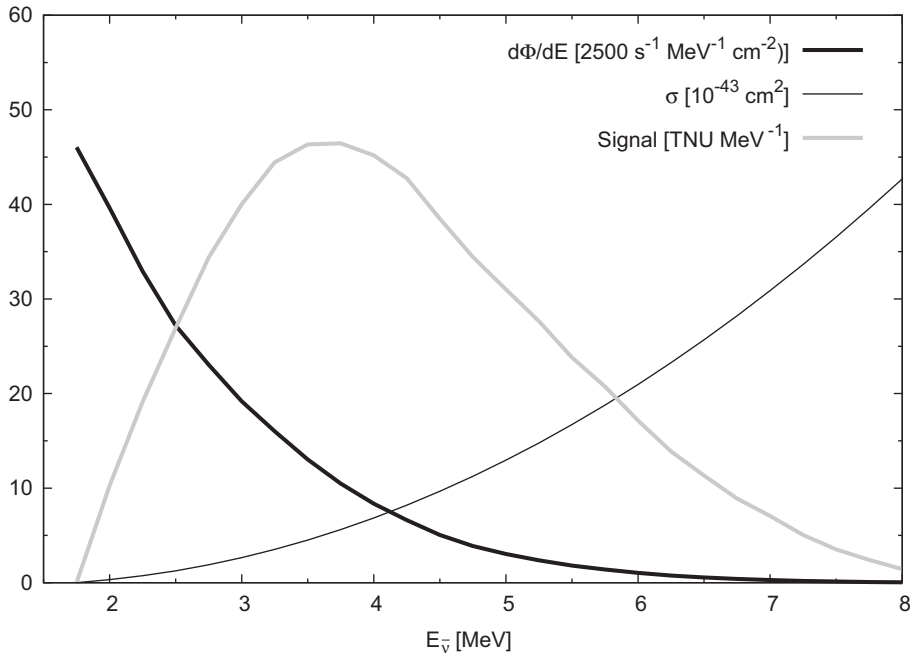

Fig. 31. Antineutrinos from reactors. The differential produced flux (no oscillations) in units of 2500 $\bar{v}_e$ s^{-1} cm^{-1} MeV^{-1}, inverse beta decay cross section in units of 10^{-43} cm^2, and the corresponding signal in TNU MeV^{-1}. The flux corresponds to 10^{20} fissions s^{-1} (or about 3 GW) in a reactor 100 km from the detector.
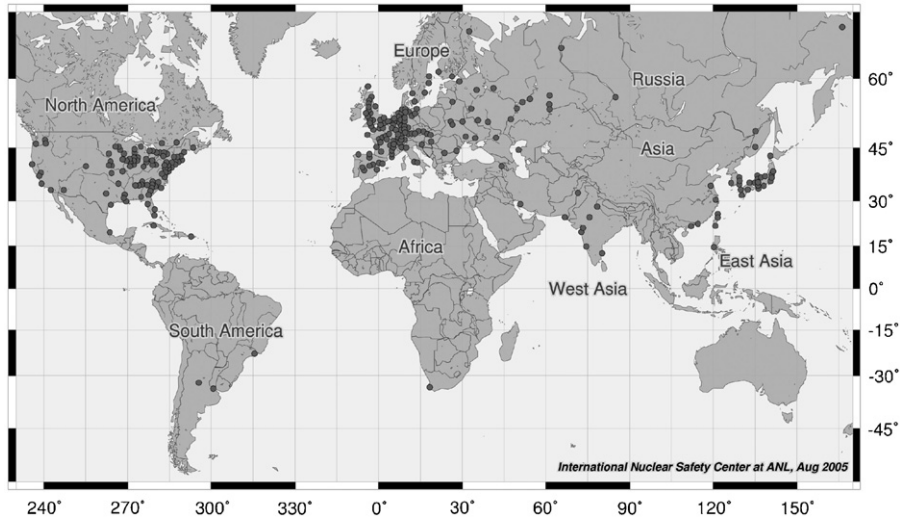
Fig. 32. Nuclear power plants in the world, from http://www.insc.anl.gov/pwrmaps/map/world_map.php.
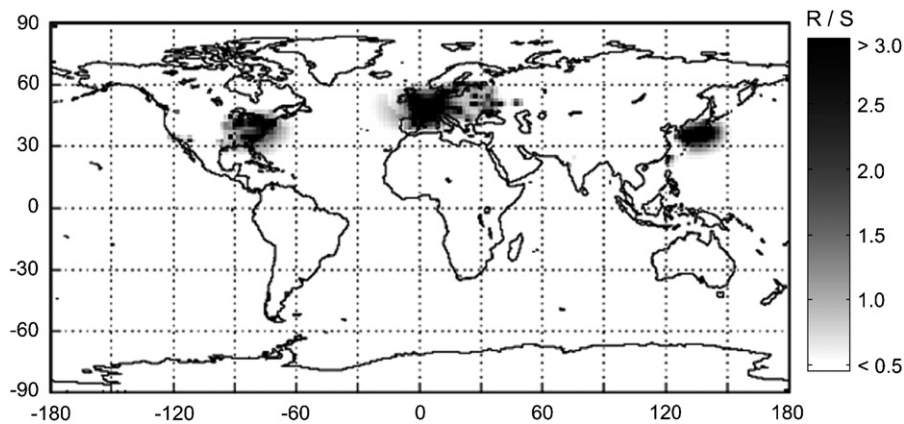

Fig. 33. The ratio of reactor anti-neutrino events (in the geo-neutrino energy region) to the expected geo-neutrino events all over the globe.

for ^{239}Pu and ^{241}Pu we used spectra from Hahn et al. (1989), for ^{235}U spectrum from Schreckenbach et al. (1985), and for ^{238}U the spectrum from Vogel et al. (1981) corresponding to 0.5 MeV neutrons. For an extensive review of reactor antineutrinos see Bemporad et al. (2002).

About 450 reactors are operational all over the world. If they all work at full power, this results in a total heat production of about 1 TW, just a factor 30 smaller than the natural heat flow from the Earth. The man-made antineutrino luminosity of the Earth is thus $\approx 10^{23}\,\mathrm{s^{-1}}$, a factor 10 below the natural luminosity in geo-neutrinos from U and Th chains.

Maps of the nuclear power plants in the world (see Fig. 32), together with information on power and operational status are provided by several organizations, e.g., the International Nuclear Safety Center, United Nations Environment Programme.

The ratio r of reactor event rate in the geo-neutrino energy window to the geo-neutrino signal $S(\mathrm{U} + \mathrm{Th})$ predicted by the reference model is shown in Fig. 33 all over the globe and its inverse $s = 1/r$ in Table 17 for eight locations. Kamioka ($s \approx 0.14$) is clearly one of the worst locations over the globe. At Gran Sasso and Sudbury the geo-neutrino event are comparable to reactor events, whereas a place like Hawaii looks much more favorable.

11. Future prospects

In summary, KamLAND has shown that the technique for exploiting geo-neutrinos in the investigation of the Earth's interior is now available. On the other hand, the determination of radiogenic heat power from geo-neutrino measurements is still affected by a 70% uncertainty. The best fit of the KamLAND result implies a radiogenic heat production close to the prediction of maximal and fully radiogenic model; however, the BSE prediction is within 1σ from it. In order to discriminate among different models of heat production in the Earth an accuracy of at least ± 7 TW is necessary. The relationship between geo-neutrino signal and radiogenic heat, $dS/dH \approx 1$ TNU/TW, implies that the experimental error has to be ± 7 TNU, i.e. a factor of four improvement with respect to present.

It looks to us that the following questions are relevant for the future:

- How shall we have definite (at least 3σ) evidence of geo-neutrinos?
- How much uranium and thorium are in the Earth's crust?
- How much in the mantle?
- What can be said about the core?

A preliminary point for establishing suitable detector locations is the reactor background. Fig. 33 shows the ratio of reactor events (in the geo-neutrino energy region) to the expected geo-neutrino events all over the globe. KamLAND location is obviously one of the worst for the study of geo-neutrinos.

The potential of different locations is summarized in Table 17, where we present the separate contributions to the geo-neutrino signal rate from crust and mantle according to our reference model, S, together with the reactor event rate in the geo-neutrino energy window, R. In the same Table we present two merit figures:

(i) $\Delta S_0 = \sqrt{S + R}$ is the square root of the total counts expected in a detector with an effective exposure of $\alpha_0 = 10^{32}$ proton yr; it represents the limiting (i.e. neglecting backgrounds other than reactors, uncertainties of oscillation parameters…) statistical error on the geo-neutrino signal which might be achieved with such a detector. For an exposure α the statistical error is $\Delta S = \Delta S_0 \times \sqrt{\alpha_0/\alpha}$.
(ii) The ratio of geo-neutrino events to reactors events in the geo-neutrino energy window $s = S/R$.

With additional statistics KamLAND should be capable of providing 3σ evidence of geo-neutrinos, but discrimination between BSE and fully radiogenic models definitely requires new detectors, with class and size similar to that of KamLAND, far away from nuclear power plants. Borexino at Gran Sasso should reach the 3σ evidence, but cannot go much further due to its relatively small size.

At Sudbury, SNO$^+$ with liquid scintillator will have excellent opportunities to determine the uranium mass in the crust, which accounts for about 80% of the geo-neutrino signal. This will provide an important test about models for the Earth's crust.

Table 17
The geo-neutrino (U + Th) signal rate expected from the crust S_C, from the mantle S_M, and their sum S, together with the reactor event rate R in the geo-neutrino energy window

Location	S_C	S_M	S	R	ΔS_0	s
Pyhasalmi	42.5	9.0	51.5	27.2	8.9	1.9
Homestake	42.3	9.0	51.3	9.4	7.8	5.5
Baksan	41.8	9.0	50.8	11.8	7.9	4.3
Sudbury	41.8	9.0	50.8	53.7	10	0.9
Gran Sasso	31.7	9.0	40.7	35.1	8.7	1.2
Kamioka	25.5	9.0	34.5	230	16	0.15
Curacao	23.5	9.0	32.5	3.3	6.0	9.9
Hawaii	3.5	9.0	12.5	1.4	3.7	9.2

ΔS_0 represents the limiting statistical error for an effective exposure $\alpha_0 = 10^{32}$ proton yr. All rates are in TNU. The s factor is the ratio between the geo-neutrino events and reactor events in the geo-neutrinos energy window.

A detector at Hawaii, very far from the continental crust, will be mainly sensitive to the mantle composition. We remind that the amount of radioactive materials in this reservoir is the main uncertainty of geological models of the Earth. Due to the absence of nearby reactors, the geo-neutrino signal can be measured with a small error, such that different models for terrestrial heat generation can be discriminated. On the other hand it is necessary that non-reactor backgrounds be kept at very small value.

For the very long term future, one can speculate about completely new detectors, capable of providing (moderately) directional information. These should allow the identification of the different geo-neutrino sources (crust, mantle and possibly core) in the Earth; in summary, *se son rose fioriranno*.[37]

Acknowledgments

Appendix A. Analytical estimates of the geo-neutrino flux

A.1. The flux from a spherical shell

Assuming spherical symmetry, the (produced) antineutrino flux at a detector on the Earth surface originated from a spherical shell centered at the Earth center and with radii R_1 and R_2 (see Fig. 34) is

$$\Phi(X) = \frac{A_X R_\oplus}{2} \left[\frac{R_2}{R_\oplus} - \frac{1}{2} \frac{R_\oplus^2 - R_2^2}{R_\oplus^2} \log \left(\frac{R_\oplus + R_2}{R_\oplus - R_2} \right) - \frac{R_1}{R_\oplus} \right.$$
$$\left. + \frac{1}{2} \frac{R_\oplus^2 - R_1^2}{R_\oplus^2} \log \left(\frac{R_\oplus + R_1}{R_\oplus - R_1} \right) \right], \tag{A.1}$$

where A is the specific geo-neutrino activity, i.e. the number of geo-neutrinos produced per unit time and volume, and X stands for U or Th.

From Eq. (A.1) one derives simple expressions for the contributions of the crust and of the mantle, when treating them as spherical shells of uniform density of heat generating elements.

A.2. Flux from the crust

In this case $R_2 = R_\oplus$ and $R_1 = R_\oplus - \Delta$, where $\Delta \approx 30$ km is the thickness of the crust. Since $\Delta \ll R_\oplus$, Eq. (A.1) simplifies to

$$\Phi_C(X) \approx \frac{A_X \Delta}{2} \left[1 + \log \frac{2R_\oplus}{\Delta} \right]. \tag{A.2}$$

In terms of the mass of the element X contained in the crust $m_C(X)$:

$$A_X \approx \frac{n_X m_C(X)}{m_X \tau_X 4\pi R_\oplus^2 \Delta}, \tag{A.3}$$

where m_X and τ_X are the mass and lifetime of the nucleus X and n_X is the number of antineutrino produced in the decay chain. This gives

$$\Phi_C(X) \approx \frac{n_X m_C(X)}{m_X \tau_X 8\pi R_\oplus^2} \left[1 + \log \frac{2R_\oplus}{\Delta} \right]. \tag{A.4}$$

Note that this result is weakly dependent on Δ.

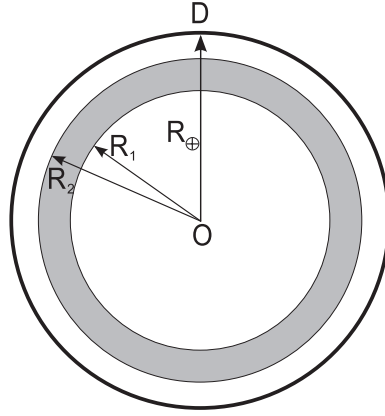[37] If they are roses, they will blossom, i.e. time will tell.

Fig. 34. Relevant variables for parameterizing source positions in the Earth relative to the detector D and spherical shell whose flux is given by Eq. (A.1).

By inserting the appropriate constants one finds

$$\Phi_C(U) = 5.1 \times 10^6 \text{ cm}^{-2}\text{s}^{-1} \times m_C(U), \tag{A.5}$$

and

$$\Phi_C(Th) = 1.1 \times 10^6 \text{ cm}^{-2}\text{s}^{-1} \times m_C(Th), \tag{A.6}$$

where U and Th masses are measured in units of 10^{17} kg.

For the values used in the reference model ($m_C(U) = 0.353$, $m_C(Th) = 1.38$) one finds

$$\Phi_C(U) = 1.8 \times 10^6 \text{ cm}^{-2}\text{s}^{-1}, \quad \Phi_C(Th) = 1.5 \times 10^6 \text{ cm}^{-2}\text{s}^{-1}. \tag{A.7}$$

This provides an order of magnitude estimate of the flux originated from the crust, however, as shown in Table 12, there can be substantial differences among different locations.

A.3. Flux from the mantle

In this case $R_2 = R_\oplus$ so that Eq. (A.1) simplifies to

$$\Phi_M(X) \approx \frac{A_X R_\oplus}{2} \left[\frac{R_\oplus - R_M}{R_\oplus} + \frac{1}{2} \frac{R_\oplus^2 - R_M^2}{R_\oplus^2} \log\left(\frac{R_\oplus + R_M}{R_\oplus - R_M} \right) \right], \tag{A.8}$$

where $R_M \approx 3500$ km is the inner radius of the mantle. The specific activity is in this case

$$A_X = \frac{3 n_X m_M(X)}{m_X \tau_X 4\pi (R_\oplus^3 - R_M^3)}. \tag{A.9}$$

This gives

$$\Phi_M(X) \approx \frac{n_X m_M(X)}{m_X \tau_X 8\pi R_\oplus^2} \frac{3 R_\oplus^2}{R_\oplus^2 + R_M R_\oplus + R_M^2} \left[1 + \frac{R_\oplus + R_M}{2 R_\oplus} \log \frac{R_\oplus + R_M}{R_\oplus - R_M} \right]. \tag{A.10}$$

By inserting the appropriate constants one finds

$$\Phi_M(U) = 2.30 \times 10^6 \text{ cm}^{-2}\text{s}^{-1} \times m_M(U) \tag{A.11}$$

and

$$\Phi_{\mathrm{M}}(\mathrm{Th}) = 0.50 \times 10^6 \, \mathrm{cm}^{-2}\mathrm{s}^{-1} \times m_{\mathrm{M}}(\mathrm{Th}). \tag{A.12}$$

For the values used in the reference model ($m_{\mathrm{M}}(\mathrm{U}) = 0.451$, $m_{\mathrm{M}}(\mathrm{Th}) = 1.76$) one has

$$\Phi_{\mathrm{M}}(\mathrm{U}) = 1.04 \times 10^6 \, \mathrm{cm}^{-2}\mathrm{s}^{-1}, \quad \Phi_{\mathrm{M}}(\mathrm{Th}) = 0.88 \times 10^6 \, \mathrm{cm}^{-2}\mathrm{s}^{-1}. \tag{A.13}$$

These values are in agreement with the numerical calculation used for the reference model, to the level of about 9%.

Appendix B. The contributed flux as function of the distance

Again assuming spherical symmetry, the contribution to the flux from the portion of the crust at a distance x from the detector is

$$\frac{\mathrm{d}\Phi_{\mathrm{C}}}{\mathrm{d}x} = \begin{cases} A/2, & x \leqslant \Delta, \\ (A/2) \times (\Delta/x), & \Delta \leqslant x \leqslant 2R_{\oplus}. \end{cases} \tag{B.1}$$

By using Eq. (A.2) the relative contribution is

$$\frac{1}{\Phi_{\mathrm{C}}} \frac{\mathrm{d}\Phi_{\mathrm{C}}}{\mathrm{d}x} = \begin{cases} (1 + \log(2R_{\oplus}/\Delta))^{-1}, & x \leqslant \Delta, \\ (1 + \log(2R_{\oplus}/\Delta))^{-1} \times (\Delta/x), & \Delta \leqslant x \leqslant 2R_{\oplus}. \end{cases} \tag{B.2}$$

This analytical estimate is shown in Fig. 35 together with the corresponding numerical result for the calculation of the reference model.

A similar calculation can be made for the mantle. The result for a single- or double-shell mantle model is presented in Fig. 36 together with the numerical result of the reference model, which considered 25 distinct shells.
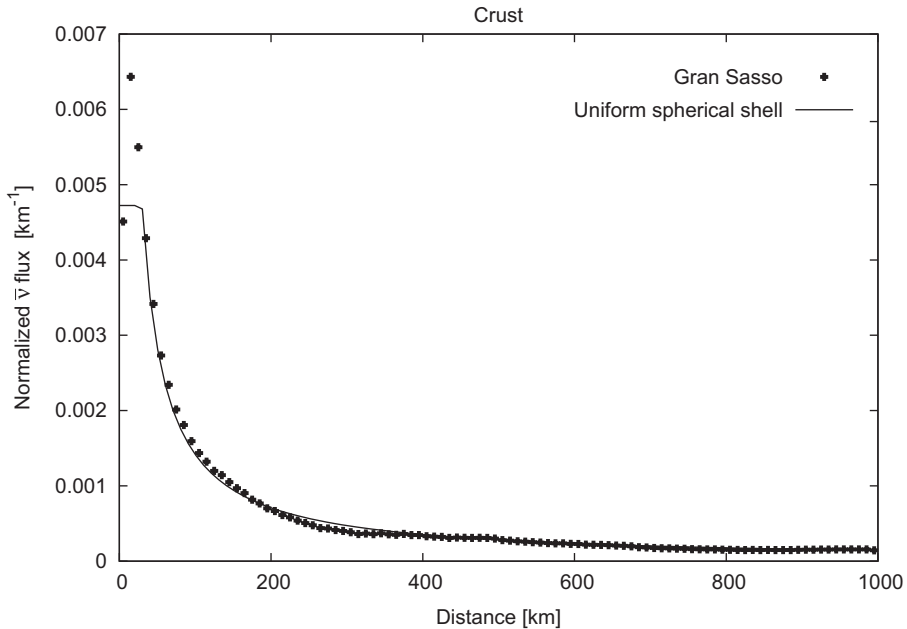

Fig. 35. Antineutrino flux from the crust as function of the distance from a detector at the Gran Sasso underground laboratory, normalized to an unitary total flux. Points corresponds to a detailed reference model (Mantovani et al., 2004). The thin line is the result of a crust model with uniform density spread over a spherical shell of thickness 30 km with the detector at its vertex, Eq. (B.2).
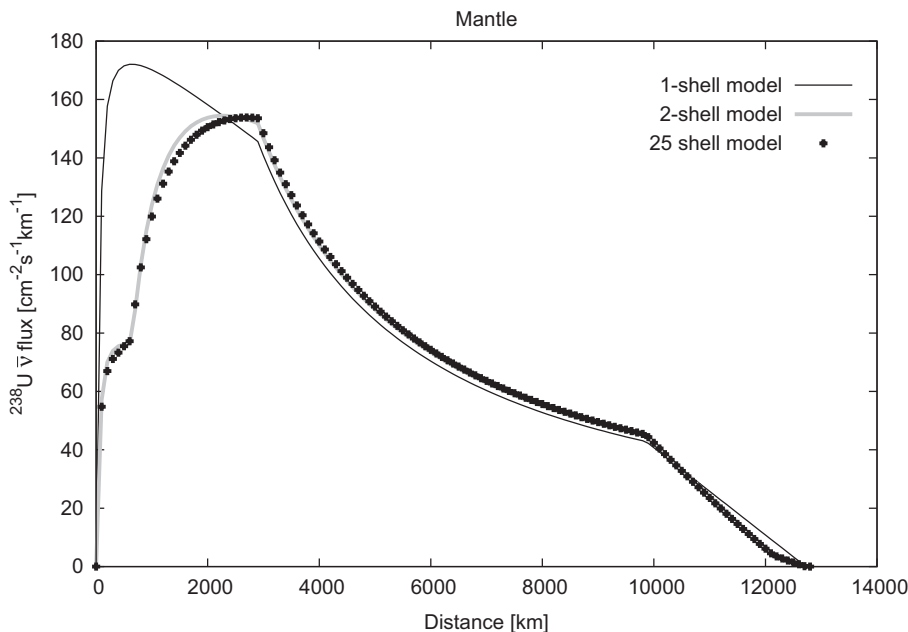
Fig. 36. Uranium antineutrino flux from the mantle as function of the distance from the detector. Points corresponds the 25-shell reference model (Dziewonski and Anderson, 1981). The thin line describes a uniform uranium density model with the same mass, with uniform uranium density $\rho_U = 5.16 \times 10^{-8}$ g cm^{-3} from a depth of 32 km up to one of 3478 km: this can be obtained with an average density $\rho = 5$ g cm^{-3} and an average abundance $a_U = 10.32$ ppb. The thick gray line shows a two-shell model, with uranium density 2.29×10^{-8} g cm^{-3} in the upper mantle and 6.48×10^{-8} g cm^{-3} in the lower mantle: this can be obtained with average densities 3.5 and 5 g cm^{-3} and average abundances $a_U = 6.55$ ppb and $a_U = 12.96$ ppb, respectively.

While the uniform model overestimates the contribution from distances smaller than about 2000 km, the two-shell model is quite close to the reference model.[38]

Appendix C. A comment on geological uncertainties

An assessment of uncertainties is most important for understanding the significance of the theoretical predictions and the relevance of geo-neutrino experiments.

In the case of geological measurements, error determination is admittedly more complex than for laboratory measurements since the quantity to be determined is often indirectly measured or extrapolated from an incomplete set of samples, important examples being the elemental abundances in the different Earth's reservoirs, and individual results are often published without quoting an error. Nevertheless it is important to have an—even if rough—estimate of the uncertainties and to propagate it onto the predicted signals.

In the following we suggest an approach for estimating and combining errors of the geological quantities relevant for geo-neutrino calculations.

C.1. Elemental abundances: selection and treatment of data

As for any experimental quantity, it is not possible to give completely objective criteria for the choice of data. It is the somewhat subjective judgment of experts in the field that selects the relevant data and uses them to extract the "best" educated estimate and its error.

---

[38] In fact the density of uranium in the mantle in our reference model is not constant for two reason: the total density grows with depth from $\rho = 3.38$ g cm^{-3} at $R = 6346$ km (depth 32 km) to $\rho = 5.41$ g cm^{-3} at $R = 2900$ km (we used 25 different layers (Dziewonski and Anderson, 1981)) and the abundance of uranium changes from $a = 6.5$ ppb in the upper mantle (above a depth of about 632 km) to $a = 13.2$ ppb in the lower mantle.

One has the choice of making his own compilation and selection of data, as in Mantovani et al. (2004) or of using some existing compilation, as in Fogli et al. (2005).

We believe that a robust procedure is to select all published results after excluding measurements that have been superseded or included in later results, or that are dependent on measurements already included, measurements that are clearly inconsistent with known more reliable information or that are based on questionable assumptions. Then all the selected measurements are averaged and the estimated standard deviation of the mean (the standard deviation of the results divided by $\sqrt{n-1}$ where n is the number of independent results) is used as error. This procedure implies that new independent measurements consistent with the existing ones reduce the error and new information can exclude inconsistent results.

In fact this is basically the procedure adopted by the Review of Particle Physics (Yao and et al., 2006), with the addition that selected data are weighted using their errors. However, geological abundances are often published without standard errors: in fact it is not easy to give a reliable estimate of the error, since the final number depends not only on the measurements of the individual samples, but also on how the samples are chosen to be representative of a much larger portion of material.

A comprehensive critical compilation of data and estimation of errors is needed.

We remark that, when discussing uncertainties of crust and upper mantle abundances, in the past our group followed a different procedure that should be upgraded: we have considered the spread of published data as a full-range error, equivalent in same, sense to a 3σ error. The numerical difference between the two procedures can be appreciated by looking at Table 9. Given the small number of independent published data, this procedure underestimates the error compared to the standard deviation divided by $\sqrt{n-1}$: the case of only two data is paradigmatic. Moreover, the errors can only become larger the more data become available.

C.2. Global and local source distributions: errors on theoretical hypotheses

In several instances, sought-after quantities depend on theoretical hypotheses or unknown parameters, e.g., distribution of elements in the mantle (see Section 4.4) or regional sources as a subducting slab under Japan (see Section 7.2). In such cases, we suggest to consider the minimal and maximal result as extremes of the $\pm 3\sigma$ interval, so that the $\pm 3\sigma$ interval cover the complete range of theoretical hypotheses.

Our group has basically followed the above-described procedure using full-range errors that included the spread of theoretical hypotheses.

C.3. Combining errors: correlations

When building a reference model for geo-neutrinos, there are several sources of uncertainties (abundances, source distributions, oscillation parameters, cross sections, etc.) and one needs to combine them to obtain the total error. When errors are independent, one can combine them quadratically, but when they are correlated (anti-correlated), this procedure underestimates (overestimates) the total error. Correlation between U and Th abundances constitutes an important example: the ratio of these abundances has a smaller fluctuation than the individual abundances, indicating strong correlation. In fact, the only other important (anti)correlation is the one between abundances in the crust and in the mantle, if we impose that the total element mass (in the mantle and crust) be constrained to either the BSE value or to a given value used as free parameter.

In principle, it would be nice to have not only good determination of errors on the abundances, but also of their correlations. Given the present situation, we believe that a correct and robust approach is to select data and use them in such a way as to reduce correlation.

As an example the U/Th correlation can be tackled by performing the complete calculation for uranium neutrinos and than scaling the result for U+Th using a fixed ratio of U/Th: this procedure is equivalent to a 100% correlation (correlation coefficient $\rho = 1$) and slightly overestimates the error.

This approach was used in Mantovani et al. (2004) and also in this paper. In fact if one uses $\rho = 0.94$ as in Fogli et al. (2005) the part of the error on the total signal due to crust abundances changes by about 1%. For instance the total error of our theoretical prediction at Kamioka is 5.9 TNU: if this error were due only to crust abundances, the use of $\rho = 0.94$ instead of $\rho = 1$ would reduce the error to 5.85 TNU: the error itself is not known with that precision.

The correlation between mantle and crust abundances is avoided not using mantle abundances as variables, but instead total (crust plus mantle) masses.

Note added in proof

After this paper was submitted the KamLAND collaboration has presented new results on geo-neutrinos at the 10th International Conference on Topics in Astroparticle and Underground Physics (TAUP), September 11–15, 2007, Sendai, Japan. Assuming the chrondritic Th/U mass ratio 3.9, they find a preliminary geo-neutrino signal of $39.4^{+14.4}_{-14.3}$ TNU. This result provides an almost 3σ evidence for geo-neutrino and the central value is close to the prediction of the reference model (Mantovani et al., 2004) 34.8 ± 5.9 TNU (see Table 11).

References

(SAGE), Abdurashitov, J.N., et al., 2002. J. Exp. Theor. Phys. 95, 181.

Albarède, F., van der Hilst, R.D., 1999. EOS Trans. AGU 80, 535–537.

(Borexino), Alimonti, G., et al., 1998. Astropart. Phys. 8, 141.

(GNO), Altmann, M., et al., 2000. Phys. Lett. B 490, 16.

Anderson, D.L., 2005. Energetics of the Earth and the missing heat source mystery. Technical Report, www.MantlePlume.org, available online at www.mantleplumes.org/Energetics.html.

Araki, T., et al., 2005a. Nature 436, 499.

(KamLAND), Araki, T., et al., 2005b. Phys. Rev. Lett. 94, 081801.

Bahcall, J.N., 1989. Neutrino Astrophysics. Cambridge University Press, Cambridge.

Bassin, C., Laske, G., Masters, G., 2000. EOS Trans. AGU 81, F897.

Bemporad, C., Gratta, G., Vogel, P., 2002. Rev. Mod. Phys. 74, 297.

Castellani, V., Degl'Innocenti, S., Fiorentini, G., Lissia, M., Ricci, B., 1997. Phys. Rep. 281, 309.

Chen, M.C., 2006. Earth Moon Planets 99, 221.

Corgne, A., Keshav, S., Fei, Y., McDonough, W.F., 2007. Earth Planet Sci. Lett. 256, 567.

Daniel, H., 1968. Rev. Mod. Phys. 40, 659.

Davies, J.H., Brodholt, J.P., Wood, B.J. (Eds.), 2002. Chemical Reservoirs and Convection in the Earth's Mantle. Royal Society London.

Domogatsky, G., Kopeikin, V., Mikaelyan, L., Sinev, V., 2006. Phys. Atom. Nucl. 69, 1894.

Dye, S.T., Guillian, E., Learned, J.G., Maricic, J., Matsuno, S., Pakvasa, S., Varner, G., Wilcox, M., 2006. Earth Moon Planets 99, 241.

Dziewonski, A.M., Anderson, D.L., 1981. Phys. Earth Planet. Inter. 25, 297.

Eder, G., 1966. Nucl. Phys. 78, 657.

(KamLAND), Eguchi, K., et al., 2003. Phys. Rev. Lett. 90, 021802.

Enomoto, S., 2005. Neutrino geophysics and observation of geo-neutrinos at KamLAND. Ph.D. Thesis, Tohoku University, available online at http://www.awa.tohoku.ac.jp/∼sanshiro/research/SanshirosDoctoralDissertation.pdf.

Enomoto, S., Ohtani, E., Inoue, K., Suzuki, A., 2005. eprint hep-ph/0508049.

Fields, B.D., Hochmuth, K.A., 2006. Earth Moon Planets 99, 155.

Fiorentini, G., Lasserre, T., Lissia, M., Ricci, B., Schönert, S., 2003a. Phys. Lett. B 558, 15.

Fiorentini, G., Mantovani, F., Ricci, B., 2003b. Phys. Lett. B 557, 139.

Fiorentini, G., Lissia, M., Mantovani, F., Vannucci, R., 2004. PoS AHEP003, 035.

Fiorentini, G., Lissia, M., Mantovani, F., Ricci, B., 2005a. Phys. Lett. B 629, 77.

Fiorentini, G., Lissia, M., Mantovani, F., Vannucci, R., 2005b. Nucl. Phys. Proc. Suppl. 145, 170.

Fiorentini, G., Lissia, M., Mantovani, F., Vannucci, R., 2005c. Earth Planet. Sci. Lett. 238, 235.

Fiorentini, G., Lissia, M., Mantovani, F., Vannucci, R., 2005d. Phys. Rev. D 72, 033017.

Firestone, R.B., Shirley, V.S. (Eds.), 1996. Table of Isotopes, Wiley, eighth edn, we use the numerical values available online: http://isotopes.lbl.gov/education/isotopes.htm.

Fogli, G.L., Lisi, E., Palazzo, A., Rotunno, A.M., 2005. Phys. Lett. B 623, 80.

Fogli, G.L., Lisi, E., Palazzo, A., Rotunno, A.M., 2006. Earth Moon Planets 99, 111.

Gao, S., Luo, T., Zhang, B., Zhang, H.Y.W., Zhao, Z., Hu, Y., 1998. Geochim. Cosmochim. Acta 62, 1959.

Gratta, G., 1999. CERN Cour. 39N3, 22.

Hahn, A.A., et al., 1989. Phys. Lett. B 218, 365.

Hall, H.T., Rama Murthy, V., 1971. Earth Planet. Sci. Lett. 11, 239.

(GALLEX), Hampel, W., et al., 1999. Phys. Lett. B 447, 127.

Harissopulos, S., et al., 2005. Phys. Rev. C 72, 062801.

Herndon, J.M., 1996. Proc. Natl. Acad. Sci. USA 93, 646.

Herndon, J.M., 1998. EOS Trans. AGU 79, 451.

Herndon, J.M., 2003. Proc. Natl. Acad. Sci. USA 100, 3047.

Herndon, J.M., Hollenbach, D.F., 2001. Proc. Natl. Acad. Sci. USA 98, 11085.

von Herzen, R., Davis, E.E., Fisher, A., Stein, C.A., Pollack, H.N., 2005. Tectonophysics 409, 193.

van der Hilst, R.D., Karason, H., 1999. Science 283, 1885.

Hofmann, A.W., 1997. Nature 385, 219.

Hofmann, A.W., 2003. Nature 425, 24.

Hofmeister, A.M., Criss, R.E., 2005a. Tectonophysics 395, 159.

Hofmeister, A.M., Criss, R.E., 2005b. Tectonophysics 409, 199.

Holland, H.D., Turekian, K.K. (Eds.), 2003. Treatise on Geochemistry. Elsevier-Pergamon, Oxford.

Javoy, M., 1995. Geophys. Res. Lett. 22, 2219.

Jochum, K.P., Hofmann, A.W., Ito, E., Seufert, H.M., White, W.M., 1983. Nature 306, 431.

Kelley, K.A., Beard, G.B., Peters, R.A., 1959. Nucl. Phys. 11, 492.

Kellogg, L.H., Hager, B.H., van der Hilst, R.D., 1999. Science 283, 1881.

Kobayashi, M., Fukao, Y., 1991. Geophys. Res. Lett. 18, 633.

Krauss, L.M., Glashow, S.L., Schramm, D.N., 1984. Nature 310, 191.

Lagage, P.O., 1985. Nature 316, 420.

Laske, G., Masters, G., Reif, C., 2001. Crust 2.0 a new global crustal model at 2×2 degrees, available online at http://mahi.ucsd.edu/Gabi/rem.dir/crust/crust2.html.

Learned, J.G., Dye, S.T., Pakvasa, S., 2006. Earth Moon Planets 99 1, Neutrino Geophysics Proceedings of Neutrino Science 2005, (Honolulu, Hawaii, December 2005).

Lewis, J.S., 1971. Earth Planet. Sci. Lett. 11, 130.

Mantovani, F., Carmignani, L., Fiorentini, G., Lissia, M., 2004. Phys. Rev. D 69, 013001.

Marx, G., 1969. Czech. J. Phys. 19, 1471.

McDonough, W.F., 1999. In: Marshall, C.P., Fairbridge, R.F. (Eds.), Encyclopedia of Geochemistry. Kluwer Academic Publishers, Dordrecht, pp. 151–156.

McDonough, W.F., 2003. In: C.R.W. (Ed.), The Mantle and Core, Elsevier-Pergamon, Oxford, vol. 2 of Treatise on Geochemistry, pp. 547–568.

McDonough, W.F., Sun, S.S., 1995. Chem. Geol. 120, 223.

McKeown, R.D., Vogel, P., 2004. Phys. Rep. 394, 315.

de Meijer, R.J., Smit, F.D., Brooks, F.D., Fearick, R.W., Woertche, H.J., Mantovani, F., 2006. Earth Moon Planets 99, 193.

Miramonti, L., 2003. First Yamada Symposium on Neutrinos and Dark Matter in Nuclear Physics—Japan, eprint hep-ex/0307029.

Nunokawa, H., Teves, W.J.C., Zukanovich Funchal, R., 2003. JHEP 11, 020.

Palme, H., O'Neill, H.S.C., 2003. In: Carlson, R.W. (Ed.), The Mantle and Core, vol. 2 of Treatise on Geochemistry. Elsevier-Pergamon, Oxford, pp. 1–38.

Pollack, H.N., Hunter, S.J., Johnson, J.R., 1993. Rev. Geophys. 31, 267.

Raghavan, R.S., 2002. eprint hep-ex/0208038.

Raghavan, R.S., et al., 1998. Phys. Rev. Lett. 80, 635.

Rama Murthy, V., van Westrenen, W., Fei, Y.-w., 2003. Nature 423, 163.

Rothschild, C.G., Chen, M.C., Calaprice, F.P., 1998. Geophys. Res. Lett. 25, 1083.

Rudnick, R.L., Fountain, D.M., 1995. Rev. Geophys. 33, 267.

Rudnick, R.L., Gao, S., 2003. In: Rudnick, R.L. (Ed.), The Crust, vol. 3 of Treatise on Geochemistry. Elsevier-Pergamon, Oxford, pp. 1–64.

Salter, V.J.M., Stracke, A., 2004. Geochem. Geophys. Geosyst. 5 (Q05004),

van Schmus, W.R., 1995. In: Ahrens, T.J. (Ed.), Global Earth Physics: A Handbook of Physical Constants, vol. 1 of Reference Shelf American Geophysical Union. pp. 283–291.

Schreckenbach, K., Colvin, G., Gelletly, W., Von Feilitzsch, F., 1985. Phys. Lett. B 160, 325.

Shibata, K., Kawano, T., Nakagawa, T., Iwamoto, O., Katakura, J., Fukahori, T., Chiba, S., Hasegawa, A., Murata, H.M.T., Ohsawa, T., Nakajima, Y., Yoshida, T., et al., 2002. J. Nucl. Sci. Technol. 39 1125, available online at http://wwwndc.tokai-sc.jaeri.go.jp/jendl/jendl.html.

Strumia, A., Vissani, F., 2003. Phys. Lett. B 564, 42.

Strumia, A., Vissani, F., 2005. Nucl. Phys. B 726, 294.

Taylor, S.R., McLennan, S.M., 1985. The Continental Crust: its Composition and Evolution. Blackwell Scientific, Oxford.

Taylor, S.R., McLennan, S.M., 1995. Rev. Geophys. 33, 241.

Togashi, S., Imai, N., Okuyama-Kusunose, Y., Tanaka, T., Okai, T., Koma, T., Murata, Y., 2000. Geochem. Geophys. Geosyst. 1 2000GC00083.

Undagoitia, T.M., von Feilitzsch, F., Göger-Neff, M., Hochmuth, K.A., Oberauer, L., Potzel, W., Wurm, M., 2006. J. Phys. Conf. Ser. 39, 287.

Verhoogen, J., 1980. Energetics of the Earth. National Academy of Sciences.

Vogel, P., Beacom, J.F., 1999. Phys. Rev. D 60, 053003.

Vogel, P., Schenter, G.K., Mann, F.M., Schenter, R.E., 1981. Phys. Rev. C 24, 1543.

Wedepohl, K.H., 1995. Geochim. Cosmochim. Acta 59, 1217.

Workman, R.K., Hart, S.R., 2005. Earth Planet Sci. Lett. 231, 53.

(Particle Data Group), Yao, W.M., et al., 2006. J. Phys. G 33, 1.

Zartman, R.E., Haines, S., 1988. Geochim. Cosmochim. Acta 52, 1327.

Zhao, D., Horiuchi, S., Hasegawa, A., 1992. Tectonophysics 212, 289.